DISSERTATION | DOCTORAL THESIS

Titel | Title

Tailoring confined carbyne

verfasst von | submitted by

Dipl.-Ing. Clara Freytag BSc

angestrebter akademischer Grad | in partial fulfilment of the requirements for the degree of

Doktorin der Naturwissenschaften (Dr.rer.nat.)

Wien | Vienna, 2025

Studienkennzahl lt. Studienblatt | Degree programme code as it appears on the student record sheet:	UA 796 605 411
Dissertationsgebiet lt. Studienblatt | Field of study as it appears on the student record sheet:	Physik
Betreut von | Supervisor:	Univ.-Prof. Mag. Dr. Thomas Pichler

Abstract

Carbyne, the carbon allotrope consisting of an sp^1-hybridized linear carbon chain, is a novel material with remarkable properties and potential applications. It is a true one-dimensional material with an interesting bonding situation, tunable electronic band gap and unparalleled mechanical properties. Free-standing carbyne is, however, not stable due to exothermic collapse of the chain or cross-linking with other chains. The first successful synthesis of carbyne was achieved by confining the chain inside a double-walled carbon nanotube. The interaction with the tube stabilizes the chain and sterically prevents cross-linking or collapse. In recent years, many different pathways for confined carbyne synthesis were developed, mainly based on high-temperature high-vacuum annealing. Unfortunately, no robust method for consistently high yields of confined carbyne exists yet. One of the main obstacles to developing such a synthesis method is the lack of a reliable determination of the bulk yield. Raman spectroscopy is the preferred method for analyzing confined carbyne due to the high Raman scattering cross section of carbyne, leading to high signals from the chain. Unfortunately, carbyne also has a highly irregular resonance behavior which makes the Raman peak of carbyne a poor indicator for yield.

In this thesis, a new model was developed which does not rely on the resonance behavior of the chain, but rather on Raman modes following the more regular resonance behavior of the surrounding nanotube host. These are coupled modes which were recently described by anharmonic phonon-phonon interactions. The coupled mode yield evaluation model is fast, robust and not dependent on the incident laser energy, providing an easy way to determine the bulk yield of carbyne confined in double-walled carbon nanotubes. Additionally, the model considers the diameter distribution of the sample, since only a narrow window of diameters is suitable to grow inner tubes with the appropriate diameter for the growth of carbyne. Relating the bulk yield to the fraction of theoretically fillable nanotubes in the sample provides the realized growth potential, which is an essential metric when comparing samples from different starting materials and determining the efficiency of the synthesis.

Using the novel model, quantitative assessments of the influence of the main parameters in the carbyne synthesis were made. The studied parameters were the filling of the host tubes with carbonaceous precursor, temperature and annealing step sequences. These results provide crucial insights into the fundamental formation mechanisms of confined carbyne, advancing our understanding of this promising hybrid nanomaterial system.

In order to create new structures based on the confined carbyne system, heteroatoms were introduced during the synthesis. Nitrogen doped precursors were filled into the nanotube hosts

to create doped carbyne chains. The incorporation of nitrogen atoms into the chains and the surrounding carbon nanotube hosts was confirmed using Raman spectroscopy. The doping of carbyne was also achieved by treating the carbon nanotube hosts with a boron-nitride precursor using chemical vapor deposition. From the doped carbon nanotube hosts, doped carbyne chains were grown. The results demonstrate the possibility to tailor the confined carbyne system and unlock new properties.

Reliable synthesis methods and controllable properties as presented here are an important step in the advancement of technology using confined carbyne. In the future, this material has great potential in applications such as molecular sensing, thermometry, and nano-electronics.

Kurzfassung

Carbin ist ein Allotrop des Kohlenstoffs, das aus einer linearen Kette aus sp^1 hybridisiertem Kohlenstoff besteht und beeindruckende Eigenschaften und ein enormes Anwendungspotenzial hat. Es ist ein eindimensionales Material mit einer interessanten Bindungssituation, kontrollierbaren elektronischen Eigenschaften und einzigartiger mechanischer Stabilität. Allerdings ist freistehendes Carbin nicht stabil, da es zu einem stark exothermischen Zusammenfall der Kette oder Reaktion mit anderen Ketten kommen würde. Die erste erfolgreiche Synthese von Carbin wurde erzielt, indem die Kohlenstoffketten direkt in einem doppelwandigen Kohlenstoffnanoröhrchen hergestellt wurden. Die Kohlenstoffnanoröhrchen dienen als Nanoreaktor und stabilisieren die Kette, indem sie die Reaktion der Kette mit sich selbst oder anderen Ketten sterisch verhindern. In den letzten Jahren wurden verschiedene Synthesepfade für Carbin entwickelt, die hauptsächlich auf der Hochtemperaturbehandlung im Hochvakuum beruhen. Es gibt allerdings noch keinen reproduzierbaren Weg für die Carbinsynthese, der konsistent hohe Ausbeute liefert. Eines der größten Hindernisse dafür ist das Fehlen einer verlässlichen Methode für das Bestimmen der Ausbeute. Raman Spektroskopie ist die bevorzugte Methode zur Untersuchung von Carbin in Kohlenstoffnanoröhrchen, da Carbin einen extrem hohen Streuquerschnitt hat. Dadurch hat Carbin ein sehr starkes Signal im Raman Spektrum. Allerdings ist das Resonanzverhalten der Carbinketten sehr irregulär, weshalb das Signal im Ramanspektrum kein guter Indikator für die Ausbeute ist.

In dieser Arbeit wurde eine neue Methode für die Bestimmung der Ausbeute entwickelt, die nicht auf dem irregulären Resonanzverhalten des Carbinsignals beruht, sondern auf Ramanmoden, die dem stabilen Resonanzverhalten der umgebenden Nanoröhrchen folgen. Diese Moden sind gekoppelte Moden zwischen der Kette und dem Nanoröhrchen, die erst kürzlich mit anharmonischer Phononenwechselwirkung beschrieben wurden. Das Modell, das auf den gekoppelten Moden basiert, ist einfach, schnell und unabhängig von der Laserenergie, mit der das Raman Spektrum aufgenommen wurde. Zusätzlich berücksichtigt das Modell die Durchmesserverteilung in der Probe, da nicht jeder Durchmesser an Kohlenstoffnanoröhrchen geeignet ist, die richtigen inneren Röhrchen zu wachsen, in denen auch die Ketten gut wachsen und stabilisiert werden können. Wenn man die Ausbeute in Relation zu den Anteilen an passenden Nanoröhrchen setzt, ergibt sich dadurch eine Metrik, die besagt, wie sehr das Potenzial einer bestimmten Probe ausgeschöpft wurde. Mit dem neuen Modell wurden quantitative Erkenntnisse über den Einfluss verschiedener Parameter auf die Ausbeute von Carbin gewonnen. Die untersuchten Parameter waren das Füllen mit kohlenstoffhaltigen Molekülen (z.B. Fullerene) als Kohlenstoffquelle für

das Wachstum der Carbinkette, die Temperatur während der Hochtemperaturbehandlung und die Wiederholungen der Hochtemperaturbehandlungen. Die Ergebnisse liefern wertvolle Erkenntnisse zu den grundlegenden Mechanismen, die das Wachstum von Carbin in Kohlenstoffnanoröhrchen bestimmen.

Um neue Materialien auf Basis von Carbin herzustellen, wurden Heteroatome in das System eingeführt. Es wurden mit Stickstoff dotierte Fullerene in die Nanoröhrchen gefüllt und dann in Carbinketten umgewandelt. Mithilfe von Ramanspektroskopie konnte nachgewiesen werden, dass Stickstoffatome in die Kette eingefügt wurden. Eine weitere Methode, um Heteroatome in das System einzubinden war das Behandeln der Nanoröhren mit einem Bornitrid Präkursor mittels chemischer Abscheidung aus der Gasphase (CVD). Auch mit dieser Methode konnten Carbinketten mit Heteroatomen hergestellt werden. Diese Ergebnisse zeigen, dass es möglich ist, das System Carbin/Kohlenstoffnanoröhre maßzuschneidern und eventuell neue Eigenschaften zu entdecken.

Methoden für zuverlässige Syntheses und kontrollierbare Eigenschaften sind ein wichtiger Baustein für den Fortschritt in Carbin-basierten Technologien. Carbin hat großes Potenzial in Anwendungen wie Sensoren, Thermometrie und Nanoelektronik.

Acknowledgments

I would like to express my gratitude to all the people who have supported me during my work. I would like to especially thank (in no particular order of importance)...

... my supervisor **Prof. Thomas Pichler** for his dependable support, guidance and advice, the many - sometimes loud, but always fruitful - discussions, as well as providing the funding for my research.

... my past and present colleagues (and friends) **Christin Schuster**, **Dido Denier van der Gon**, **Emil Parth**, **Joselyn Benalcazar**, **Dr. Valeria Milotti**, **Ivan Verbitskii** and **Dr. Weili Cui**, for the teamwork, great collaboration and support during my studies.

... **Prof. Paola Ayala** for her academic mentorship.

... **Dr. Christian Kramberger-Kaplan** for the academic guidance, proof-reading and countless outdoor physics lectures.

... **Prof. Kazuhiro Yanagi** for giving me the opportunity to visit his laboratory in Tokyo and providing the arc-discharge carbon nanotubes I used for many experiments.

... **Dr. Takeshi Saito** for providing the eDIPs carbon nanotubes used in many of my experiments.

... **Dr. Nikos Tagmatarchis** and **Dr. Rubén Cantón-Vitoria** for providing the nitrogen doped fullerenes used in my attempts to synthesize hybrid structures.

... **Stefan Loyer** and **Andreas Stangl** for the quintessential technical support.

... **all the other colleagues** in the Electronic Properties of Materials group, for providing a supportive working environment.

... **Ixy** and **Manti** for spreading joy in the office with their presence.

... the **Doctoral College of Advanced Functional Materials (DCAFM)** members for the great interdisciplinary cooperation and the great seminars and retreats.

... the **Vienna Doctoral School in Physics (VDSP)**, especially **Dr. Christiane Maria Losert Valiente-Kroon** and **Mag. Julia Just** for providing great opportunities and networking for all PhD students of the faculty and for giving me the opportunity to shape the school as a student representative.

... my parents **Brigitte** and **Stefan** for financially supporting me throughout my entire bachelor's and master's degree, making it possible for me to focus entirely on my studies and their interest in my work.

... my **friends** and **family** for their support, patience, and encouragement.

... **Dr. Maximilian Raab** for unwavering support in scientific and personal matters since our first day of university together in more than 10 years ago.

The studies performed as part of the present work were supported by the projects:

"Doctoral College Advanced Functional Materials - Hierarchical Design of Hybrid Systems" Austrian Science Fund (FWF), doc.funds 10.55776/DOC85.
"**MO**mentum and position **RE**solved mapping **T**ransmission **E**lectron energy loss **M**icroscope" European Research Council (ERC) Synergy Project, Grant No. 951215

Contents

1

Introduction

Carbon is the most versatile element on earth, as it forms more chemical compounds than all other elements on earth combined. It is a non-metallic element with the atomic number 6 that has three naturally occurring isotopes, with ^{12}C being the most abundant. ^{13}C is also a stable isotope (1.1% abundance), while ^{14}C is a radionuclide that is often used for carbon dating. Carbon has 4 electrons in its valence shell which means it can form 4 bonds, making it the basis of the organic molecules that make up life on earth.

Carbon also forms a wide array of allotropes with vastly different properties, depending on its hybridization (fig. 1.1). Depending on the hybridization, different bonding geometries arise.

1.1 Allotropes of carbon

In the case of sp^3-hybridized carbon, a tetrahedral bonding environment leads to the diamond structure which forms naturally under high pressures and temperatures. Diamond is known and loved for its brilliance (it is "sparkly") but also its physical properties. It has the highest hardness on the Mohs scale of any natural material and a high thermal conductivity. It is an electrical insulator with a band gap between 4.5 eV and 6 eV [1]. In graphite, another common allotrope, the

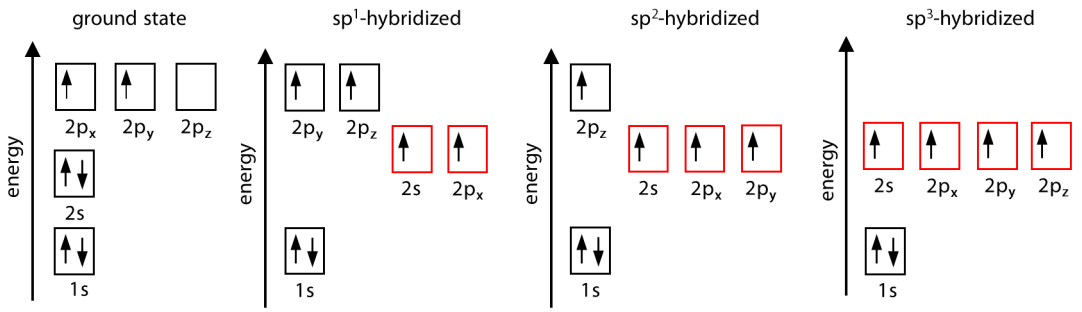

Figure 1.1: Different hybridizations of carbon.

sp^2-hybridization leads to a trigonal planar bonding environment, resulting in a stack of planar carbon sheets consisting of hexagonally arranged carbon atoms. Graphite is the stable allotrope of carbon under ambient conditions. Graphite appears black or gray, is an electrical conductor and can be used as a lubricant or for pencils. The name "graphite" is even derived from this application, as it comes from the Greek "graphein" - to write. In the past decades, other forms of sp^2-hybridized carbon have been synthesized. Those include fullerenes, which were first theoretically predicted in the 1970s by Eiji Osawa [2]. The first paper about the synthesis of C_{60} and C_{70} fullerenes was published in 1985 [3] and some of its authors Robert F. Curl, Harold W. Kroto and Richard E. Smalley were awarded the Nobel Prize in Chemistry for this discovery in 1996. A method for the bulk synthesis of fullerenes was reported by Krätschmer *et al.* in 1990 [4]. The first synthesis and characterization of helical microtubules of graphitic carbon or - as they are now more commonly referred to - carbon nanotubes is often credited to Sumio Iijima in 1991 [5], even though similar structures of "hollow carbon fibers" had already been observed in the 1970s [6], [7]. These were multi-walled carbon nanotubes synthesized during the pyrolysis of organic compounds in the presence of catalyst particles or from arc-discharge. In 1993, Iijima [8] and Bethune [9] independently discovered methods to produce single-walled carbon nanotubes. Carbon nanotubes can have very varying properties depending on their individual structure, e.g. some nanotubes are semiconducting, while others are metallic. Due to the curvature of fullerenes and nanotubes, they are not considered fully sp^2-hybridized, but as having a small amount of sp^3 character. Another important milestone in the world of carbon allotropes was the isolation of graphene, a single layer of graphite [10], for which Andre Geim and Kostya Novoselov were awarded the Nobel Prize in Physics in 2010. Graphene is highly conductive to electrons, has a remarkable strength and an interesting electronic structure, it is a zero gap semiconductor.

The most elusive, however, of the carbon allotropes is the one made of sp^1-hybridized carbon. In this case, the hybrid orbital geometry leads to a linear bonding environment, specifically a linear chain of carbon atoms. Organic compounds with such a bonding geometry are called alkynes, the shortest of which is acetylene, which has a carbon-carbon triple bond and hydrogen atoms as end groups. If further carbon atoms are added to the chains, the resulting compounds are called polyynes. An "infinitely long" carbon chain is called carbyne. This means that the properties become independent of the chain length and it is no longer regarded as a molecule, but a material [11]. The potential existence of such a material has been a rather controversial topic for a long time.

A whole host of carbon materials have been discovered and engineered in recent years which contain a mixture of carbon hybridizations, such as graphynes (carbon hexagons connected by linear carbon chains), yne-diamonds (mix of sp^3 and sp^1 carbon) or carbon dots (CDs) and graphene quantum dots (GQDs), which contain all three hybridizations [1], [12]. A ternary "phase diagram" as shown in figure 1.2 was first suggested at a seminar in Japan in 1992 to classify the discovered, as well as hypothetical and speculative allotropic forms of carbon, and published in 1997 [13].

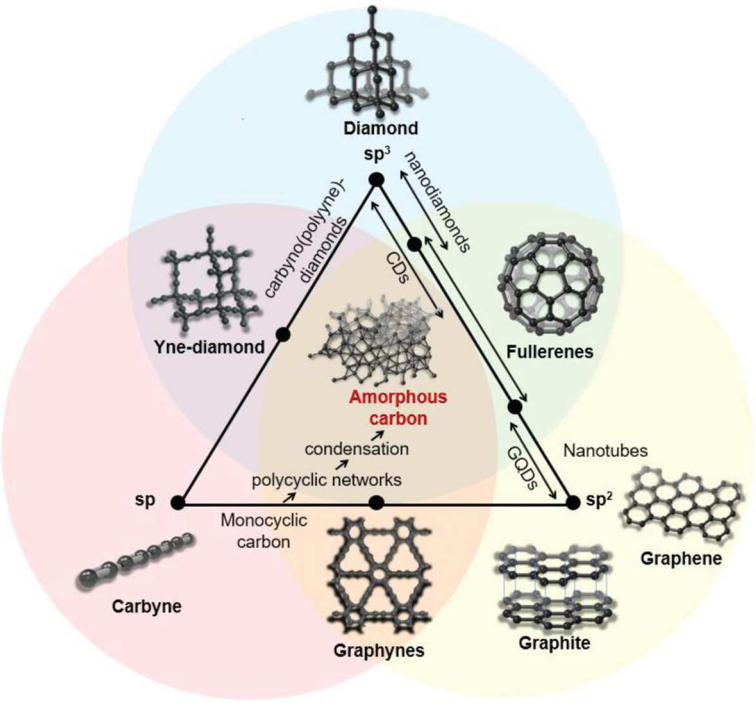

Figure 1.2: Allotropic forms of carbon resulting from the different hybridizations, from [1].

1.2 History and contention over carbyne

The first attempts on making polyynes were published in 1885 by Adolf von Baeyer [14]. He attempted to polymerize acetylene dicarboxylic acid, but was not able to isolate the desired end product tetraacetylene. He was, however, cautiously optimistic that it would be possible to create longer polyynes, if the "slight" problem of the instability of the carbon-carbon triple bond was solved. The interest in polyynes was renewed when natural polyynic compounds were isolated from plants and fungi [15]–[17]. This led to more attempts of bottom-up synthesis, where polyynes with up to 20 carbon atoms in the chain were synthesized [18]. The basis of these methods is the attachment of bulky end groups to the polyynes in order to prevent cross-linking, for example aromats, heterocycles or large organometallic compounds [19], only limited by the creativity of organic chemists. The highest number of carbon atoms (44) with such methods was achieved using a tris(3,5-di-t-butylphenyl)methyl moiety as the end-capping group [20].

A pivotal discovery in the history of carbyne was made in Germany in 1968, where "a new allotropic form of carbon" was proposed from a mineral found in the Ries Meteorite Crater in Bavaria [21]. The mineral appeared different from the graphitic rock surrounding it, with white lamellae embedded in the rock, and the analysis showed that the phase is composed of pure carbon. At the same time, Russian scientists, who were also responsible for the name "carbyne", allegedly discovered a material made only from carbon composed mostly of linear carbon chains [22]. It was then proposed that carbyne might be the allotrope of carbon that occurs at high temperatures, forming from graphite. A new phase diagram was proposed that included the

carbyne forms [23]. Even in interstellar dust, claims of carbyne structures were presented [24].

However, improved analysis methods showed that many of the early identifications were wrongly attributed to carbyne and that the signals originated from impurities, e.g. from talc, and the meteorites were composed mostly of poorly ordered graphite [25]. In 1975, another publication countered the supposed evidence of carbyne by explaining its diffraction patterns as the product of double scattering of electrons in twinned graphite with specific twinning angles [26]. Doubts were cast again over even the possibility of the existence of carbyne in minerals. H.W. Kroto, one of the Nobel prize winners for fullerenes, even said [27]:

"The existence of carbyne is myth based on bad science and perhaps even wishful thinking."

- H.W. Kroto

Chemists have long since doubted the possibility of stable long linear carbon chains, as our experiences tell us that carbon-carbon triple bonds are unstable and the chain would collapse onto itself in a strongly exothermic way, or as R.B. Heimann phrased it [26]:

"Organic chemists tend to look at the pile-up of double and triple bonds connecting the carbon atoms in the chains and take cover."

- R.B. Heimann

Some even gave up on the pursuit after minor accidents in the laboratory [28]. In 2015, a paper claimed to have successfully synthesized carbyne crystals using laser ablation in liquid [29], to which the greatest naysayer in the world of carbyne said [11]:

"I know that they can't have made carbyne because they are still alive."

- H.W. Kroto

Quickly following, another paper proposed that the material made was more consistent with carbon-gold clusters than with pure carbon chains [30]. It seems, some of the animosity on this topic is also concerning semantics, disagreements on nomenclature and gate-keeping of the name "carbyne".

Nonetheless, a host of sp^1-hybridized carbon containing materials have been synthesized using physical methods, for example laser vaporization of graphite [31], laser ablation of graphite particles in liquid [32] or arc-discharge between graphite electrodes [33]. Another method is the irradiation of a sheet of graphene in the TEM, where the "bridges" of linear carbon chain remain between graphene structures after the removal of carbon atoms from the lattice due to radiation damage. [34]. Short-lived carbon chains have also been made *in situ* in a scanning tunnel microscope, using gold contacted graphene flakes and applying a current [35]. Carbon wires can also be made in field electron microscopes, where high voltage is applied to needle

shaped specimen of carbon fibers at low temperatures. This unravels singular carbon chains from the tip surface [36].

A third approach to stabilize linear carbon chains is to confine them inside carbon nanotubes. It was observed that linear carbon chains of 20 nm, corresponding to more than 100 carbon atoms, appear inside multi-walled carbon nanotubes made from carbon electrodes by arc-discharge evaporation in hydrogen gas [37]. It is also possible to fill single-walled carbon nanotubes with polyynes, e.g., $C_{10}H_2$ under vacuum [38]. From polyyne-filled carbon nanotubes, longer chains can be formed by fusing the polyynes together at high temperatures under vacuum [39]. In 2016, a breakthrough was achieved, where carbon chains with lengths of more than 6000 carbon atoms were synthesized directly inside small-diameter double-walled carbon nanotubes using high temperature annealing under high vacuum (fig. 1.3) [40], which is considered the closest we have come to true carbyne [41].

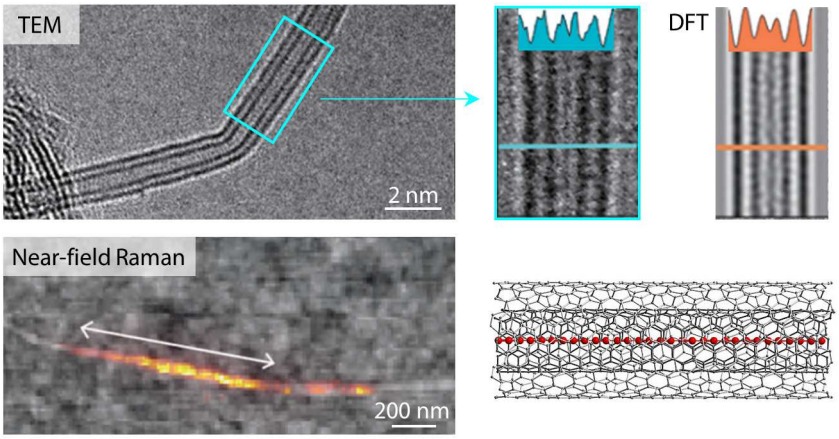

Figure 1.3: Long linear carbon chains inside double-walled carbon nanotubes, adapted from [40].

1.3 Raman spectroscopy

This chapter largely follows references [42] and [43].

Raman spectroscopy is the main tool for the study of confinded carbyne in this thesis. It is based on the inelastic scattering of light, also called Raman scattering or Raman effect. This effect was first predicted by Adolf Smekal in 1923 [44] and observed by Sir Chandrasekhara Venkata Raman in 1928 [45], who received the Nobel Prize in Physics in 1930 for his work on the scattering of light and the discovery of the Raman effect. Raman spectroscopy probes quasiparticles, such as vibrational modes, in a molecule or crystal. The peaks in a Raman spectrum correspond to the quantized excitations or quasiparticles, most often optical phonons, in the sample. In contrast to elastic scattering (Rayleigh scattering), where the wavelength of the incident light is not changed after scattering, a shift in the wavelength both to longer and shorter wavelengths is observed in Raman scattering. The shift to longer wavelengths (quasiparticle creation) is referred to as Stokes scattering and the shift to shorter wavelengths (quasiparticle destruction) is called Anti-Stokes scattering (fig. 1.4). Both Rayleigh scattering and Raman scattering intensities scale with ω^4 or λ^{-4}, the frequency or wavelength of the light. The Rayleigh scattering process is significantly more likely, which leads to higher intensity compared to peaks resulting from Raman scattering. In the resonance Raman effect, the energy of the photons matches the electronic transition energies, significantly enhancing the intensity.

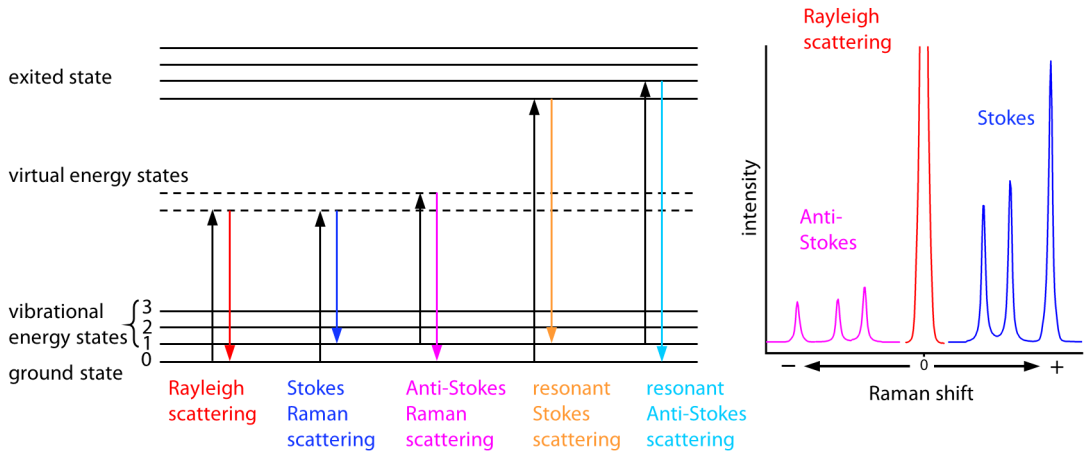

Figure 1.4: Elastic scattering (Rayleigh scattering), Stokes and Anti-Stokes scattering and resonant Stokes/Anti-Stokes scattering. On the right side, a schematic Raman spectrum is shown.

In practice, the Raman shift is usually denoted as ν and measured in wavenumbers (cm^{-1}). The wavenumbers can be converted to electron volt according to equation 1.1. Note that spectroscopic wavenumbers are defined without the factor of 2π. This energy corresponds to the energy of the created or annihilated quasiparticle. The Raman shift in wavenumbers is independent from the incident laser wavelength, which means the peak positions do not depend on the laser wavelength.

$$8065\,\mathrm{cm}^{-1} = 1\,\mathrm{eV} \tag{1.1}$$

Scattering cross section

The total Raman scattering cross section σ_T refers to the probability of inelastic scattering at a Raman shift ν into any solid angle Ω (eq. 1.2). The total Raman scattering cross section is an integral over the differential scattering cross sections σ_ν and σ_Ω, which refer to the probability that a photon is inelastically scattered with Raman shift ν in any direction and the probability that a scattered photons travels into the direction (θ, ϕ) of the steradian Ω. The double differential scattering cross section $\sigma_{\nu,\Omega}$ describes the probability of an incoming photon being inelastically scattered in the direction Ω and acquiring the Raman shift ν.

$$\sigma_T = \frac{I_0}{I_T} \qquad \sigma_\nu = \frac{\partial \sigma_T}{\partial \nu} \qquad \sigma_\Omega = \frac{\partial \sigma_T}{\partial \Omega} \qquad \sigma_{\nu,\Omega} = \frac{\partial^2 \sigma_T}{\partial \nu \partial \Omega} \tag{1.2}$$

Molecular scattering

In order for a phonon peak to be observable in the Raman spectrum, the vibration needs to modulate the polarizability α of the molecule or crystal (eq. 1.3), which occurs due to the periodical change in the interatomic distances or bond angles. The frequency of the quasiparticle is Ω.

$$\alpha(t) = \alpha_0 + \alpha_1 \cos(\Omega t) \tag{1.3}$$

The interaction of an electric field E(ω) with a molecule with polarizability α leads to a dipole moment $P_D(\omega)$ (eq. 1.4 and eq. 1.5), which acts as the source of an evanescing electromagnetic wave.

$$P_D(\omega) = \alpha E(\omega) \tag{1.4}$$

$$P_D(\omega) = \alpha E_0 \cos(\omega t) \tag{1.5}$$

When introducing the modulated polarizability (eq. 1.3) into equation 1.5 we receive equation 1.6, and subsequently, by trigonometric sum rules, equation 1.7.

$$P_D(\omega) = \alpha_0 E_0 cos(\omega t) + \alpha_1 E_0 \cos(\Omega t)\cos(\omega t) \tag{1.6}$$

$$P_D(\omega) = \alpha_0 E_0 cos(\omega t) + \alpha_1 E_0 \frac{1}{2}\Big(\cos((\omega - \Omega)t) + \cos((\omega + \Omega)t)\Big) \tag{1.7}$$

The evanescing electromagnetic wave is therefore a superposition of the original incoming frequency ω and two sidebands $\omega \pm \Omega$. The sidebands correspond to the Stokes and Anti-Stokes shifted wavelengths.

Even though Raman activity follows selection rules, most molecules and solids have at least one Raman active mode. The Raman active modes of a molecule or solid can be determined from

their symmetry and group theory. Vibrational modes are only Raman active if the derivative of the polarizability α as a function of the deformation Q at $Q = 0$ is non-zero. In figure 1.5, examples for vibrational modes of diatomic and triatomic molecules are shown and their Raman activity is discussed.

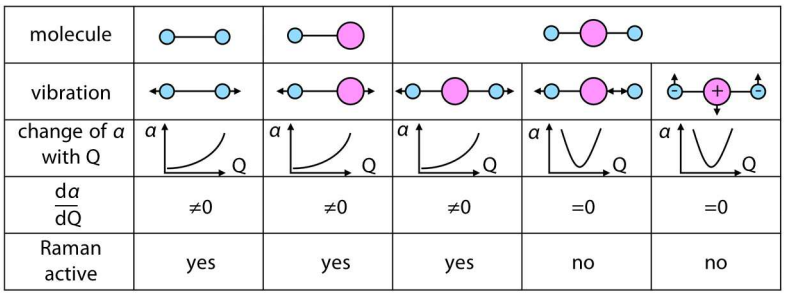

Figure 1.5: Raman active vibrations for diatomic and triatomic molecules, adapted from [43].

Raman scattering in solids

For the case of crystals, one must use a susceptibility tensor χ_{ij} instead of the scalar polarizability α. The displacements of the atoms are denoted by the normal coordinates Q_k of the oscillations. The susceptibility can be expanded around the equilibrium $\vec{Q} = 0$ with a Taylor expansion, which is terminated after the linear term (eq. 1.8).

$$\chi_{ij}(\vec{Q}) = \chi_{ij}(0) + \sum_k \left.\frac{\partial \chi_{ij}}{\partial Q_k}\right|_0 Q_k + ... \tag{1.8}$$

If the Raman scatterers oscillate with specific eigenfrequencies Ω_k, the susceptibility is modulated by the same frequencies (eq. 1.9) in analogy to equation 1.3.

$$\chi_{ij}(t) = \chi_{ij}(0) + \sum_k \left.\frac{\partial \chi_{ij}}{\partial Q_k}\right|_0 Q_k \cos(\Omega t) \tag{1.9}$$

The partial derivative of the susceptibility χ_{ij} with respect to the normal coordinate Q_k is called the Raman tensor $[\chi_{ij}]_k$ (eq. 1.10).

$$[\chi_{ij}]_k = \left.\frac{\partial \chi_{ij}}{\partial Q_k}\right|_0 \tag{1.10}$$

The components of the tensor have three indices: i and j extend over the coordinates of the tensor and k runs over the 3N-3 normal coordinates for the vibrations, where N is the number of atoms in the unit cell. There is a rank-2 tensor for every individual mode with frequency Ω_k, which have been tabulated [46]. The scattering intensity of a Raman mode is proportional to the square of the Raman tensor (eq. 1.11), where I_0 is the intensity of the incident light, σ_M is the measured scattering cross section, F_i and F_f are resonance enhancement factors for the initial (i) and final (f) wavelengths, $\vec{e}_i$ and $\vec{e}_f$ are unit vectors of the initial and the final electric fields,

and $[\chi_{ij}]_\nu$ is the Raman tensor of a specific vibration. The measured scattering cross section σ_M arises from the limitations of the recording of all possible angles of scattering.

$$I = I_0 \sigma_M F_i F_f \left| \vec{e}_f \cdot [\chi_{ij}]_\nu \cdot \vec{e}_i \right|^2 \tag{1.11}$$

Raman thermometry

The Raman signal is dependent on the temperature. The intensity ratio of the Stokes and Anti-Stokes peak is affected, as occupation of higher vibrational energy levels/existence of quasiparticles is necessary for the appearance of the Anti-Stokes peak (eq. 1.12). At higher temperatures, the higher energy states are more occupied in accordance with the Boltzmann distribution. Additionally, peaks are shifted towards lower wavenumbers in case of strong temperature dependence of the phonons themselves. Thermal broadening of peaks occurs as a result of diffuse motions of phonons.

$$\frac{I_S}{I_{AS}} = \left(\frac{\omega - \Omega}{\omega + \Omega} \right)^4 e^{\frac{h\Omega}{k_B T}} \tag{1.12}$$

Isotope effect

The frequency of vibrational modes is correlated with the masses of the atoms participating in the vibration. Equation 1.13 [47] describes the shift in frequency resulting from changes in the mass, where ν is the frequency belonging to the altered mass, ν_0 the frequency of the unaltered mass, m_0 is the unaltered mass, m_x is the mass of the isotope, and c is the relative concentration of the isotope.

$$\frac{\nu_0 - \nu}{\nu_0} = 1 - \sqrt{\frac{m_0}{m_0 + (m_x - m_0)c}} \tag{1.13}$$

Raman spectrometers

The instrumentation of Raman spectroscopy in its most simple form includes a light source, usually a laser, an optical path including mirrors, filters, gratings, a beamsplitter and a monochromator, an objective, a spectrometer and a detector (e.g. CCD) to record the scattered light (fig. 1.6).

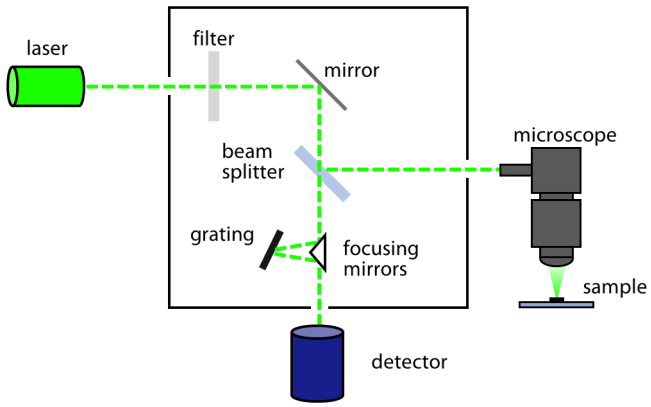

Figure 1.6: Schematic set-up for confocal Raman microscopy.

Raman spectroscopy is a useful method for the identification of samples using their characteristic Raman finger print and studying material properties such as strain, crystallinity, doping, band gaps and phase transitions. Raman thermometry can be used to determine the temperature in the sample. If the Raman cross section of the sample is known, quantitative analysis is also possible. Raman spectroscopy can be applied to gases, liquids or solid samples and is generally non-destructive, as long as the laser power is low enough to not cause thermal damage to the samples. For this reason, it is often also applied to analyze sensitive materials, such as biological samples or pigments of artworks.

1.4 Carbon nanotubes

1.4.1 Structure of carbon nanotubes

This chapter largely follow reference [48].

Carbon nanotubes can be conceptually thought of as a rolled up sheet of graphene. Depending on the orientation of the axis with respect to the graphene lattice, the geometry of the carbon nanotube can differ (fig. 1.7). The axis is perpendicular to the vector of helicity C_h (eq. 1.14), which is the sum of the lattice vectors a_1 and a_2 multiplied by integers n and m, respectively. The different vectors of helicity result in chiral (n,m) and achiral nanotubes. The achiral nanotubes can be further divided into zigzag (n,0) nanotubes and armchair (n,n) nanotubes.

$$\mathbf{C_h} = n\mathbf{a_1} + m\mathbf{a_2} \tag{1.14}$$

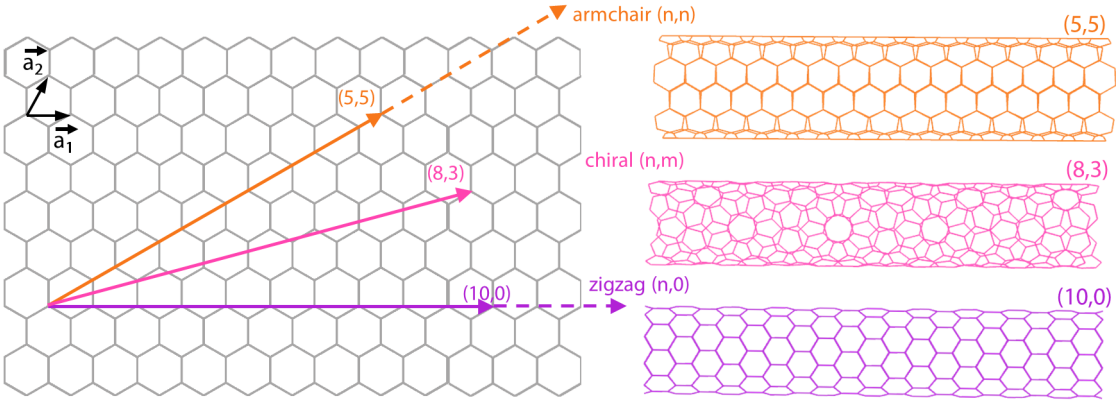

Figure 1.7: Carbon nanotubes formed by rolling up a sheet of graphene.

The diameter of carbon nanotubes typically ranges between 0.4 nm [49] and 2.5 nm [50]. The lower limit exists due to the high stress on the carbon-carbon bonds while the cylindrical shape is not stable much above 2.5 nm and the tubes would collapse [51]. As compromise between strain on the carbon bonds and stability of the cylinder, carbon nanotubes with a diameter of about 1.35 nm seem to be the most favorable, as this is the diameter that grows predominantly during synthesis from solid carbon sources in the absence of catalysts [50]. The diameter can be calculated from the vector of helicity (eq. 1.15), where a_{cc} is the bond length between carbon atoms.

$$D = \frac{|C_h|}{\pi} = \frac{a_{cc}\sqrt{3(n^2 + nm + m^2)}}{\pi}, \tag{1.15}$$

The bond length varies slightly depending on the radius of curvature, as the carbon-carbon bond is elongated compared to that of flat graphene. The lower limit is 1.42 Å, which is the carbon-carbon bond length in graphite, and 1.44 Å, is reasonably assumed to be the upper limit, which corresponds to the carbon-carbon bond length in C_{60} fullerenes [50]. The length of single-

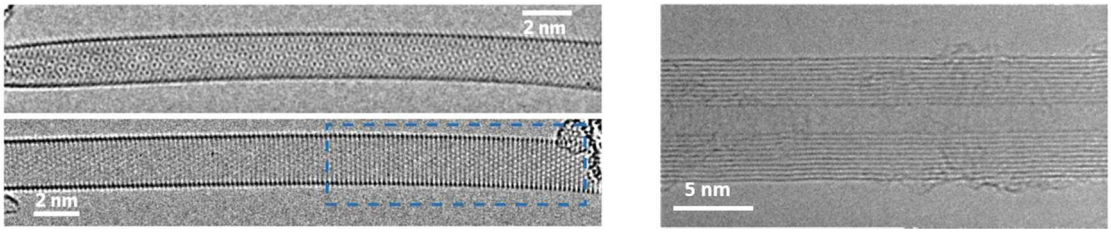

Figure 1.8: Left: single-walled carbon nanotubes (top: chiral; bottom: zigzag); Right: multi-walled carbon nanotube; adapted from [56] and [57], respectively.

walled carbon nanotubes (SWCNT) is dependent on the synthesis method and can range from 500 nanometers up to several millimeters. One of the longest reported carbon nanotubes was 0.55 meters long [52]. Due to their extremely high aspect ratios, carbon nanotubes exhibit properties of truly one-dimensional solids. Their behavior is similar to that of polyacetylene polymers with more than 100 carbon atoms, where the properties become independent of length. However, polyacetylene, which should be metallic considering only a combination of molecular orbitals, due to Peierl's distortion, becomes a semiconductor or insulator [53], [54]. Carbon nanotubes are stable against Peierl's distortion [48] and therefore exhibit properties of one-dimensional metals, such as Luttinger liquid behavior.

Double- or multi-walled carbon nanotubes (DWCNT/MWCNT) are Russian-doll like structures of coaxial single-walled carbon nanotubes with increasing diameter. Their diameter can range from 1.4 - 30 nm and they are, in contrast to flexible single-walled carbon nanotubes, rod-like rigid structures [55]. In figure 1.8, transmission electron microscopy (TEM) images of single-walled carbon nanotubes and multi-walled carbon nanotubes are shown.

1.4.2 Properties of carbon nanotubes

In order to understand the electronic properties of carbon nanotubes, it is useful to first look at the electronic band structure of graphene. Graphene has a hexagonal Brillouin zone, and the π and π* bands touch only at the corner points of the Brillouin zone, labeled K and K' (fig. 1.9a and b), where the density of states is zero [58]. This is why graphene is neither a true metal nor a true semiconductor, but is often referred to as a semi-metal or a zero-gap semiconductor. When the graphene sheet is rolled up into a carbon nanotube, periodic boundary conditions are imposed on the structures perpendicular to the tube axis and only a limited amount of k states are allowed, which are shown by the red lines in figure 1.9c and d. The distance between the quantization lines is determined by the diameter D of the nanotube. Depending on the geometry of the nanotube, this results in metallic, tiny-gap semiconducting or large-gap semiconducting nanotubes. If the K and K' points are included in the allowed k states, the nanotube is metallic, if it is not included, the tube is a semiconductor. This can be seen by the depiction of the Dirac cones (linear dispersion relation of the energy bands at the K and K' points), where the offset of the quantization line from the K/K' point leads to the opening of a band gap (fig. 1.9d). Armchair (n,n) nanotubes are always metallic, in the case of zigzag (n,0) or chiral (n,m) nanotubes, a general rule can be

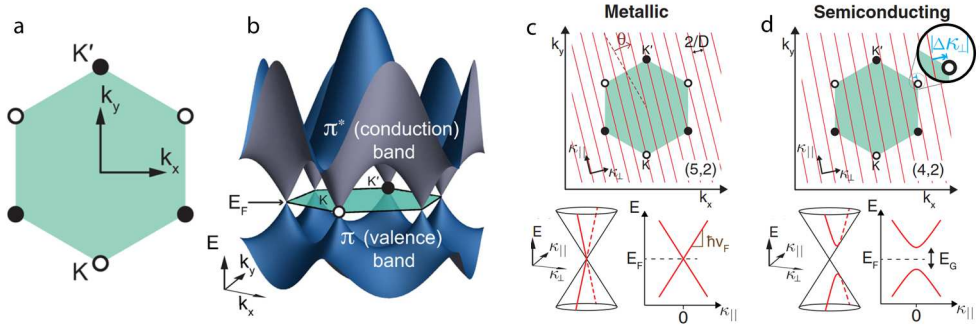

Figure 1.9: Electronic band structure of graphene and carbon nanotubes, adapted from [58]: a) Brillouin zone of graphene; b) energy bands of graphene close to the Fermi level, the π and π* bands touch at the K and K' points; c) Brillouin zone of a metallic carbon nanotube, the allowed k states (red lines) include the K and K' points; d) Brillouin zone of a semiconducting carbon nanotube, the allowed k states do not include the K and K' points, the Dirac cone below shows how the offset from the K/K' points leads to the opening of a band gap.

found in equation 1.16. If j is a nonzero integer, the nanotube is a tiny-gap semiconductor, in all other cases the tube is a large-gap semiconductor. When only considering the zone-folding model, the nanotubes that follow equation 1.16 should be metallic, but a tiny gap can open due to tube curvature effects in cases where j is nonzero. Armchair nanotubes always remain metallic, since even taking curvature into account, the shift of the wave vector is along an allowed line of the graphene Brillouin zone [59]. However, the band gaps of tiny-gap semiconductors are so small that they appear metallic under ambient conditions [60].

$$n - m = 3j, \tag{1.16}$$

As single-walled carbon nanotubes are one-dimensional solids, the density of states exhibits interesting features. Compared to three-dimensional systems, where the density of states has a monotonic increase with energy, one-dimensional systems show sharp maxima at certain energies with a decaying tail (fig. 1.10a). These are called Van Hove singularities. Due to these well-defined energy maxima, single-walled carbon nanotubes behave almost like molecules in terms of electron excitations and optical transitions. Depending on the structure of the nanotube, different discrete transitions occur, which are denoted as E_{ii} in figure 1.10b [61]. A systematic plot of single-walled carbon nanotube optical transitions as a function of diameter, the so-called Kataura plot [62], can be found in figure 1.10c. This plot is useful in order to select the correct excitation wavelength to study a certain nanotube or, inversely, determine the diameter of the nanotube from the optical absorption properties. Semiconducting carbon nanotubes also exhibit photoluminescence, which is a useful tool to characterize them [63]–[65].

The electronic and optical properties of carbon nanotubes are, in practice, strongly influenced by the environment. For example, in (metallic) armchair nanotubes, bundling together the nanotubes into a rope will lead to repulsion of the bands between neighboring tubes. This causes a pseudogap of up to 0.3 eV to open, drastically changing the electronic properties [67]. As

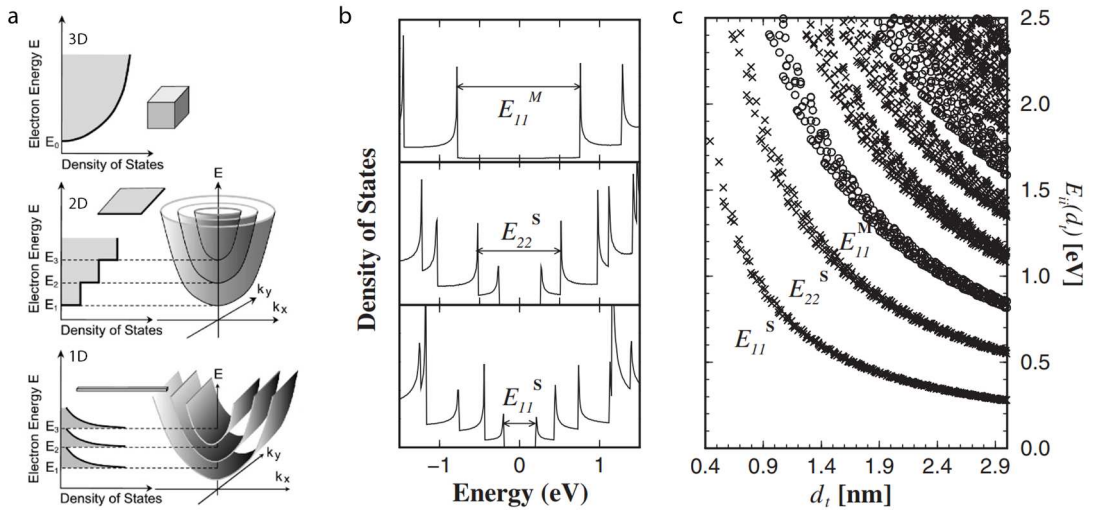

Figure 1.10: a) Density of states of 3D, 2D and 1D systems, adapted from [66]; b) density of states for an armchair (10, 10) metallic single-walled carbon nanotube (top), a chiral (11, 9) semiconducting single-walled carbon nanotube (middle) and a zigzag (22, 0) semiconducting single-walled carbon nanotube (bottom), adapted from [42]; c) Kataura plot of electronic transitions E_{ii} as a function of nanotube diameter, adapted from [42].

mentioned above, semiconducting carbon nanotubes exhibit photoluminescence, but only individually isolated single-walled carbon nanotubes have a strong photoluminescence signal. In case of nanotube bundles the signal is quenched due to non-radiative relaxation of the excitons [64].

The phononic properties of carbon nanotubes can also be derived from graphene. In graphene, there are 6 phonon branches. Four of them are in-plane phonon branches, namely transverse acoustic (TA), longitudinal acoustic (LA), transverse optical (TO) and longitudinal optical (LO) and two out-of-plane branches, one acoustic (ZA) and one optical (ZO) [68]. A closer look into the phonon dispersion of graphene revealed two Kohn-Anomalies at the Γ and K points (fig. 1.11b) [69]. The phonon branches of graphite, measured using inelastic X-ray scattering (IXS) and modeled using GW calculations, are shown in figure 1.11 [70]. The three highest branches (LO, TO and LA) are almost triply degenerate around the K point. The study by Grüneis *et al.* also enabled the disentangling of the phonon branches at the K points [70]. Many-body effects needed to be considered to correctly reflect experimental results, which could not be explained using density functional theory (DFT).

The electronic and optical properties of carbon nanotubes make them interesting materials for a wide range of applications, such as nano-scale light emitters [71], field effect transistors [72] or even biosensing applications [73].

Carbon nanotubes also have remarkable mechanical properties, such as high tensile strength of around 45 GPa for single-walled carbon nanotubes [74] and around 150 GPa for defect free multi-walled carbon nanotubes [75]. Steel in comparison only has a tensile strength of 0.45-2.35 GPa, depending on the structure, while being significantly heavier [76]. The Young's modulus

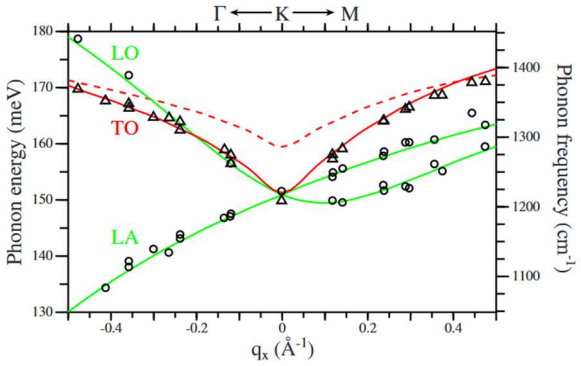

Figure 1.11: Phonon dispersion of graphite along the the ΓKM direction. The points are extracted from IXS measurements, full lines represent the GW calculations. The dashed lines correspond to DFT calculations, illustrating the importance of considering electron-electron correlations (GW approach) to achieve good agreement with experimental values, adapted from [70].

of carbon nanotubes is exceptionally high, in the TPa range [77]. Carbon nanotubes also have high resilience, meaning that they can significantly change their shape, e.g., bending, torsion or flattening without irreversible atomic rearrangements [78]. Due to their superb mechanical properties, low density and high aspect-ratios, carbon nanotubes are ideal candidates for high performance composite fibers [79]. Composites of nanotubes with metal, ceramic or polymer matrices are extensively studied, as carbon nanotubes promise major advances for the properties of such materials [50].

1.4.3 Raman spectroscopy of carbon nanotubes

Raman spectroscopy is a useful tool to study carbon nanotubes and related systems, as they have many Raman active modes that are directly related to their properties such as diameter, chirality and purity. In figure 1.12, the Raman spectrum of a single-walled carbon nanotube is shown and the characteristic modes are marked.

The radial breathing mode (RBM) describes a synchronous vibration of all carbon atoms in the radial direction, comparable to the movement of the thorax when breathing. The typical Raman shifts of radial breathing modes are in the range of 100-500 cm^{-1}. The RBM is very useful for the characterization of carbon nanotubes, as its frequency is dependent on the diameter of the nanotube roughly according to equation 1.17, where ω is the frequency of the RBM, D is the nanotube diameter and A and B are constants to be determined empirically. For isolated single-walled carbon nanotubes the values $A = 248$ and $B = 0$ and for bundles the values $A = 234$ [cm^{-1}nm] and $B = 10$ [cm^{-1}] have been found [80]. However, this relation is only accurate for nanotubes between 1.2 and 1.8 nm in diameter, as below a diameter of 1 nm, lattice distortions lead to a chirality dependence of the frequency of the radial breathing mode [80], [81].

$$\omega_{\mathrm{RBM}} = \frac{A}{D} + B \tag{1.17}$$

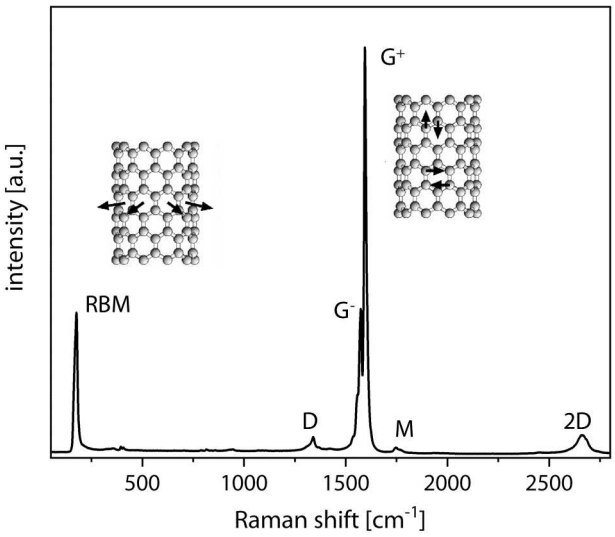

Figure 1.12: Raman spectrum of single-walled carbon nanotubes measured with a 568 nm laser. The vibrations of the RBM and G modes are shown schematically, adapted from [80].

Using resonant Raman scattering and the Kataura plot (fig. 1.10c), the RBM frequency can even be used to identify the chirality of a single nanotube [82]. The Stokes/Anti-Stokes intensity ratio can also be used for the determination of electronic transitions and subsequently, chirality of individual single-walled carbon nanotubes [83]. It is important to note that equation 1.17 does not take into account environmental effects, which also causes shifts in the RBM frequency [84]. Double-walled carbon nanotubes exhibit radial breathing modes from both the inner and the outer tubes, which are shifted towards higher frequencies compared to single-walled carbon nanotubes with the same diameter [85]. The inner and the outer tube can be considered as two oscillators connected by a spring [86]. It can also be observed that the inner tube RBMs exhibit a characteristic splitting into multiple components for each outer tube due to interactions between the shells [87].

The tangential modes in carbon nanotubes originate from the optical phonons in graphite and are characterized by a displacement parallel to the nanotube wall, either along the circumference, the axis or a mixed direction in-between. As these modes involve mostly the strong sp^2 carbon bonds, they appear at high frequencies. The Raman active tangential modes are the G-mode ("G" as in "graphite") at around 1585 cm^{-1}, sometimes also referred to as the high energy mode (HEM) and the 2D-mode [86]. In graphite, the longitudinal optical (LO) mode and transverse optical (TO) mode are degenerate at the Γ point, leading to a single peak [81]. However, due to their curvature, the G-mode is a multi-peak feature in carbon nanotubes, where the most intense peaks, labeled G^+ and G^-, originate from the breaking of symmetry along the tube axis and along the circumference, respectively. The G-mode is also dependent on the diameter and metallicity [80]. While the frequency of the G^+ mode is relatively independent of the nanotube diameter, the G^- frequency increases with increasing diameter (fig. 1.13b). However, for metallic tubes, *ab-initio* calculations have rejected previous assignments of the LO- and TO-mode to G^+ and G^-

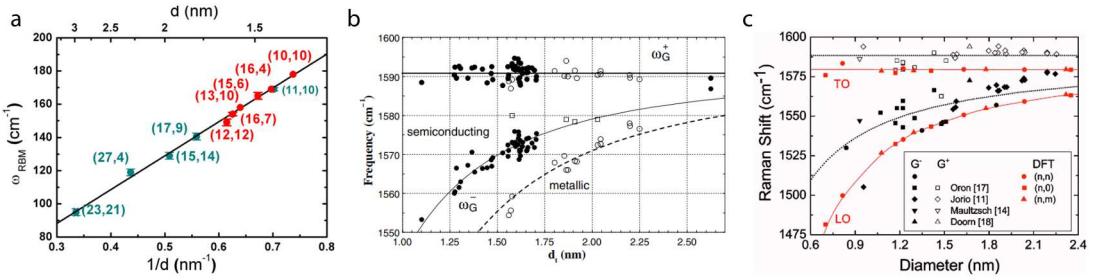

Figure 1.13: Diameter dependence of the the Raman modes of carbon nanotubes: a) diameter dependence of the RBM (adapted from [89]); b) diameter dependence of the G-mode (adapted from [80]); c) opposite mode assignment for the G-mode of metallic single-walled carbon nanotubes (adapted from [88]).

and assigned the modes the opposite way (fig. 1.13c) [88]. Using the difference in frequency of G^+ and G^- bands, the diameter can be estimated. This is however not as accurate as determination from the radial breathing mode. The diameter dependence of the radial breathing mode is shown in figure 1.13a.

The D-mode ("disorder-induced" mode), also a tangential mode, is located at around 1350 cm^{-1} and appears in the Raman spectrum of carbon nanotubes in the presence of defects, such as heteroatoms, vacancies, impurities, heptagon-pentagon pairs, kinks or grain boundaries [80], [81]. This mode is not visible in the Raman spectrum of a perfect carbon nanotube structure, as it is associated with the K point of the Brillouin zone and only modes at the center of the Brillouin zone (Γ point) can be measured due to momentum conservation. Breaking the translational symmetry due to defects in the structure leads to a breakdown of momentum conservation by activating phonons at the K points of the Brillouin zone. The disorder-induced lattice distortions could also lift other symmetry-based selection rules, thus also activating phonons that are forbidden by the symmetry of the unperturbed crystal structure [42]. The origin of the mode is based on a double-resonance process, coupling phonons and electrons [90]. The frequency, linewidth and intensity can provide information on the structure of the carbon nanotubes, their degree of disorder and mechanical properties such as compressive or tensile strain [81]. A comparison of the ratio of the D-band and G-band intensities as a function of distance between defects in graphite is shown in figure 1.14 [91]. However, resonance behavior has to be considered when comparing D-band intensities with other Raman features.

The 2D-band, also often called G'-band, appears at even higher frequencies, between 2500-2800 cm^{-1}. This band arises from the anti-parallel second harmonic of the D-band at the K point. The cancellation of the momentum renders this mode optically active. It is highly dispersive and therefore useful to probe the electronic and phononic structure of sp^2 carbon materials. Despite its name, it is not dependent on defects in the structure. Its frequency, linewidth and and intensity are, however, sensitive to strain [81]. Both the D- and the 2D-bands are dependent on carbon nanotube diameter and chiral angle.

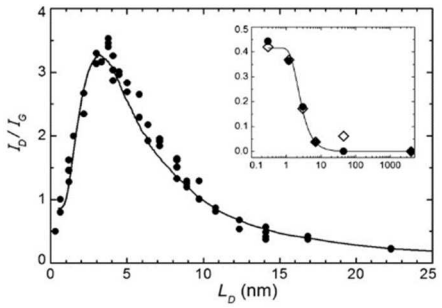

Figure 1.14: Ratio of D-band to G-band intensities in the Raman response of graphite as a function of distance between defects, adapted from [91].

1.4.4 Synthesis, purification and sorting of carbon nanotubes

Synthesis

The main methods of carbon nanotube synthesis are arc-discharge, laser ablation and chemical vapor deposition [92]. In the arc-discharge method, carbon electrodes are evaporated in an inert gas using high currents. The temperatures can reach 3000°C-4000°C. Single-walled and multi-walled carbon nanotubes with high crystallinity can be synthesized by arc-discharge. Arc-discharge was also the method used by Iijima in 1991, who used the method typically used for fullerene synthesis and discovered carbon nanotubes [5]. The first larger scale synthesis of multi-walled carbon nanotubes using arc-discharge was reported in 1992, where high pressures of helium gas (500 Torr) were used [93]. Synthesis of single-walled carbon nanotubes through arc-discharge requires a metal catalyst in the carbon anode. In 1993, substantial amounts of single-walled carbon nanotubes could be synthesized using carbon anodes with a small percentage of cobalt [9]. High yields of 70-90% of single-walled carbon nanotubes could be achieved with 1 at.% Y and 4.2 at.% Ni as catalysts [94].

In laser ablation, laser pulses are used to ablate a target in a furnace, while a flow of inert gas, e.g. argon, carries the produced nanotubes into a cooler zone to be collected. This method was pioneered in 1995 to make multi-walled carbon nanotubes [95] and single-walled carbon nanotubes [96]. The single-walled carbon nanotubes were synthesized from metal-graphite composite targets containing cobalt and nickel or cobalt and platinum with a furnace temperature of 1200°C.

In chemical vapor deposition (CVD), a catalyst is heated inside a furnace and a hydrocarbon gas flows over the catalyst. The catalysts are usually transition-metal nanoparticles, e.g. iron, cobalt or nickel, and ethylene or acetylene are typical feedstock gases. Temperatures for CVD growth of multi-walled carbon nanotubes commonly range between 550°C and 750°C. First reports of such methods for growing multi-walled carbon nanotubes by acetylene decomposition over iron catalyst particles at 700°C came out in 1993 [97]. In order to grow singe-walled carbon nanotubes from CVD, generally higher temperatures are required, as smaller diameter single-walled carbon nanotubes have higher strain energies. It is important to consider the feedstock gas at high temperatures, as self-pyrolysis into amorphous carbon is unfavorable for the yield [92]. For example, high-quality single-walled carbon nanotubes were grown using methane as a carbon

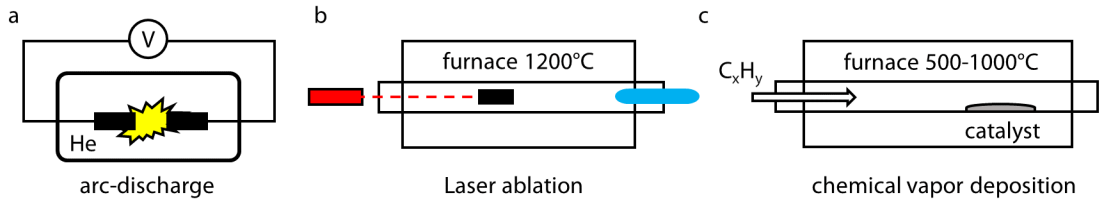

Figure 1.15: Common synthesis methods for carbon nanotubes: a) arc-discharge; b) laser ablation; c) chemical vapor deposition.

source and supported Fe_2O_3 catalysts at 1000°C [98]. Generally, there are many parameters in CVD (feedstock gas, partial pressures, temperatures, catalyst, catalyst supports) which can and have been tuned in the past decades in order to improve the yield of high-quality nanotubes and even make aligned carbon nanotubes, which is possible due to the catalyst pores acting as growth templates [99].

A sketch of the three main methods for nanotube synthesis is shown in figure 1.15. All three methods have some advantages and limitations [100]. In arc-discharge, near perfect single-walled and multi-walled carbon nanotubes can be synthesized. However, high temperatures are required and only batch production is possible. The growth parameters are not easily controllable and the tubes are typically short and deposited in random positions and orientations. Laser ablation is relatively costly due to the need for expensive lasers, but compared to arc-discharge, the growth conditions can be well controlled. It primarily produces single-walled carbon nanotubes with a well defined diameter which are cleaner than the tubes made from arc-discharge. In CVD, the yield can be extremely high, the tubes can be very long and it is the most easily scalable at an industrial level. Unfortunately, the tubes are often high in defects, which is disadvantageous to their properties. In recent years however, CVD methods have been greatly improved in this regard, basically eliminating this issue.

A variation of the CVD method for carbon nanotube synthesis is enhanced direct injection pyrolytic synthesis (eDIPS) (fig. 1.16) [101]. This method uses a vertical ceramic furnace tube with a temperature gradient, where an organic solvent solution of the catalyst precursor is injected via a spray nozzle under a hydrogen carrier gas flow. A second carbon source, e.g. ethylene, flows trough the reactor. The reaction temperature is around 1200°C. The nanotubes are collected in a filter at the bottom. For example, ferrocene is used as a catalyst precursor in a toluene solution, which sublimates and decomposes into iron clusters/nanoparticles with increasing size. The diameter of the nanotubes can be controlled through the decomposition temperature of the carbon source. It is assumed that carbon precursors decomposing at lower temperatures will yield smaller diameter nanotubes, as the catalyst particle clusters in this furnace zone are smaller.

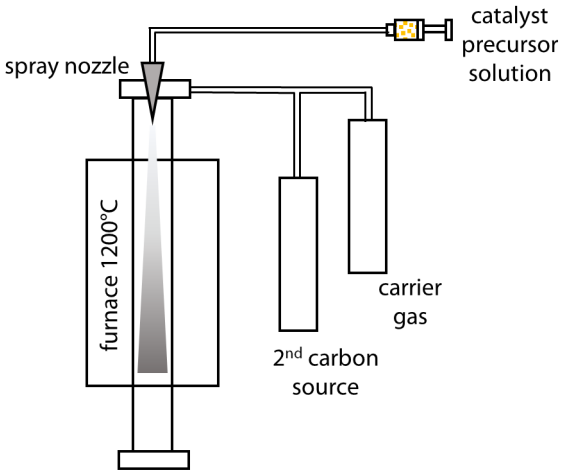

Figure 1.16: Enhanced direct injection pyrolytic synthesis (eDIPS), adapted from [101].

Purification

As-grown carbon nanotubes with any method always contain a certain amount of impurities [102]. In the case of CVD, undesired side products often include amorphous carbon, aromatic carbon, polyhedral carbon, carbon nanoparticles and metal particles. In arc-discharge and laser ablation, common by-products are fullerenes, graphitic polyhedrons, also with catalyst particles enclosed, and amorphous carbon. There are several purification methods based on chemical oxidation processes, these include gas-phase oxidation, liquid phase oxidation using acid treatment and electrochemical oxidation. These methods are based on the principle that amorphous carbon and carbon nanoparticles are less stable towards oxidation than the carbon nanotubes. However, these chemical processes can damage the nanotubes, e.g. open the end-caps, modify their surface structure and add functional groups. While this is unwanted for some applications, the modified nanotubes can serve as starting materials for further interesting chemical reactions. For example, opening the end-caps is necessary for filling carbon nanotubes with other molecules, such as fullerenes to create "peapods" [103]. To avoid the chemical modifications by the various types of oxidation treatments, physical methods of sample purification can also be used. Common methods include filtration, centrifugation, chromatography, electrophoresis, and high temperature (1400–2800°C) annealing. While these methods are generally non-destructive, for most of them the nanotubes need to be in solution, requiring surfactants and sonication for dispersion.

Separation

For many applications, e.g. optoelectronics, it is necessary to not only purify carbon nanotubes, but also to separate the nanotubes themselves according to their properties, such as diameter, band gap, metallicity or chirality.

One of the most common methods for nanotube separation is density gradient ultracentrifugation (DGU). This technique is based on the different buoyant densities of carbon nanotubes with different structures. The centrifugation is performed in solution with a density gradient and the

resulting centripetal force on the particles causes them to spatially separate according to their buoyant densities. Using successive iterations of ultracentrifugation, very small diameter distributions can be achieved [104]. In the first attempts, the single-walled carbon nanotubes were wrapped in DNA strands and separated by diameter in a density gradient solution of iodixanol [105]. This method had some significant drawbacks, including the limited stability of DNA in aqueous solutions, difficult removal and non-sensitivity to metallicity, which is why other surfactants were explored. Bile salts such as sodium cholate (SC), sodium deoxycholate (DOC) and anionic-alkyl amphiphiles such as sodium dodecyl sulfate (SDS) are often used. The surfactants form encapsulation layers around the carbon nanotubes which are sensitive to slight differences in the structure. With these surfactants, also metallicity sorting is possible, as the surfactants interact differently with metallic and semiconducting nanotubes. It has been suggested that metallic nanotubes interact more strongly with the surfactants via π interactions than semiconducting nanotubes [106]. The packing density of the surfactants is also sensitive to electrostatic screening of the nanotubes. Partial charge-transfer between metallic nanotubes and the surfactants could also play a role [104]. Using nonlinear density gradients, different chiral single-walled carbon nanotubes can be enriched [107]. Even the right and left handed enantiomers of single-walled carbon nanotubes can be separated with DGU using the chiral surfactant sodium cholate [108] and nonlinear density gradients [107].

Co-polymer isolation is based on the different dispersability of carbon nanotubes in different polymers. With this method, carbon nanotubes can be sorted by length [109], diameter [110], chirality [111] and enantiomer [112].

Aqueous two-phase extraction (ATPE) is another common method for the separation of carbon nanotubes [113]. In this method, two water-soluble polymers are mixed together in an aqueous solution. At certain concentrations, a transition occurs and the mixture separates from one phase into two phases. When the other components of the mixture have different affinity to the two phases, they will also be enriched in the respective phases, allowing a separation. Surfactant concentrations are used in single-walled carbon nanotube separation to control the affinity to the polymer phases, typically polyethylene glycol (PEG) and dextran (DEX). Carbon nanotubes covered with SC or DOC tend to gather in the dextran-rich phase and nanotubes with SDS into the PEG rich-phase. Using several steps of separations with varying surfactant concentrations, highly enriched fractions can be collected. Separation according to diameter, metallicity, band gap and enantiomeric sorting are possible with ATPE. This method is generally very practical, as it requires no expensive equipment, has low energy cost, low material costs and high throughput.

Different types of chromatography have also been applied for the separation of carbon nanotubes. In general, chromatography is a separation technique based on differences in the interaction of the components in the sample with the material of a column. At first, size-exclusion chromatography was used to separate the multi-walled carbon nanotubes by length, using SDS to disperse the sample and controlled pore glass as a chromatography column [114]. Using agarose gel and single-walled carbon nanotubes dispersed in SDS, a separation of metallic and semiconducting nanotubes can be achieved [115]. Single-chirality separation could also be achieved, e.g. by using gel chromatography with an alkyl-dextran based gel [116]. Ion exchange chromatography can also be applied for diameter sorting [117] and chirality sorting [118]. Using

gel permeation chromatography, even double-walled carbon nanotubes can be separated into four fractions according to the metallicity of both the outer and the inner nanotubes [119].

In electrophoresis, the application of an electric field leads to the sorting of a sample according to the mobility of its components in a medium. For example, semiconducting and metallic single-walled carbon nanotubes can be dispersed in SDS and separated using agarose gel electrophoresis in only 20 minutes [120]. This method is fast, low cost and high yield.

The "holy grail" of nanotube synthesis would be to find methods where only one single chirality of nanotube is produced. Even if this has not yet been achieved, synthesis pathways that lead to the enrichment of one type of nanotube have been developed in recent years, such as total organic synthesis, cloning and catalyst engineering [121].

1.4.5 Functionalization of carbon nanotubes

Carbon nanotubes can be modified to enhance or change certain properties or for specific applications. Such modifications include, but are not limited to, doping (substitutional, endohedral or exohedral), intercalation, functionalization, coating and endohedral filling [122]. Heteronanotubes and filled nanotubes are discussed in further detail in the following sections.

Intercalated nanotubes

Intercalation compounds of nanotubes refer to structures where heteroatoms, often alkali metals such as lithium or potassium, are found between single-walled carbon nanotubes in bundles. The heteroatoms act as electron donors or acceptors, modifying the electronic structure of the nanotubes [122], [123].

Different levels of charging can be observed in the Raman frequency for potassium intercalated nanotubes [124]. Intercalated nanotubes can be synthesized using two-zone vapor transport [125]. Intercalated nanotubes are structurally closely related to graphite intercalation compounds (GIC), which makes GICs well-suited models for the study of electronic doping on sp^2-hybridized nanocarbon. For intercalated graphite, different effects were observed on the Raman frequency, specifically the G-mode and the 2D-mode of graphite [126] (fig. 1.17). Charge transfer causes upshifts in Raman frequencies, while the strain caused by the deformation of the lattice and subsequent elongation of the carbon-carbon bond leads to downshifts in the Raman frequency. For the G-band, a mode originating at the Γ point, both effects occur, but the effect of charge transfer dominates, resulting in a net increase of the Raman frequency. For the 2D-mode, which contrary to the G-mode originates at the K point in the Brillouin zone, only the effect of strain is observed, leading to a downshift in the Raman frequency.

The effects of electronic doping have also been observed in doped graphene. Shifts of the G-band can be correlated to changes in the Fermi level. It has been shown in simulations that the G-band in graphene will shift downwards slightly, regardless of *p*-type or *n*-type doping in very low concentrations. With increasing concentrations, both the increase and decrease of the surface electron concentration leads to an upshift of the G-band frequency (fig. 1.18a and b) [127], [128]. The "dip" at low concentrations is more pronounced at low temperatures compared to room temperature, where almost no decrease in the G-band frequency can be measured. The

full-width at half maximum (FWHM) also decreases with the change in electron concentration (fig. 1.18a and c).

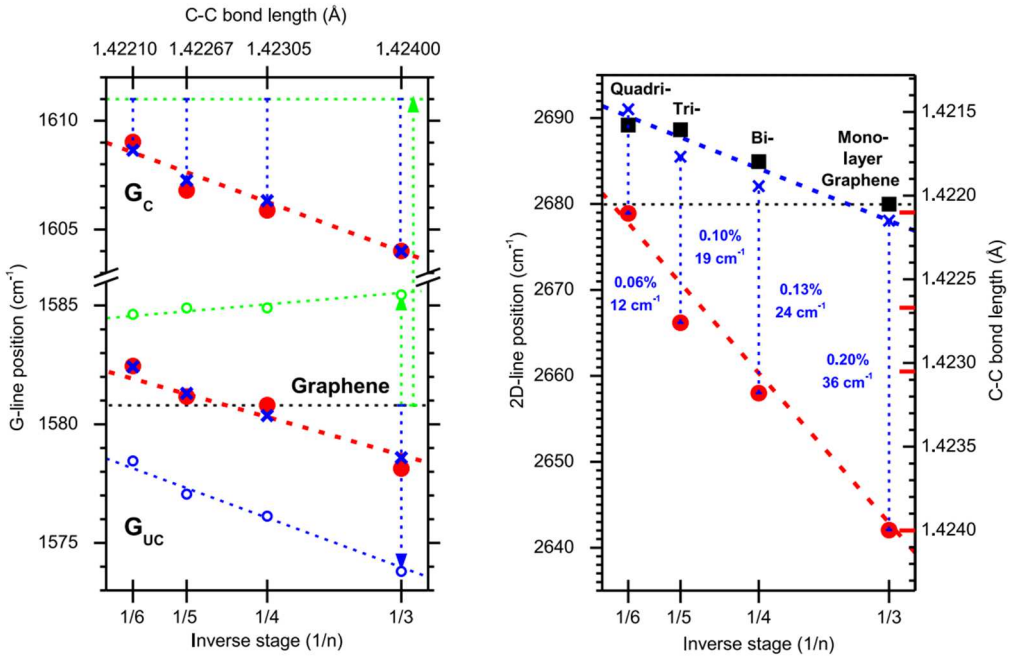

Figure 1.17: Shifts of the G-mode (left) and 2D-mode (right) in intercalated graphite as a function of inverse intercalation stage, adapted from [126].

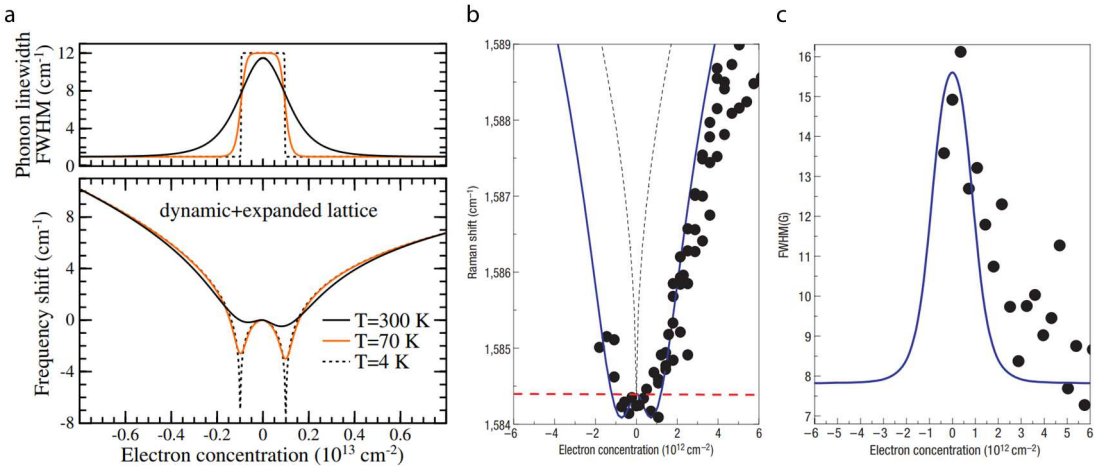

Figure 1.18: Effect of electronic doping on the G-mode of graphene: a) simulations for linewidth and frequency of the G-mode, adapted from [128]; b) experimental values for frequency shifts of the G-mode at 295 K, adapted from [127]; c) experimental values for the linewidth of the G-mode, adapted from [127].

Apart from doping, the effect of charging on carbon nanotubes has been studied using gating. Nanotubes are promising materials for field-effect transistors. The increase in the G-band frequency has been observed also for applying a positive gate voltage, i.e., adding charges into the material [129].

Heteronanotubes

Carbon atoms in the structure can be replaced with heteroatoms such as boron, nitrogen or even phosphorus without changing the honey-comb lattice structure (heteronanotubes) [130], [131]. The substitution of a carbon atom with a boron atom leads to the creation of an electronic hole, as boron has only three valence electrons, compared to four valence electrons in carbon. Therefore, boron doped carbon nanotubes are *p*-type "nanoconductors". Nitrogen, on the other hand, has five valence electrons, so three-coordinated nitrogen can be substituted into the structure and the nanotube will exhibit *n*-type doping. The nitrogen can substitute a carbon atom in the lattice and be bonded to three carbon atoms (graphite-type doping) (fig. 1.19a), or it can be bonded to only two carbon atoms (pyridine-type doping), in which case another carbon needs to be removed from the lattice, creating a structural "hole" (fig. 1.19b). Such nanotubes have localized electronic states above and below the Fermi-level.

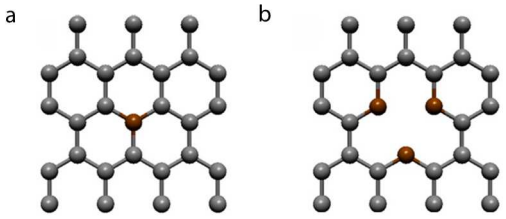

Figure 1.19: Different types of nitrogen doping in carbon nanotubes: a) graphite-type doping; b) pyridine-type doping, adapted from [131].

Heteronanotubes can be synthesized with the same methods as pristine carbon nanotubes, e.g. CVD, arc-discharge or laser ablation, by changing the gas atmosphere or the targets to include the desired dopant atoms [131]. Other methods include ion implantation [132] and substitution reactions [133].

The Raman spectrum of nitrogen doped single-walled carbon nanotubes (N-SWCNT) differs from the Raman spectrum of pure single-walled carbon nanotubes in a few different ways [134]. The radial breathing mode (RBM) intensity is lowered, the higher the concentration of nitrogen in the doped tubes. The defect band (D-band) intensity can increase with higher concentrations of nitrogen. For boron doped single-walled carbon nanotubes (B-SWCNT), an increase in the intensity of the D-band was observed, as well as a downshift of the 2D-band and variations in RBM and G-band intensity [135]. Since the defect band (D-band) intensity is correlated to the amount of defects in the structure, it is not surprising that doping leads to higher intensity compared to undoped single-walled carbon nanotubes.

In multi-walled doped carbon nanotubes, downshifts of the D-band for boron doped MWCNTs, upshifts for the D-band for nitrogen doped MWCNTs and downshifts of the G-band can be observed regardless of doping with boron or nitrogen [136].

The isotope effect discussed in section 1.3 can also be applied to calculate frequency shifts for heteronanotubes, following equation 1.13. For N-SWCNT with 1% nitrogen, the G-band at 1585 cm^{-1} would shift downwards by about 1.3 cm^{-1}. For B-SWCNT, with 1% boron, the G-band would shift upwards by 0.8 cm^{-1} as a result of the lower mass of boron compared to carbon.

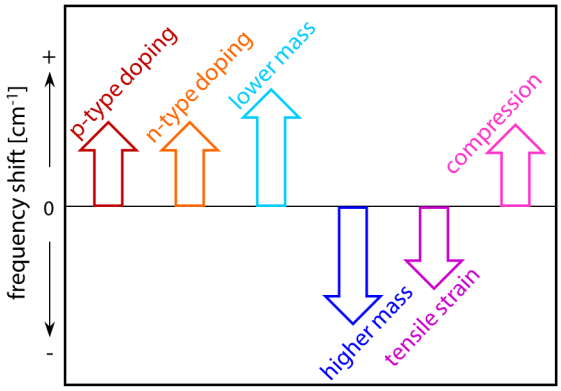

Figure 1.20: Different effects leading to frequency shifts in the Raman spectrum.

The different effects changing the Raman frequency occur simultaneously (fig. 1.20). The effect of electronic charge transfer can be more or less pronounced depending on the system. In the case of boron doping, both the mass and charge transfer effects shift into the same direction, since the lower mass leads to an upshift in frequency and the frequency also increases due to the change in the electronic structure. For nitrogen doping, the effects push the frequency in opposite directions, since from the mass, a downward shift can be observed, while the increase in electronic density will lead to an upshift. Additionally, tensile strain and elongation of carbon-carbon bonds can lead to downshifts [126]. Conversely, compression would lead to an upshift in the Raman frequency. This makes the evaluation of Raman shifts for doped single-walled carbon nanotubes rather complex. Even if no shifts are observed, it does not necessarily mean that there is no doping.

Endohedral filling of carbon nanotubes

Another possibility to modify carbon nanotubes is by filling them with metals, oxides, salts, gases or molecules, commonly denoted as X@SWCNT. The filling is commonly done in solution, with molten-state precursors or with sublimated molecules and is usually preceded by an oxidation step in order to open the end-caps of the nanotubes [50]. Such structures are promising candidates for a wide array of applications [137]. Especially the concept of carbon nanotubes as nanoreactors to synthesize and stabilize exotic phases or molecules is of great significance for this work.

Single-walled carbon nanotubes can be filled with fullerenes, creating so-called "peapods", as their structure somewhat resembles the legume (fig. 1.21a). This structure was first observed in 1998, where it was discovered that fullerenes can be trapped inside carbon nanotubes, both made using pulsed laser vaporization of graphite [138]. Especially C_{60} fullerenes, which have a diameter of 0.7 nm can be well accommodated inside carbon nanotubes with a diameter of 1.4 nm. This is due to the Van der Waals radius of carbon of 0.17 nm [139]. The spacing between the nanotube and any molecule or inner tube is ideally two times the Van der Waals radius from both sides, meaning a total difference of four times the Van der Waals radius (0.68 nm), between the diameter of the nanotube and the fullerene. A different synthesis pathway to peapods is the

filling of C_{60} into acid-purified nanotubes at 450°C [140]. Here, it is proposed that the fullerenes are first adsorbed on the outside of the nanotubes and diffuse along the carbon nanotube until a defect or an opening is found, where the fullerenes will get sucked into the nanotubes. Another method is the sublimation of fullerenes and filling into carbon nanotubes inside an evacuated glass ampoule at 650°C [141]. The vapor filling method was optimized by adding a nanotube oxidation step (10-30 minutes at 400-450°C) before the actual filling in order to open the end-caps of the carbon nanotubes [142].

The filling of the carbon nanotubes with fullerenes can be observed in TEM, however, this technique only provides very local information. The bulk yield can be determined with X-ray diffraction [143] or electron energy loss spectroscopy (EELS) [144]. ^{13}C nuclear magnetic resonance can also be used to count the fullerenes inside the nanotubes, if isotope enriched fullerenes are used [47]. It is also possible to determine the yield using Raman spectroscopy, from the C_{60} $A_g(2)$-mode (pentagonal pinch mode) at $\sim$ 1468 cm^{-1} [145]. Using a 488 nm laser for excitation, the ratio of the $A_g(2)$ mode to the G-mode of the nanotube is 4.6×10^{-3}, if the entire available volume (94%) is filled with fullerenes for nanotubes with a mean diameter of 1.4 nm. The available volume can be estimated from the diameter distribution of the single-walled carbon nanotubes, as only nanotubes with a diameter of more than 1.2 nm can be filled with fullerenes.

Under electron beam irradiation, the fullerenes coalesce into short, small diameter end-capped nanotubes inside of the surrounding carbon nanotubes [146]. As this method leads to a high amount of defects in both the outer and the inner tube, experiments with high temperature vacuum annealing at 1200°C were carried out, which produced longer double-walled carbon nanotubes with few defects [147]. A TEM image of double-walled carbon nanotubes grown from peapods by annealing is shown in figure 1.21c. It is also possible to combine heating and electron beam irradiation in order to tune the process of inner tube formation [148]. Another method for double-walled carbon nanotube synthesis from peapods is pulsed laser annealing [149]. A growth mechanism of the inner tubes proposed in ref. [150] (fig. 1.21b) is based on a (2+2) cycloaddition between two fullerenes followed by a series of bond rotations called generalized Stone-Wales transformations [151]. The resulting structure (C_{120}) can be imagined as a short nanotube end-capped with two fullerene hemispheres. The polymerization of C_{60} and C_{70} fullerenes into short nanotubes with an average diameter of roughly 0.7 nm inside the surrounding nanotube was experimentally observed using Raman spectroscopy [152]. In this study, the inner nanotubes were grown over several days at relatively low temperatures of 800°C in order to study the intermediates the polymerization process. The characteristic radial breathing mode (RBM) of the inner tube can be directly associated with a specific chirality of nanotube. A C_{120} nanotube would be an armchair (5,5) nanotube with pentagonal rings at the tips of the end-caps, energetically inhibiting further polymerization. However, if a (9,0) zigzag nanotube (C_{140}) is formed, hexagonal rings are at the tip of the end-caps, in which case further polymerization can continue like a chain reaction. Additionally, 6 carbon atoms are released from the structure that can migrate and assist in the polymerization. Freely-moving carbon atoms significantly lower the activation barrier of the polymerization and structural relaxation compared to pure Stone-Wales transformations.

The observation of very small diameter inner tubes grown from C_{70} peapods challenged the polymerization growth model [154]. It was also shown that double-walled carbon nanotubes

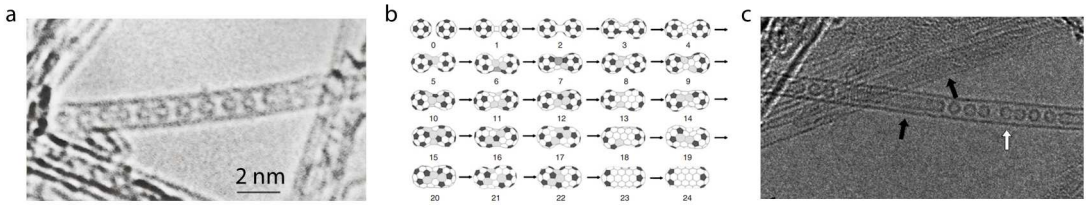

Figure 1.21: C_{60} filled carbon nanotubes ("peapods"): a) TEM image of peapods, adapted from [138]; b) Proposed mechanism of C_{60} dimerization, adapted from [150]; c) TEM image of double-walled carbon nanotubes made from peapods using annealing, black arrows indicate DWCNTs, white arrows peapods and intermediates, adpated from [153].

can be synthesized using organic solvents, e.g., toluene and benzene as a carbon source, inside a single-walled carbon nanotubes in addition to fullerenes, which act as stoppers to prevent the small organic molecules from evaporating before the growth of inner tubes [155]. Inner nanotubes can also grow in single-walled carbon nanotubes filled with ferrocene [156]. In these cases, a decay of the molecules into fragments inside the nanotube and subsequent formation of the inner tube is suggested as the mechanism of inner tube growth. However, experiments with ^{13}C enriched fullerenes showed little diffusion of carbon along the tube axis during inner tube formation [157], supporting the polymerization growth model for inner tubes from peapods.

Currently, there are no industrial scale uses for peapods, but some possible applications have been demonstrated on small scales. Peapods can be used in transistors, as they have better suited band gaps than unfilled single-walled carbon nanotubes. Using metallofullerene peapods such as $Gd@C_{82}$, a band gap of 0.1 eV can be achieved [158] and a working device could be manufactured [159]. Due to their ability to separate charges, peapods are also an interesting candidate for solar cells [160]. More generally, filled nanotubes can be used for drug delivery in medicine [161]. In combination with external nanotube functionalization, filled nanotubes are good vessels for transporting molecules to specific organs and even anti-cancer drugs directly to a targeted tumor [162]. Some more theoretically envisioned application of peapods are photonic crystals, peapods as "shuttle" memory, high frequency oscillators and quantum computing [122]. A very honorable mention goes to the "nanogun" [163]: simulations have shown that a positively charged tube could cause the fullerenes inside to be driven out of the tube with a speed of over 1 km/s. In case of negative charge applied to the tube, the fullerenes are driven to oscillation and electrically neutral molecules can be "inhaled" into an open end of the tube, which I will call a "nano vacuum cleaner".

Coaxial Van der Waals heterostructures

An interesting hybrid system containing single-walled carbon nanotubes are coaxial tubes. These systems are made from layers of Van der Waals structures, such as transition metal dichalcogenides (e.g. MoS_2), graphene and boron nitride, which are, conceptually speaking, rolled up into a coaxial cable of tubes. A combined boron nitride and carbon nanotube could be synthesized using chemical vapor deposition [164] (fig. 1.22). Using X-ray photoelectron spectroscopy (XPS), only boron-nitrogen and carbon-carbon bonds and no boron-carbon or nitrogen-carbon bonds were observed, confirming they are two separate tubes and there is no exchange of atoms between the two tubes. Downshifts in the Raman signal of the combined system could be observed compared to pure single-walled carbon nanotubes. Boron nitride coating was shown to protect single-walled carbon nanotubes against oxidation, raising the temperature of where the single-walled carbon nanotubes remain intact in air from 400°C to 700°C. The coaxial single-walled carbon nanotube and boron nitride nanotube cable was theoretically predicted to be a topological insulator [165].

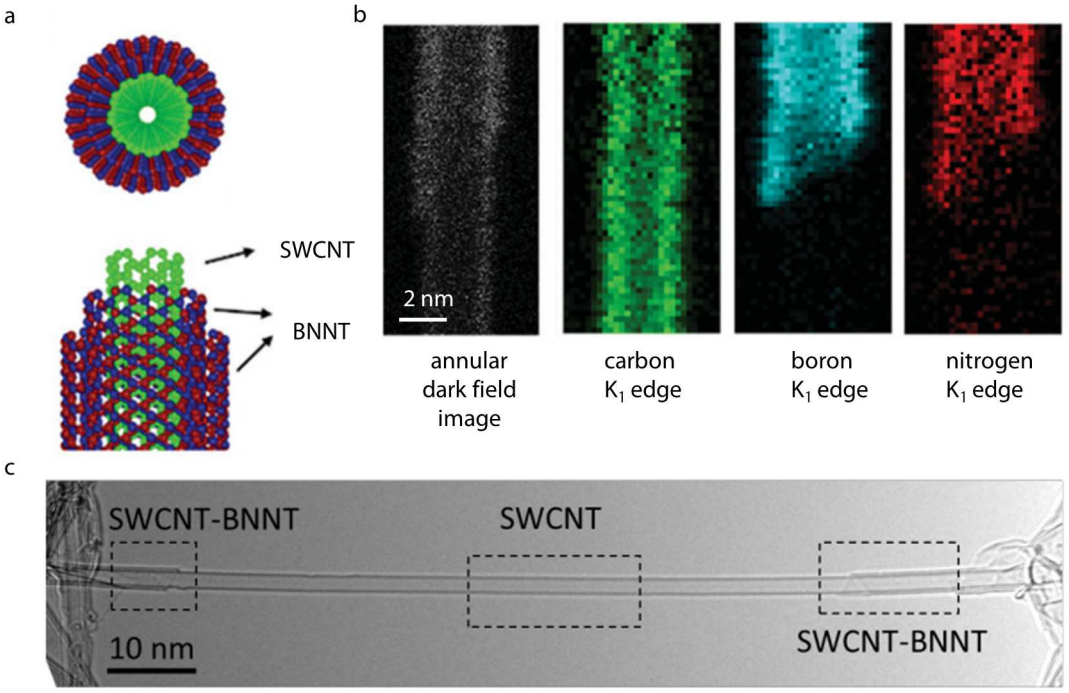

Figure 1.22: Coaxial Van der Waals heterostructures: a) schematic of a single-walled carbon nanotube (SWCNT) surrounded by boron nitride nanotubes (BNNT); b) annular dark field image and EELS mapping of a carbon nanotube partially surrounded by a boron nitride tube, c) TEM image of a single-walled carbon nanotube partially surround by a boron nitride nanotube adapted from [164].

1.5 Linear carbon chains and carbyne

1.5.1 Structure and properties of linear carbon

Linear carbon chains are the allotropic form of sp^1-hybridized carbon. The two hybrid orbitals (see fig. 1.2) form covalent bonds in opposite directions (180°), making the linear carbon chain a true one-dimensional material. Carbon atoms can form four covalent bonds, and in the case of the linear carbon chain, two bonding geometries are possible (fig. 1.23). The structure where the chain consists only of double bonds is called cumulene. This structure is not always energetically favorable, resulting in a breaking of the symmetry called Peierl's distortion into alternating single and triple bonds, leading to a doubling of the unit cell [53], [166]–[168]. In contrast to cumulene, where all bonds are the same length, this structure is called polyyne and it exhibits bond length alternation (BLA) as the triple bond is shorter than the single bond. The π-electrons in cumulene are uniformly distributed across the chain, whereas the π-electrons in the polyyne are localized at the triple bond [169] while the single bond is depleted. Cumulene is therefore metallic, polyyne a semiconductor (fig. 1.23).

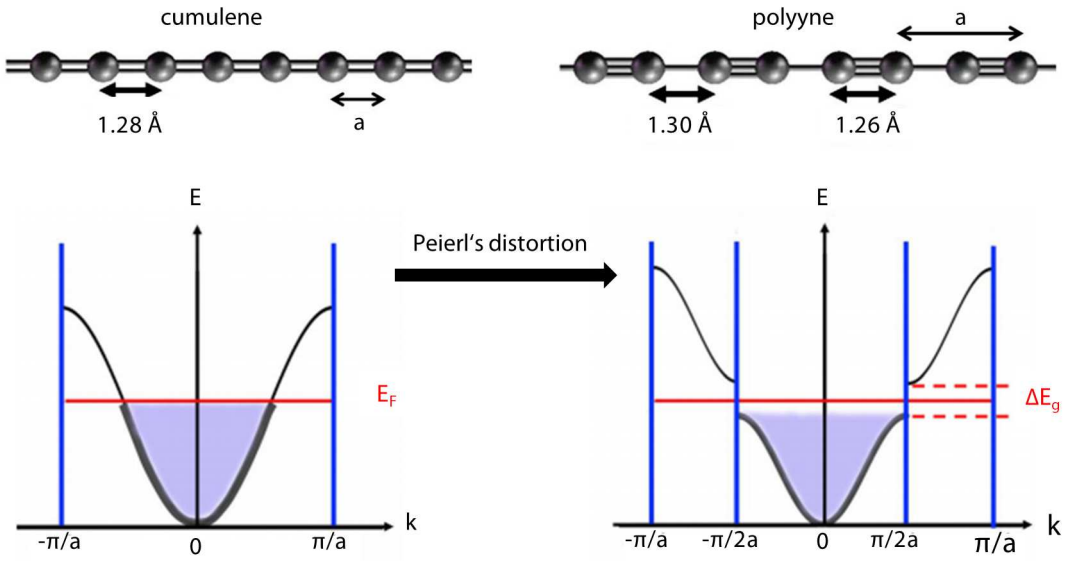

Figure 1.23: Different bonding configurations of linear carbon chains: cumulene (left) has only double bonds and is metallic, polyyne (right) has alternating single and triple bonds and is a semiconductor; adapted from [169].

The preferred configuration of the carbon chain is an interplay between several contributing factors, such as electronic energy, zero-point vibrations and strain. The opening of the band gap leads to a lowering of the electronic energy, stabilizing the polyyne. However, a reverse effect stabilizing the cumulene comes from zero point vibrations [170]. Mechanical strain to the chain induces the cumulene to polyyne transition [171]. Increasing the mechanical strain on the chain also leads to an increase in the bond length alternation due to stretching of the weaker single bond and a widening of the band gap [35]. At a critical strain, the band gap switches from a direct band gap to an indirect band gap [167]. An additional contribution to the bonding

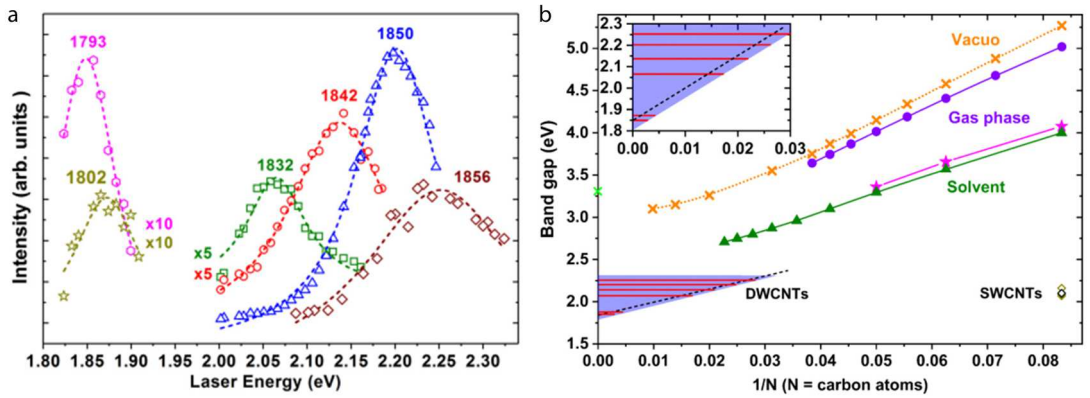

Figure 1.24: Band gaps of linear carbon chains as a function of chain length: a) Raman resonance excitation profiles for six different carbyne chains; b) the band gap decreases as the chain gets longer, different band gaps can be observed for chains in different matrices (gas phase, solution, confined inside carbon nanotubes); adapted from [175].

situation in the carbon chain is imposed by the terminating groups in finite chains [170]. In case of hydrogen terminated chains, sp^3 groups (e.g. -CH_3) increase the bond length alternation, while sp^2 groups (e.g. =CH_2) decrease the bond length alternation in comparison to an infinite unterminated chain. In addition to the influence of the end-capping groups, the chain length affects the bond length alternation, with longer chains leading to lower bond length alternation [172]. Through the bond length alternation, the chain length and band gap are correlated (fig. 1.24). The band gap is dependent on the matrix, showing differences for chains in the gas phase, in liquid phase and confined inside double-walled carbon nanotubes. The decrease of the band gap in finite hydrogen-capped linear carbon chains was observed in the gas phase [173] and in organic solvents [174] using UV-spectroscopy. The same trend of decreasing band gap with chain length was observed for polyynes with up to 44 carbon atoms end-capped by large organic molecules (tris(3,5-di-t-butylphenyl)methyl moiety), measured by UV-Vis spectra in hexane [20]. In this study, a convergence of the band gap to around 2.2 eV was estimated. The band gap values for the confined carbon chains were determined from resonance Raman spectroscopy [175]. In the case of confined carbyne, the band gap is not directly related to the chain length anymore, as the properties become length independent at a certain threshold (marked in blue in fig. 1.24). In this regime, the bond length alternation, and therefore band gap, are related to the geometry of the host nanotube [176]. The full resonance profiles of confined carbyne were recently measured by Martinati *et al.* [177].

Carbyne has extraordinary predicted mechanical properties. It was calculated that the tensile stiffness is $\sim 10^9$ N m/kg, which is around double the value of graphene and carbon nanotubes (4.5×10^8 N m/kg) and three times the value of diamond (3.5×10^8 N m/kg) [178]. Carbyne also outperforms any other known material in specific strength. The Young's modulus of carbyne was calculated to be 32.7 TPa [178], compared to graphene's 1 TPa [179]. In theoretical investigations in finite carbon chains, the mechanical properties are dependent on the chain length [180]. For example, longer chains have a higher elastic modulus and odd numbered chains have higher strength than even numbered chains up to a chain length of 12 carbon atoms. The strength of

carbon chains produced *in situ* in a field emission electron microscope (sec. 1.5.3) was measured at low temperatures, revealing a strength of 270 GPa at 5 K and 251 GPa at 77 K [181].

1.5.2 Raman spectroscopy of linear carbon

Raman spectroscopy is an important technique for studying linear carbon chains and carbyne because it has a very high Raman cross section of 10^{-22} cm^2 sr^{-1} per atom, which makes it the strongest Raman scatterer ever reported [182]. The strongest visible Raman mode of linear carbon chains is sometimes referred to in literature as the "$\mathcal{R}$" or "effective conjugation coordinate" (ECC) mode and is characteristic for π-conjugated systems. For an infinite polyynic carbon chain, the linear optical phonon at q = 0 is described as a stationary wave in which both carbon-carbon single and triple bonds simultaneously oscillate out-of-phase in the whole structure [183]. This mode usually appears in the range of 1800-2300 cm^{-1}.

A Raman spectrum of confined carbyne inside a carbon nanotube is shown in figure 1.25. The mode at around 1840 cm^{-1} is the characteristic LO-mode of the carbyne chain (CC-mode). The familiar modes of the carbon nanotube also appear, however, the G-mode and the 2D-mode have visible shoulders that arise from coupling of the modes of the carbyne chain with the inner and outer tubes of the double-walled carbon nanotube host. These modes were recently described by anharmonic phonon-phonon interactions between the carbyne chain and the nanotube hosts [184].

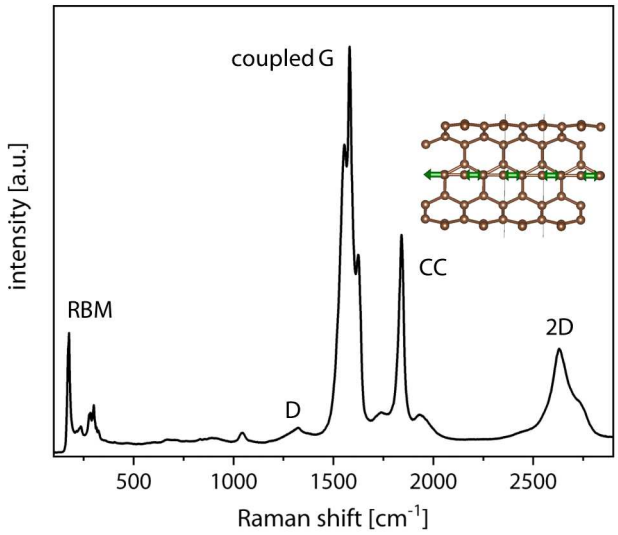

Figure 1.25: Raman spectrum of confined carbyne inside a double-walled carbon nanotube, measured with a 568 nm laser. Compared to the spectrum of a single-walled carbon nanotube (fig. 1.12), RBMs corresponding to the inner tubes appear, as well as a mode from the chain itself and coupled modes appear in the area of the G-mode of the carbon nanotube. The inset shows the vibration of a carbyne chain inside the host nanotube, made with VESTA [185].

As discussed above, the Raman frequency of the LO-mode of confined carbyne is dependent on the host inner tube geometry and diameter, leading to the appearance of the peak in the spectrum

at different frequencies (fig. 1.26) [176]. The inner tube diameter of the double-walled carbon nanotube hosts influences the frequency of the confined carbyne mode (CC-mode) a smaller diameter leads to a lower peak position in the Raman spectrum.

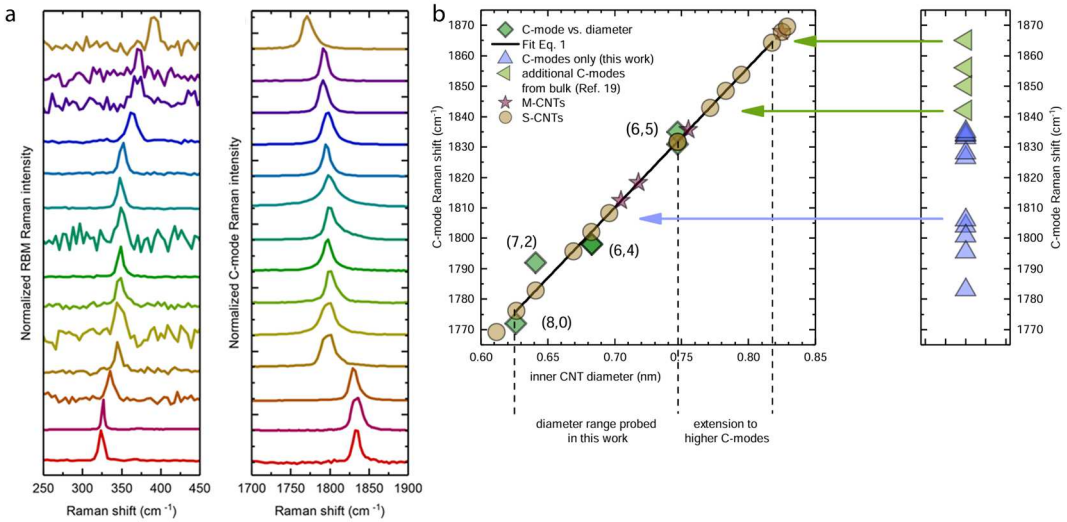

Figure 1.26: Dependence of the Raman mode of linear carbon chains on inner tube host diameter, adapted from [176]: a) pairs of tip-enhanced Raman spectra (TERS) for 14 carbyne chains and their surrounding inner nanotube hosts; b) frequency of the carbyne as a function of inner tube diameter.

When not considering infinite chains or carbyne, the frequency of the Raman modes of linear carbon chains (e.g. polyynes) is strongly dependent on the chain length as well as the bond length alternation [186], [187] (fig. 1.27). The Raman frequencies of hydrogen-capped short chain polymers have been measured in liquid, showing a shift from 2172 cm^{-1} for C_8H_2 downwards to 2031 cm^{-1} for $C_{16}H_2$ [188].

In experimental results, the matrix of the chain has to be considered, as for example shifts to lower frequencies can be observed for chains inside carbon nanotubes as opposed to chains in solution [189]. This also means that the band gap of the linear carbon chains is tunable by choosing the corresponding nanotubes as host tubes [190]. A linear relation can be observed between the Raman frequency and the band gap, which is related to the bond length alternation. The bond length alternation is dependent on chain length and, in the case of strong confinement inside small-diameter inner tubes, the geometry of the inner host tube. However, in the combined system of confined carbyne inside carbon nanotubes, the strong interaction with the host nanotubes governs the band gap and any effect of differing bond length alternations due to chain length is inconsequential, as carbyne, per definition, is a material where the properties are independent of chain length.

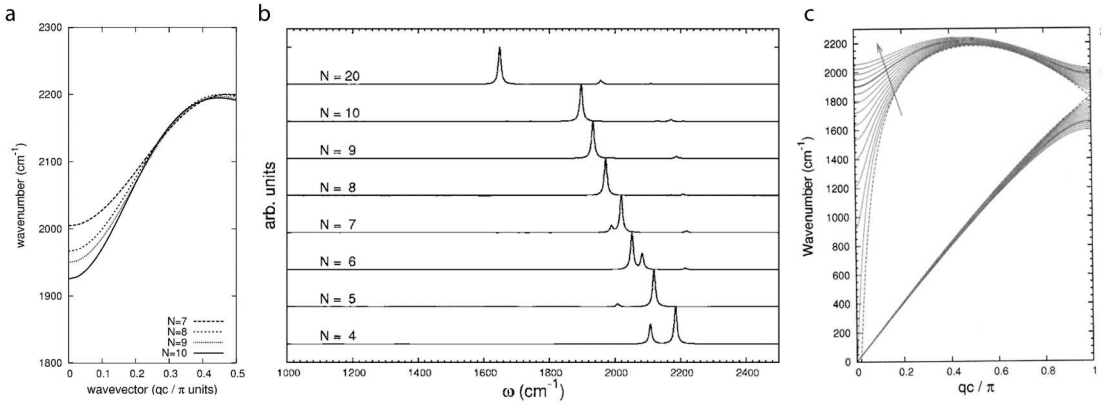

Figure 1.27: Dependence of the Raman mode of linear carbon chains on chain length and bond length alternation: a) calculated linear optical phonon dispersion (LO) for chains with different lengths, adapted from [191]; b) calculated Raman spectra for H-capped polyynes from 4-20 carbon-carbon triple bonds, adapted from [187]; c) dependence of the LO-mode on the bond length alternation (BLA), the arrow indicates increasing bond length alternation, the dashed line represents cumulene with a bond length alternation of zero, adapted from [186].

1.5.3 Synthesis of linear carbon

The field of organic synthesis has long since attempted the synthesis of linear carbon chains. The synthesis of short-chained cumulenes was pioneered in the 1930s, where it was discovered that the reduction of tetraphenyl-butyne-diol with e.g. hydroiodic acid leads to the removal of the alcohol groups and the creation of a chain of double bonds [192]. The cumulene series is denoted according to the number of double bonds in the chain. An [n]cumulene is structure with n carbon-carbon double bonds and n+1 atoms in the chain. Synthesis methods have been developed for the bottom-up synthesis of cumulenes with up to 10 carbon atoms ([9]cumulene) with end-capping groups [193]. Some pathways to [3]cumulenes include the dimerization of carbenes/carbenoids [194] (fig. 1.28a), elimination of trihaloalkanes [195] and reduction of acetylenic diols [196]. The formation of [4]cumulenes can be achieved, for example, *via* dibromo-1,4-pentadienes and base-induced elimination [197] or addition of dichlorocarbene to a [3]cumulene [198]. [5]Cumulenes can be synthesized similarly to the [3]cumulenes *via* dimerization of carbenes [199], addition of carbenes to [3]cumulenes [200], or oxidative homocoupling of acetylenic diols and subsequent reductive elimination [192]. Only one synthesis method has been reported for a [6]cumulene, which is based on an acetylenic cross-coupling reaction and ferrocene end groups [201]. The synthesis of [7]cumulenes is similar to the pathways for [3] and [5]cumulenes, from triyne dioles [196]. Due to their instability, these longer cumulenes are difficult to assemble and isolate, however, even [9]cumulenes have been synthesized from acetylenic diol derivates [193].

While the first "bottom-up" organic synthesis attempt of polyynes is credited to Adolf von Baeyer in 1885 [14], the basis for his work was the discovery of acetylenic coupling reactions by Carl Glaser in 1869 [204]. After renewed interest in polyynes in the 1950s, synthesis methods based mainly on polymerization of butindiols were developed [205]. The main methods

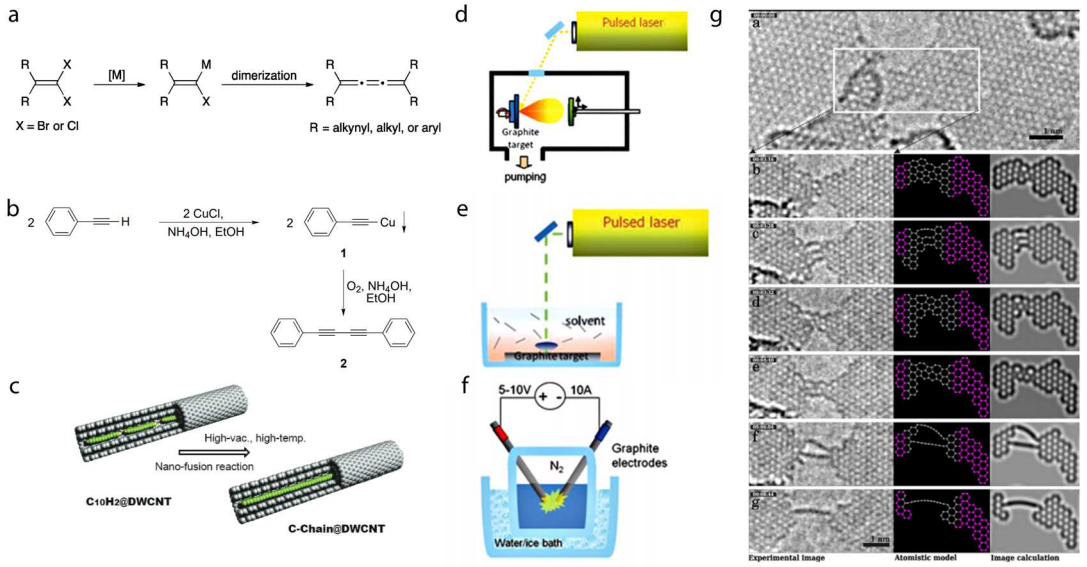

Figure 1.28: Synthesis methods for linear carbon chains: a) synthesis of [3]cumulenes based on the dimerization of carbenes/carbenoids, adapted from [193]; b) acetylenic coupling, adapted from [202]; c) fusion of short chain polyynes inside double-walled carbon nanotubes, adapted from [39]; d) laser ablation of graphite in vacuum, adapted from [203]; e) laser ablation of graphite in liquid solvents, adapted from [203]; f) arc-discharge in liquid, adapted from [203]; g) TEM irradiation of graphene, adapted from [34].

for the synthesis to date are based on acetylenic homo- or heterocoupling reactions [202] (fig. 1.28b) or elimination reactions to form the polyyne in the last step [206]. The boundaries of what chain lengths are considered possible to synthesize and stabilize/isolate have been pushed further and further. Through cross coupling reactions, chain extensions of up to 28 carbon atoms were achieved using Pt-containing large organic end-capping groups [207]. Many types of end groups have been used to stabilize the chains, mainly organic or organometallic moieties [19]. Using tris(3,5-di-t-butylphenyl)methyl as the end-capping group, chains consisting of 44 atoms were synthesized in 2010 [20]. Recently, with additional stabilization of the chain during synthesis using masking groups, which are then eliminated in the final step, and threading the chains through organic macrocycles, even longer chains with up to 68 carbon atoms have been synthesized [208]. Another interesting "bottom-up" method is the growth of carbon chains using Pt atoms on graphene [209]. In this study, it was observed in a TEM how free carbon atoms on a graphene sheet are trapped by Pt atoms, which serve as nucleation sites for the growth of carbon chains, terminated by Pt atoms on one or both ends. The chains were however only stable for a little over a minute. Another possible pathway to free standing chains is atomic manipulation of organometallic precursors inside an atomic force microscope [210]. With this method, a chain with 120 carbons could be manufactured and studied on a metallic surface using scanning probe microscopy.

Polyynes can be formed during laser ablation of graphite in a He carrier gas with chain lengths

of up to 22 carbon atoms [31] (fig. 1.28d). With this method, hydrogen, nitrogen or cyano end groups terminate the chains. Laser ablation can also be used to make polyyne chains up to 12 carbon atoms from C_{60} suspended in hexane or methanol [211]. Similarly, carbon chains with up to 16 carbon atoms can be formed using laser ablation of graphite particles in organic solvents [32] (fig. 1.28e). Arc-discharge has also been used to synthesize polyyne chains with up to 18 carbon atoms, by submerging electrodes in organic solvents [33], [212] (fig. 1.28f). Recently, the growth dynamics of polyynes made with pulsed laser ablation in liquid were studied *in situ* using a tunable synchrotron radiation Raman excitation source, where the size and solvent-dependent growth rates were evaluated [213].

Another approach for the synthesis of linear carbon chains are "top-down" methods. In a TEM, carbon atoms can be removed from a graphene sheet until only a chain remains between two areas of graphene [34], [214] (fig. 1.28g). Carbon chains can also be created *in situ* from graphene flakes mechanically by pulling them apart after electrical contacting to a gold tip inside a TEM and then measured using scanning tunnel microscopy (STM) [35]. Inside a field ion microscope, high voltage can be applied to a needle shaped sample with carbon fibers, unraveling chains of carbon from the tip [36].

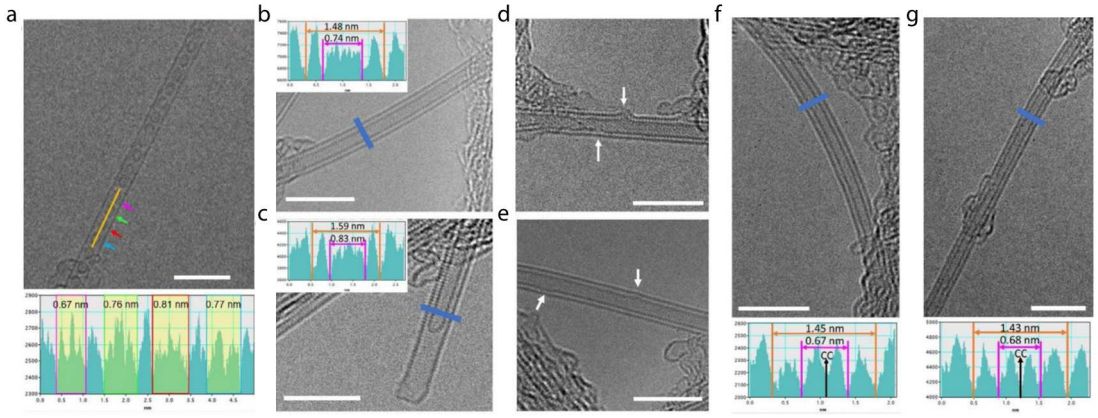

Figure 1.29: HRTEM images of the steps of the multi-step annealing process for confined carbyne synthesis from single-walled carbon nanotube peapods: a) C_{70} peapods; b) and c) double-walled carbon nanotubes made from the peapods; d) and e) defective double-walled carbon nanotubes after oxidation; f) and g) confined carbyne inside double-walled carbon nanotubes, adapted from [215].

The problem of the instability of longer linear carbon chain was overcome by synthesis methods where the chains are grown inside carbon nanotubes. Apart from stabilizing the structure sterically and through interaction with the surrounding tube, confinement inside carbon nanotubes also modifies the mechanical properties of carbyne, such as its compressive stiffness [216]. Such hybrid structures of carbon chains inside carbon nanotubes ("confined carbyne") can be formed as "side-products" during nanotube synthesis by arc-discharge [37], [217]. Inside multi-walled carbon nanotubes, linear carbon chains of more than 100 carbon atoms have been observed. It is also possible to fill short chain polyynes made e.g. from laser ablation in liquid into carbon nanotubes [38]. Using double-walled carbon nanotubes filled with short chain polyynes, annealing leads to the fusion of the polyynes into longer carbon chains [39], [218], [219] (fig. 1.28c). The longest

observed carbon chains inside double-walled carbon nanotubes (6000 atoms) were synthesized using high temperature high vacuum annealing of CVD-grown double-walled carbon nanotubes [40]. The CVD double-walled carbon nanotubes contain other carbon based molecules as well as amorphous carbon from the synthesis process which act as carbon sources for the growth of the carbyne chain. The diameter of the inner nanotube is crucial for the formation of carbon chains and the ideal diameter is around 0.7-0.8 nm. This synthesis can also be performed using laser annealing of double-walled carbon nanotubes in vacuum [220]. In order to optimize the yield, the carbon nanotube host tubes can be filled with molecules such as methanol [221] or fullerenes (peapods) [215], [222] in order to increase the amount of carbonaceous feedstock. The yield can be further increased by following a multi-step annealing process, where the fullerene filled single-walled carbon nanotubes are first annealed to form double-walled carbon nanotubes at 1300°C, then oxidized to create defects, and then annealed at 1500°C [215] (fig. 1.29). Recently, low temperature annealing at only 400°C has been used to synthesize weakly confined carbyne from ammonium deoxycholate as a carbonaceous precursor inside single-walled carbon nanotubes [223]. This system could pave the way for studying the properties of carbyne more independently from the surrounding host tubes.

1.6 Optical absorption

This chapter largely follows reference [43].

Optical absorption spectroscopy (OAS) is based on the different transmitted intensities of wavelengths after interacting with a sample. Photons corresponding to discrete allowed energy transitions are absorbed and electrons in the material are excited from a lower molecular orbital or the valence band to a higher orbital or the conduction band (fig. 1.30a). The transitions must be in resonance according to equation 1.18, where E_i and E_f correspond to the energies of the initial and final states and $h\nu$ describes the photon energy.

$$\left|E_f - E_i\right| = h\nu \tag{1.18}$$

The electrons leave behind a positively charged hole in the band structure. The bound state of the electron and hole is referred to as an exciton. For carbon nanotubes, the optical response arises from the excitonic states beyond the electronic band structure [224]–[226] and the strong interaction of electron and hole needs to be considered to accurately describe the observed spectra [227]. Excitonic effects are typically very small in bulk systems due to screening of the separated charges, but for low-dimensional nanostructures, electron-hole correlations are more prominent.

For an interaction between a molecule (solid) and electromagnetic radiation to occur, the molecule most have a dipole or temporary dipole with which the electromagnetic field can interact. The probability p of a transition is described by equation 1.19. The wavefunctions of the initial and final states Ψ_i and Ψ_f are connected *via* the dipole operator $\hat{\vec{\mu}}$, integrated over all coordinates.

$$p_{f\leftarrow i} = \int \Psi_f^* \, \hat{\vec{\mu}} \, \Psi_i \, d^3r \tag{1.19}$$

In order for a transition to be allowed, the integral must be non-zero. In other words, the product of the three functions in the integral must have even parity (behavior against inversion). The dipole operator itself has odd parity, s- and d-orbitals have even parity and p-orbitals have odd parity. When multiplying, even, odd and even (e.g. s, $\hat{\vec{\mu}}$ and s) give an odd product, which means a transition from s- to s-orbitals is forbidden. In the case of s, $\hat{\vec{\mu}}$ and p, the product is even, meaning that transitions from s- to p-orbitals are allowed. Transitions from s- to d-orbitals are forbidden.

Using photons, only direct transitions can be achieved due to momentum conservation, as photons cannot transfer momentum. In summary, transitions must be in resonance (eq. 1.18), the dipole selections rules must be followed and the total momentum must be conserved.

The transmitted intensity I from a simple viewpoint of absorption of incident light with intensity I_0 in a medium is described by an exponential decay (Lambert-Beer law, eq. 1.20), where ϵ_λ is the specific extinction coefficient of the material at a specific wavelength λ, c is the concentration of the absorbing molecule and d is the length of the path of the light in the medium (fig. 1.30b).

$$I = I_0 \, e^{\epsilon_\lambda \, c \, d} \tag{1.20}$$

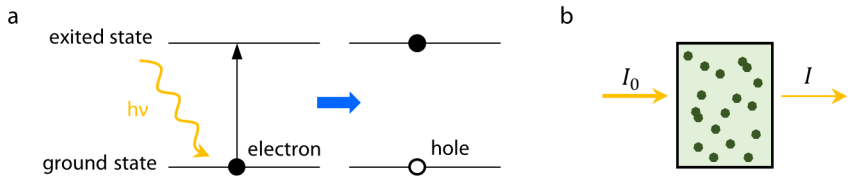

Figure 1.30: Principles of optical absorption: the absorption of a photon, excitation of an electron to a higher energy level and creation of a hole; b) intensity of incident and outgoing light in an absorption experiment (Lambert-Beer law).

In a dispersive geometry, the absorption spectrum is calculated from the sample spectrum and a "blank" reference spectrum. A typical set-up for optical absorption includes a light source, a monochromator, a beam splitter to create the two beam paths for the reference and the sample and detectors. The reference should be an identical cuvette containing the solvent or matrix the sample is dissolved or dispersed in in order to eliminate matrix effects from the resulting spectrum. Certain wavelengths of the incident light (usually in the range between IR and UV) will be absorbed due to the quantized electronic transitions in the sample.

Fourier-transform (FT) spectrometers are also often used for optical absorption measurements. In this case, an interferometer is set before the sample. The reference spectra are recorded sequentially. A schematic of the optical beam path of an FT-spectrometer is shown in section 2.4.

Optical absorption is a useful technique to study the properities of carbon nanotubes, as the electronic transitions of carbon nanotubes fall into this energy range. A systematic study of the diameter dependent electronic transitions in carbon nanotubes was performed by Kataura in 1999 [62] (fig. 1.10). The optical absorption spectra can be used to estimate the mean diameter of a sample of carbon nanotubes (eq. 1.21), where E_{11}^{S} is the transition energy in eV, a_0 is the carbon-carbon bond length in graphene (0.142 nm), γ_0 is the tight binding nearest neighbor overlap integral ($\sim$ 3 eV) and d is the diameter of the nanotubes in nm [228]. Newer studies provdide empirical formulas to determine the diameter dependent transition energies [229], which are applicable for chirality-sorted metallic and semi-conducting nanotubes in the range between 1 and 2 nm. When considering the different peaks for metallic and semiconducting nanotubes, the quality of metallicity sorting can be reviewed [230].

$$E_{11}^{\mathrm{S}} = \frac{2a_0\gamma_0}{d} \tag{1.21}$$

2

Experimental methods

2.1 Preparation of metallicity-sorted arc-discharge carbon nanotubes

The metallicity sorting of the arc-discharge carbon nanotubes was performed in the laboratory of Prof. Kazuhiro Yanagi at the Tokyo Metropolitan University in Japan. The following protocol was followed to prepare arc-discharge nanotubes from MEIJO Nano carbon:

- … Add ca. 80 mL methanol to the carbon nanotubes
- … Sonicate for 30 minutes in the bath sonicator
- … Filter the sample using a 0.2 µm PTFE membrane and wash with methanol 3 times
- … Add methanol and sonicate for 15 minutes, filter the sample
- … Add ca. 80 mL toluene
- … Sonicate for 30 minutes
- … Add toluene, sonicate for 20 minutes, filter the sample 2 times
- … Add methanol, sonicate for 20 minutes, filter the sample
- … Wash with 100°C ultrapure water 3 times
- … Add methanol, sonicate 20 minutes, filter the sample
- … Wash with 100°C ultrapure water 5 times
- … Disperse the sample in 2% sodium deoxycholate (DOC) solution (FUJIFILM Wako Pure Chemical Corporation)

... Homogenize for 3 hours using a tip sonicator

... Centrifuge the homogenized solution at 3600 rpm for 2 hours

For the density gradient centrifugation (DGU), 6 solutions with different concentrations of iodixanol (Optiprep, COSMO BIO) (40%, 35%, 32.5%, 30%, 27.5% and 5%) were prepared. First, for each solution, 1.2 g of sodium dodecyl sulfate (SDS, Sigma Aldrich) were dissolved in ultrapure water and sonicated for 10 minutes. Then, the appropriate amount of iodixanol was added and the mixture was sonicated for 10 more minutes. Using a peristaltic pump, the density gradient solutions were then layered into a plastic tube from highest (40%) to lowest (27.5%) concentration of iodixanol. The homogenized carbon nanotube solution is layered on top. The solutions were then centrifuged at 50000 rpm for 9 hours. After the centrifugation, the separated nanotube solution was pumped into small vials using a peristaltic pump. The separated fractions were then measured to determine the quality of separation using UV/Vis spectroscopy. Measured optical spectra are shown in figure 2.1 for the semiconducting and metallic fractions of the separated carbon nanotubes. For the highest purity (dark blue and dark red spectra), there is no visible peak in the region of the M_{11} or S_{22} peaks, respectively, for the lower purities (light blue and light red spectra), small peaks in those areas can be seen.

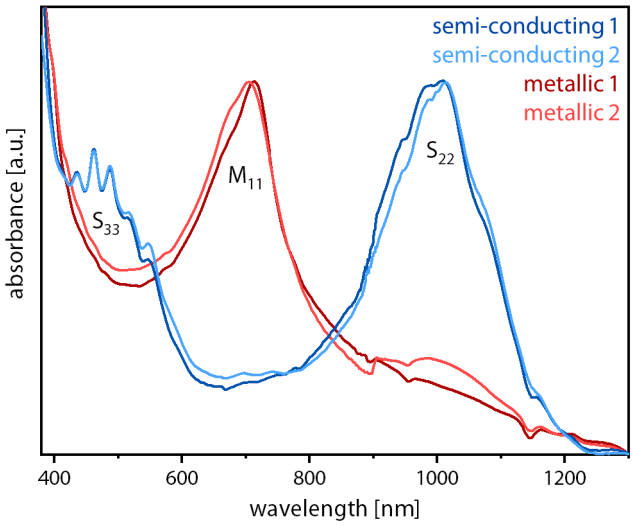

Figure 2.1: Optical spectra of the metallicity-sorted 1.4 nm arc-discharge carbon nanotubes: red spectra are metallic nanotubes, metallic 1 is the highest purity, metallic 2 a lower purity, blue spectra are semi-conducting nanotubes, semi-conducting 1 is the highest purity, semi-conducting 2 a lower purity.

From the highest purity fraction of semiconducting nanotubes, a bucky paper was prepared, which was then used to synthesize confined carbyne. In order to prepare the bucky paper, the nanotube solution from the centrifugation was treated as follows in order to bundle the nanotubes and remove the surfactants and the iodixanol:

... Add equal volume of methanol to the nanotube solution

... Filter the sample using a 0.2 µm PTFE membrane and wash with methanol 3 times

... Wash with 100°C ultrapure water

... Add methanol and sonicate for 10 minutes, filter the sample, wash with methanol and 100 °C ultrapure water 3 times

... Add toluene, sonicate 20 minutes, filter the sample

... Add methanol, sonicate 10 minutes, filter the sample

... Let the nanotubes dry on the filter and peel off the bucky paper

2.2 Synthesis process for confined carbyne

Many different processes were tested during this thesis for confined carbyne. The specific details will be discussed in the respective chapters in the results. Generally, the steps involve filling the host tubes with fullerenes and multiple steps of annealing at high temperature and in high vacuum and with oxidation steps in-between under the following conditions:

... Oxidize nanotubes at 450°C in air for 30 minutes (opening end-caps)

... Put the nanotubes and the fullerenes inside a glass ampoule and evacuate to ultra-high vacuum

... Seal the glass ampoule under vacuum

... Heat the ampoule inside a furnace for 12 hours at 550°C (filling the nanotubes)

... Anneal the nanotubes under high vacuum at 1500-1600°C for 1 hour (direct growth of confined carbyne OR anneal the nanotubes under high vacuum at 1300°C for 2 hours (growth of double-walled carbon nanotubes)

... Oxidize the nanotubes at 600 mbar at 500°C for 2 hours (opens end-caps of inner tubes and introduces defects)

... Anneal the nanotubes under high vacuum at 1500-1600°C for 1 hour

The opening of the end-caps is necessary in order to allow the fullerenes, or other molecules, to be filled into the nanotubes. The molecules inside the carbon nanotube hosts act as carbonaceous feedstock for the growth of carbyne chains. High temperature high vacuum annealing leads to the growth of inner walls and carbyne chains. In the oxidation step, a temperature is chosen where single-walled carbon nanotubes are less stable than double-walled carbon nanotubes, which leads to preferential etching of the parts of the nanotube hosts where no inner tubes were grown [231]. Since the maximum fraction of carbon nanotubes that can be filled with inner walls is around two thirds, governed by the fullerenes from which they are grown, some parts of the sample are still only single-walled carbon nanotubes. During the subsequent annealing step, more inner tubes grow, leading to a higher fraction of double-walled nanotubes, as the free carbon from the destruction of some of the single-walled parts can be used to form more inner

walls and carbyne. While this may lead to a fracturing of long nanotubes into shorter segments, it ultimately increases the fraction of nanotube hosts with inner walls where carbyne can grow. The oxidation step also ensures opening of end-caps of the double-walled inner nanotubes and partial destruction of the double-walled carbon nanotubes and introduces defects which help the growth of confined carbyne [222].

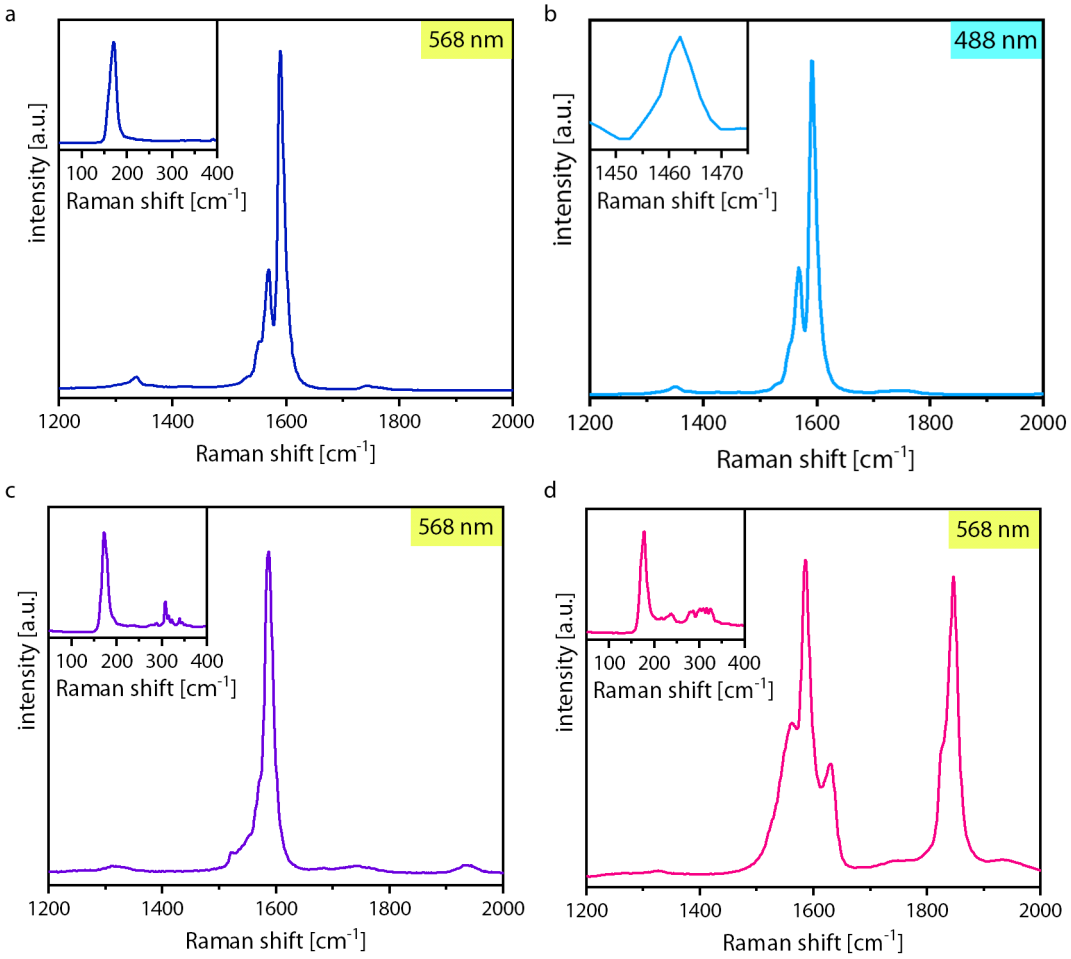

Figure 2.2: Example: Raman spectra of precursors, intermediates and end products of confined carbyne synthesis: a) single-walled carbon nanotubes, the inset shows the RBM area, measured with a 568 nm laser; b) C_{60} peapods, the inset shows the characteristic peapods peak, measured with a 488 nm laser; c) double-walled carbon nanotubes (568 nm laser); d) confined carbyne (568 nm laser).

In Figure 2.2, Raman spectra of the starting material, intermediates and the end product, confined carbyne, are shown. For the single-walled carbon nanotubes, which is the starting material of the synthesis, two main peaks of the G-mode (G^+ and G^-) and one main feature in the RBM region are present, which indicates a narrow diameter distribution, as the RBM frequency is diameter dependent. Using equation 1.17, the diameter is estimated to be 1.45 nm. For the peapods, no significant changes in the characteristic modes of the carbon nanotubes are observed, however, using the 488 nm laser, a peak at around 1460 cm^{-1} can be observed, which is attributed to the

C_{60} pentagonal pinch mode [145]. After the double-walled carbon nanotube growth, the shape of the G-mode changes as the inner tubes also each have a main G^+ and G^- component, which are only slightly shifted compared to the modes of the outer tubes. In the RBM region, peaks at 300 to 350 cm^{-1} can be observed, which correspond to the RBM of the smaller diameter inner nanotubes. The RBM frequencies of the smaller inner tubes are not as uniform as the outer tube modes due to the 1/d scaling of the RBMs. For the confined carbyne, the G-mode has shoulders on the left and right, which arise from vibronic coupling between the carbyne chain and the surrounding nanotube host. The characteristic mode of the carbyne chain appears at 1850 cm^{-1}.

2.3 Raman spectrometer

The Raman spectra shown in this thesis were measured with a Horiba LabRAM HR Raman microscopy set-up with 800 mm focal length. The multi-frequency Ar^+/Kr^+ laser (Coherent Innova 70C) provides laser wavelengths of 458, 488, 514, 532, 568, and 647 nm. Additionally, a He-Ne laser with 633 nm is coupled into the set-up. The spectra are recorded using a liquid nitrogen cooled CCD detector. Two gratings are available in the set-up, with 600 Gr/mm and 1800 Gr/mm. A neon lamp was used to calibrate spectra. All measurements were performed using a 50x objective with a laser spot of 500 - 1000 nm in size, with a 1000 µm pinhole and a 100 µm slit. The laser power was kept below 0.5 mW to avoid thermal effects or damage to the samples.

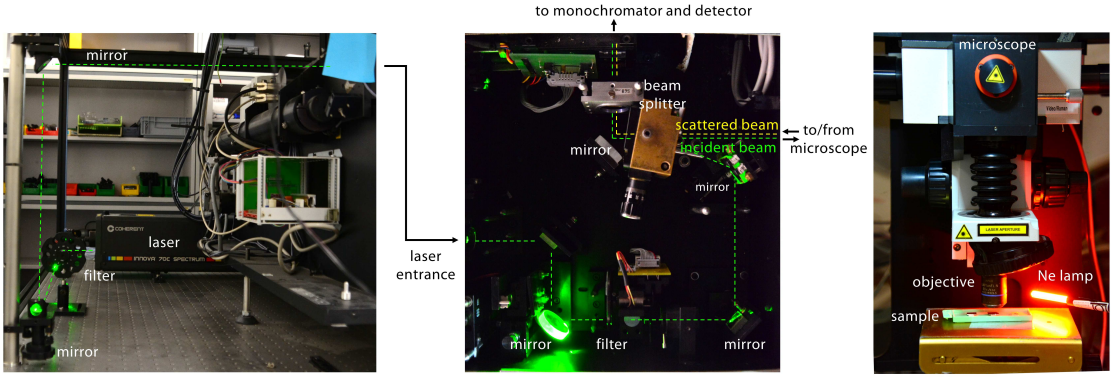

Figure 2.3: Horiba LabRAM Raman microscopy set-up.

2.4 Optical absorption spectrometer

The optical absorption measurements were made with a Bruker vertex 80v FT-IR spectrometer. This spectrometer has evacuable optics and covers a spectral range from UV to THz with a resultion of below 0.06 cm^{-1}.

The measurements were performed in reflectance on thin films on BaF_2 wedges. The samples were prepared by sonication in acetone and then airbrushed onto the wedges.

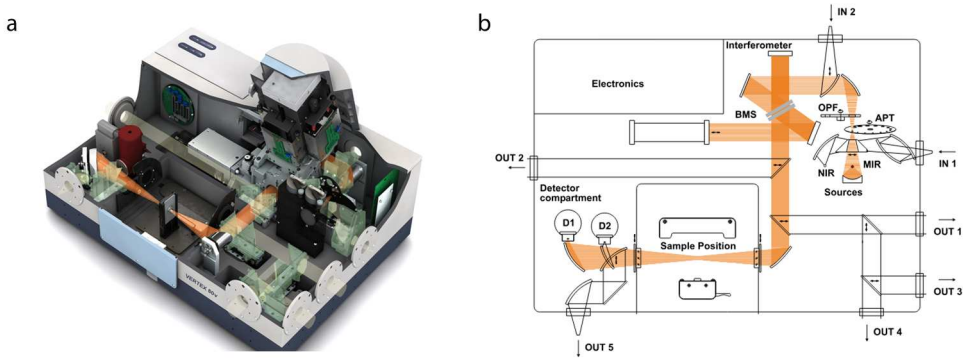

Figure 2.4: Bruker 80v FT-IR spectrometer: a) spectrometer components; b) optical beam path, adapted from [232].

2.5 Ceramic furnace for high temperature annealing

A ceramic tube (Al_2O_3) was used for high temperature high vacuum annealing. The ceramic tube is attached to an ultra-high vacuum chamber and the pressure in the tube can reach the 10^{-8} mbar range. The ceramic tube can be heated by a Carbolite furnace to 1600°C. A picture of the ceramic furnace set-up is shown in figure 2.5.

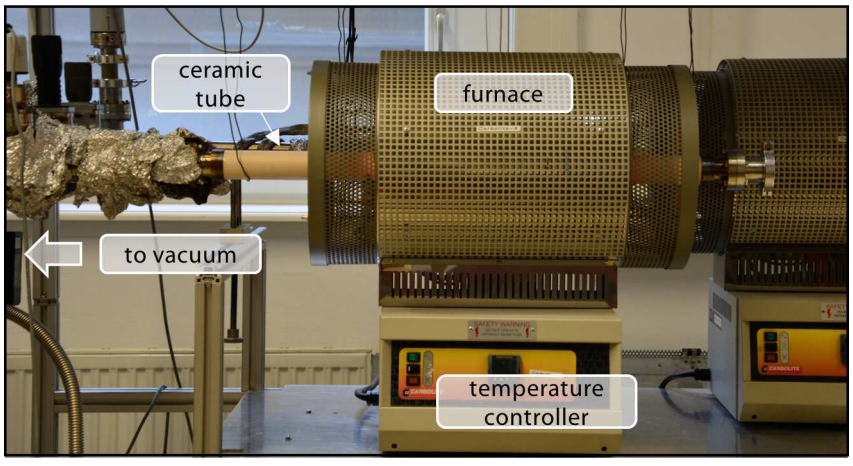

Figure 2.5: Ceramic furnace for high temperature high vacuum annealing.

2.6 Furnace for chemical vapor deposition

For the chemical vapor deposition experiments with boron nitride, the glass furnace in figure 2.6 was used. In this set-up, there are multiple home-made furnaces that can be heated separately in order to have different temperature zones during the synthesis. There is a vacuum pump (scroll pump) on one side, which can achieve a vacuum of 10^{-3} mbar. On the other side, a valve to the ultra-high vacuum chamber can be opened. The gas is introduced opposite to the scroll vacuum pump to achieve a flow, which can be regulated and monitored using a pressure gauge and leak valve.

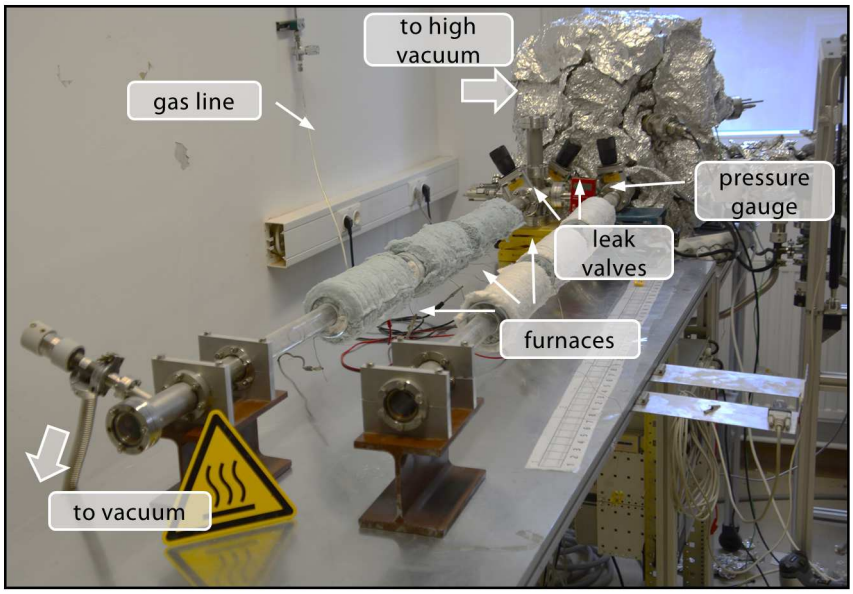

Figure 2.6: Experimental set-up for chemical vapor deposition.

3

Results: A novel method for bulk yield determination

3.1 Summary: Determining the bulk yield of confined carbyne

A novel method for determining the bulk yield of confined carbyne inside carbon nanotube hosts was developed. The model is based on a computational study (E. Parth et al., Nature Communications [184]) which relies partially on experimental data by me and my colleagues Dr. Weili Cui and Christin Schuster. The new yield determination model is published in Carbon (C. Schuster et al. [233]). For this work, the experimental data was obtained by me, Christin Schuster, Dr. Weili Cui and Prof. Lei Shi, the data evaluation and writing the manuscript was performed by Christin Schuster and I. The nanotube host tubes were provided by Dr. Takeshi Saito (eDIPS) and Prof. Kazuhiro Yanagi (arc-discharge). Below, the yield determination model is summarized.

The main work of this thesis focuses on the synthesis of confined carbyne inside carbon nanotubes. For the process of optimizing the bulk yield of confined carbyne, first, a reliable method of determining the yield had to be be found. The state of the art was to consider the intensity of the longitudinal optical (LO) mode of the carbyne chain at around 1850 cm^{-1} in the Raman spectrum to determine the yield [215]. However, this is not a reliable indicator for bulk carbyne yield for multiple reasons. Firstly, due to its extremely high scattering cross section, the signal is highly enhanced [182]. Additionally, the resonance profile of carbon chains is not constant and the chain has a narrow resonance window [175], [177]. In comparison, the resonance response of the G-band of the host nanotube is relatively constant across the visible light spectrum [184]. Apart from the appearance of the carbyne LO-mode (CC-mode) in the Raman spectrum, other changes to the spectrum of the confined carbyne/nanotube host system (CC@CNT) can be observed, specifically shoulders in the G-line and the 2D-band of the nanotubes. The shoulders

were recently explained by anharmonic phonon-phonon interactions between the carbyne chain and the nanotube host [184]. These modes of the nanotube hosts are vibrationally coupled with, but electronically decoupled from the carbyne chain, which means they follow the stable resonance behavior of the nanotube hosts. In other words, the resonance behavior, which is due to the electronic structure of the individual sub-systems (carbon nanotube and confined carbyne), is independent. In contrast, the phononic structure shows interaction features, which were explained by correlation effects from phonon-phonon interactions. This means that the area, i.e., integrated intensity, of these coupled modes could be a good indicator for determining the bulk yield of confined carbyne as they follow the more stable resonance behavior of the host tubes rather than the irregular resonance behavior of the carbyne chain. In figure 3.1, the coupled G-band and the CC-mode of a CC@CNT sample is shown for different laser energies. The left and right shoulders are denoted as G_S^- and G_S^+. The line-shape analysis was performed by fitting 6 peaks to the double-walled carbon nanotube host and an additional 2 peaks for each of the shoulders. The fit model for the double-walled carbon nanotube hosts was previously fitted from a Raman spectrum of the unfilled host tubes. The two peaks for the shoulders are correlated and have a fixed distance, corresponding to the distance between the two main features of the carbyne mode. In order to obtain the relative G-line area using the fit model, the fraction that the shoulder peak areas (A_S) make up of the total area (A_T) is evaluated (eq. 3.1).

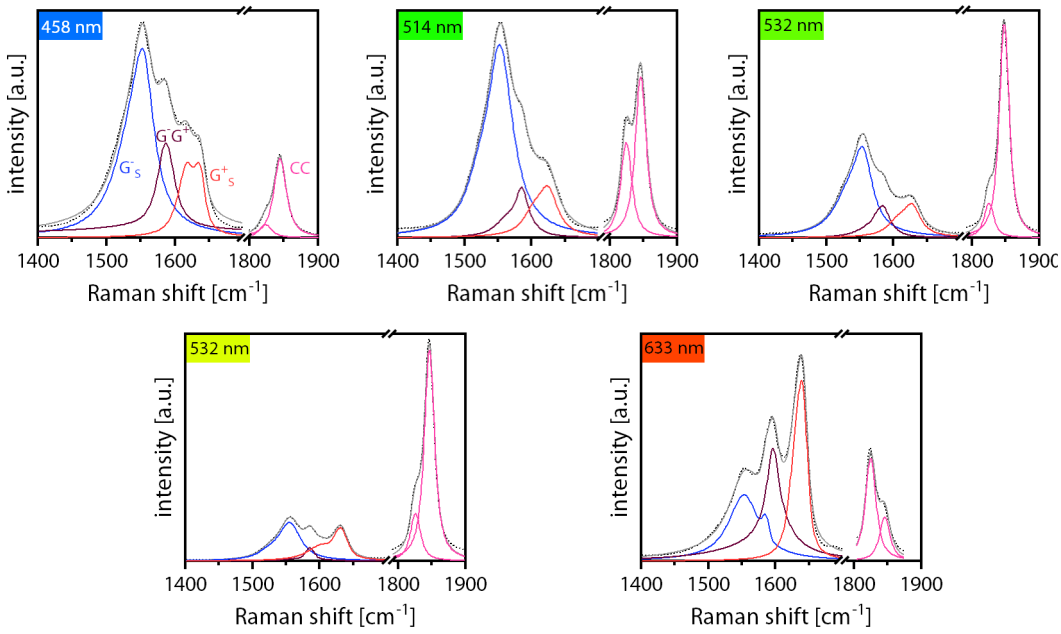

Figure 3.1: Resonance behavior and line-shape analysis of the coupled G-mode and CC-mode of CC@CNT measured at different wavelengths across the visible light spectrum.

$$\text{relative G-line area (fit model)} = \frac{A_S}{A_T} \tag{3.1}$$

The resonance behavior of the carbyne chain can be seen in figure 3.3. While the left and right shoulders vary strongly over the studied spectral range, the sum of both shoulders is reasonably

constant. In order to test if it is possible to simplify the analysis without significantly reducing the accuracy of the bulk yield determination, we compared the combined $G_S^+ + G_S^-$ area obtained by the coupled G-mode fit with a simple area comparison of filled and unfilled tubes. For this analysis, the Raman spectrum of the double-walled carbon nanotube host without carbyne is also needed. The integrated area of the G-band of the unfilled DWCNT spectrum (A_U) is subtracted from the area of the CC@DWCNT spectrum (A_F) and then divided by the area of the filled sample (A_F) to obtain the relative G-band area arising from the interaction of the tube with confined carbyne (eq. 3.2 and fig. 3.2).

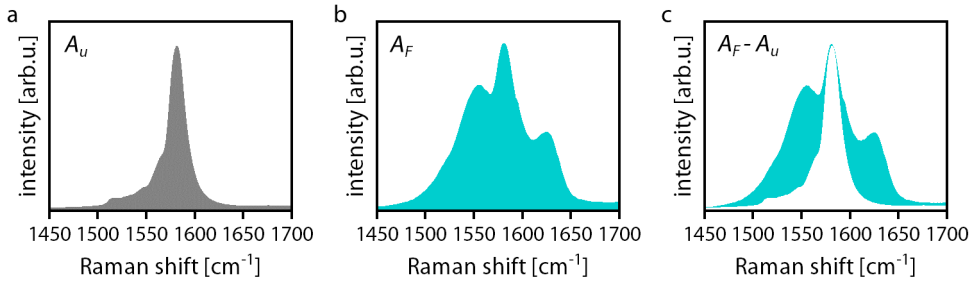

Figure 3.2: Area integration model for the determination of the bulk yield of confined carbyne: a) Raman spectrum of the unfilled double-walled carbon nanotube host; b) Raman spectrum of the double-walled carbon nanotube hosts filled with confined carbyne; c) the area of the unfilled subtracted from the spectrum of the filled nanotube hosts.

$$\text{relative G-line area (area integration model)} = \frac{A_F - A_U}{A_F} \tag{3.2}$$

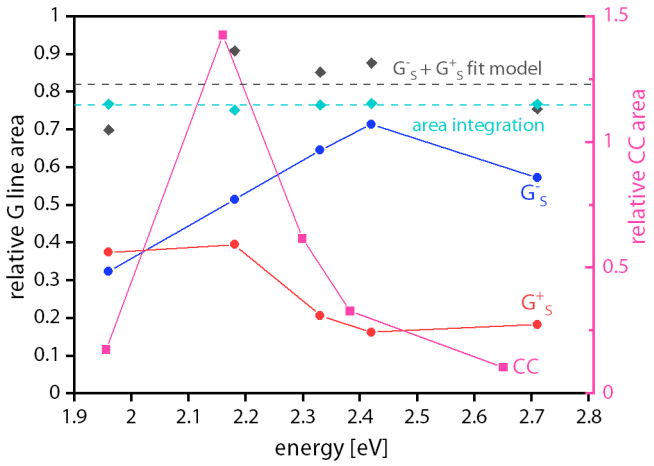

Figure 3.3: Bulk yield determination models: fit model *versus* area integration model.

In figure 3.3, the relative G-line area and CC-mode area relative to the G-band area are shown. The simplified area integration model provides an even more stable relative G-line area of around 0.75, which is within the error range of the fit model (0.82 ± 0.08). The lower stability of the fit model arises from the overestimation or underestimation of the G-line of the carbon nanotube due

to the peak fronts and peak tails of the shoulders, especially in the case of large shoulders. The area integration model also works better for samples where line-shape analysis is more difficult due to lower yields or complex line-shapes, e.g. due to the presence of metallic tubes, which have broad Fano peaks [234], [235]. The stability of the area integration over the entire measured energy range also indicates that the bulk yield can be determined using any laser from the Raman spectra of a sample and its reference. In all following chapters, the area integration model was applied for the determination of the bulk yield.

For comparing different samples of confined carbyne, the relative G-line area can be used as an indicator for which sample has a higher bulk yield of confined carbyne. However, determining absolute values of bulk yield is more complicated as there is, to my knowledge, no other method of bulk yield determination to provide a calibration point. Nevertheless, a reasonable calibration was attempted using a sample with exceptionally high bulk yield under the assumption that the sample is filled to is maximum (fig. 3.4a).

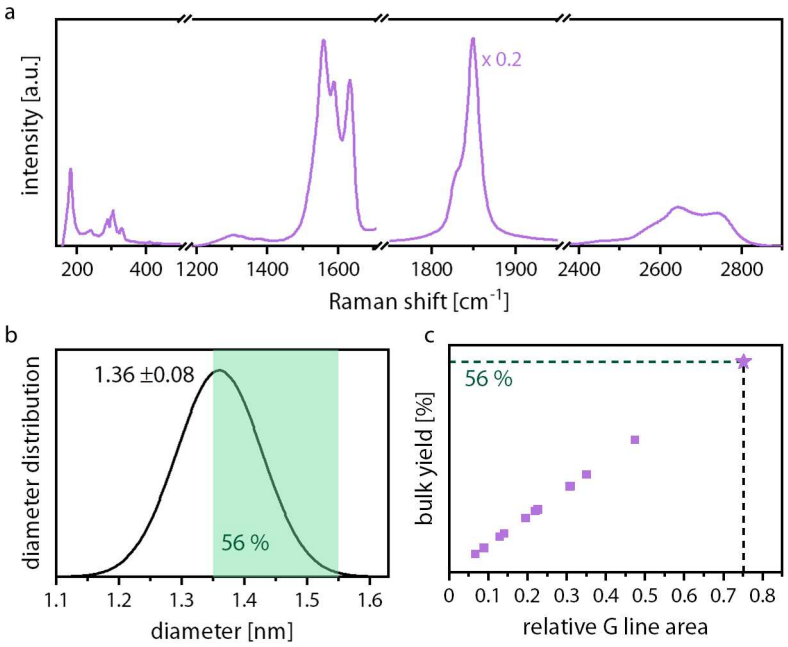

Figure 3.4: Calibration of the bulk yield of confined carbyne: a) Raman spectrum of confined carbyne used as a calibration for the bulk yield determination model; b) diameter distribution of the host nanotubes modeled by a Gaussian curve, the green area marks the diameter window where carbyne is expected to grow; c) calibration of the relative area under the assumption that this sample is filled to its maximum (lilac star) and calculated bulk yield values for other samples with the same nanotube hosts obtained from sonication experiments of the same sample.

Some considerations regarding the diameter of the host nanotubes need to be made in order to determine the calibration point, as not all nanotubes are suitable for the growth of inner walls and carbyne. While the diameter of the inner tubes suitable for carbyne growth is not definitively known, one can rely on experimental observations, where confined carbyne was observed in nanotubes in a diameter range of 0.63 to 0.83 nm [176]. It is also empirically known that the

optimal spacing between inner and outer walls of carbon nanotubes is 0.36 nm [236]. Even though the Van der Waals radius of carbon is 0.17 nm, the slightly higher value of 0.18 nm for the spacing of nanotubes is expected due to curvature. This means that the difference of the diameter between inner and outer tubes is 0.72 nm and carbyne growth should mainly take place in carbon nanotube hosts with an outer tube diameter between 1.35 and 1.55 nm. If the diameter distribution of the carbon nanotube hosts is known, the percentage of host tubes suitable for carbyne growth can be determined. The nanotube sample used for the calibration point has a diameter distribution of 1.36 ± 0.08 nm [184], which was modeled using a Gaussian curve (fig. 3.4b). Here, the diameter distribution was estimated from the RBM frequencies measured with multiple laser energies. From integrating between the boundaries of 1.35 and 1.55 nm, it was determined that 56% of the nanotubes have the correct diameter for carbyne growth. Under the assumption that all suitable tubes are filled with carbyne, this value was used to calibrate the relative G-line areas (fig. 3.4c).

Another consideration, additionally to comparing bulk yields, is the realized growth potential. Since not all carbon nanotubes have a suitable diameter for the growth of confined carbyne, the fraction of carbon nanotubes in the sample for which confined carbyne growth is possible was derived from optical absorption data [62], [229], [237]. The excitonic E_{11} peak was measured for the carbon nanotube hosts before the synthesis of confined carbyne using optical absorption spectroscopy. From the diameter distribution, the percentage of suitable hosts within the boundaries of 1.35 nm and 1.55 nm can be determined.

From this data, the bulk yield can be transformed into a relative yield, or realized growth potential (eq. 3.3). This metric shows how many of the fillable tubes contain confined carbyne, while the bulk yield only gives the yield on the entire sample, not removing the unfillable tubes from the calculation. The realized growth potential provides important information about the synthesis as it shows the success in relation to the potential of the specific host nanotubes. If the realized growth potential is almost entirely fulfilled, it would not make sense to change the synthesis further in the pursuit of higher bulk yields. It is also important to consider the different diameter distributions when different host tubes are compared. With only the bulk yield, the comparison would not reflect the difference in fraction of fillable tubes of the different host and might lead to wrong conclusions about synthesis pathways.

$$\text{realized growth potential [\%]} = \frac{\text{bulk yield [\%]}}{\text{fraction of fillable tubes}} \tag{3.3}$$

Carbon 234 (2025) 119979

Contents lists available at ScienceDirect

Carbon

journal homepage: www.elsevier.com/locate/carbon

Quantifying the bulk yield of carbyne confined in different carbon nanotube hosts

Christin Schuster [a,*], Clara Freytag [a,**], Weili Cui [b], Lei Shi [b], Emil Parth [a], Dido Denier van der Gon [a], Takeshi Saito [c], Kazuhiro Yanagi [d], Thomas Pichler [a,***]

[a] Faculty of Phyiscs, University of Vienna, Boltzmangasse 5, Vienna, 1090, Austria
[b] State Key Laboratory of Optoelectronic Materials and Technologies, Guangdong Basic Research Center of Excellence for Functional Molecular Engineering, Nanotechnology Research Center, School of Materials Science and Engineering, Sun Yat-sen University, No. 135, Xingangxi Road, Guangzhou, 510275, China
[c] Nanomaterials Research Institute, National Institute of Advanced Industrial Science and Technology (AIST), 1-1-1 Higashi, Tsukuba, 305-8565, Japan
[d] Department of Physics, Tokyo Metropolitan University, 1-1 Minami-Osawa, Tokyo, 192-0397, Japan

ARTICLE INFO

Keywords:
Confined carbyne
Raman spectroscopy
Bulk yield

ABSTRACT

Carbyne can be successfully synthesized inside carbon nanotubes with exceptionally high yield. However, the exact determination of its bulk yield remains challenging because of the lack of an available analysis method. Raman spectroscopy is the preferred method for the analysis of confined carbyne, as confined carbyne has the highest observed resonance Raman cross section. However, the resonance window is narrow and depends on the host carbon nanotube and its interaction with the confined carbyne, which results in challenges accounting for the bulk yield of confined carbyne in different environments. Here, we propose a model to quantify the yield of confined carbyne using distinct changes in the vibrational response induced by the anharmonic coupling between the carbon nanotube and the carbyne chain. This allows us to quantify the bulk yield of carbyne confined in different carbon nanotube environments without relying on the narrow resonance window of carbyne, paving the way for optimizing the bulk yield of confined carbyne and achieving the full growth potential.

1. Introduction

Carbyne is the sp^1 hybridized allotrope of carbyne, forming an infinitely long one-dimensional chain with excellent predicted mechanical, optical and electronic properties [1–8]. Many pathways have been explored to build materials with linear carbon bonds, for example laser vaporization of graphite [9], laser ablation of graphite particles in liquid [10] or arc-discharge between graphite electrodes [11]. Following organic synthesis pathways, large end-capping groups have been used to sterically stabilize linear carbon chains with up to 44 carbon atoms [12]. The possibility to form long chains with carbon-carbon double bonds or alternating single and triple bonds from polymers using high energy radiation has recently been demonstrated [13]. Extremely long carbon chains, which have reached the threshold of being considered “infinite” carbyne, have been successfully synthesized inside carbon nanotube (CNT) hosts [14] and the synthesis was steadily improved in recent years [15–18].

Its growth mechanisms have been intensively investigated, showing that confined carbyne (CC) can only grow in the presence of carbonaceous precursors inside the host tubes [19]. The synthesis of CC is possible either directly inside an as-grown CNT [14] or in a stepwise process from single-walled carbon nanotube (SWCNT) hosts [17], first forming inner tubes and then growing the CC in a second step. Both of these processes can be improved by introducing additional carbonaceous material inside the CNT host instead of relying on the amorphous carbon already present inside the CNT after its synthesis. The added carbon feedstock for the CC growth can be provided by filling the nanotubes with precursors, *e.g.* methanol [18], fullerenes [17] or short chain linear polyynes [20], or oxidation of the double-walled carbon nanotube (DWCNT) host prior to the CC synthesis [19]. Confined carbyne can also be formed directly inside multi-walled carbon nanotubes during arc-discharge nanotube synthesis [21,22]. The most common synthesis methods for CC is high temperature annealing in high vacuum [23], but low temperature annealing [24] and photothermal synthesis

* Corresponding author.
** Corresponding author.
*** Corresponding author.
E-mail addresses: christin.schuster@univie.ac.at (C. Schuster), clara.freytag@univie.ac.at (C. Freytag), thomas.pichler@univie.ac.at (T. Pichler).

https://doi.org/10.1016/j.carbon.2024.119979
Received 15 November 2024; Received in revised form 20 December 2024; Accepted 30 December 2024
Available online 31 December 2024

[16] have also shown success. Recently, weakly confined carbyne has been synthesized inside large single-walled carbon nanotubes at a very low temperature [25]. The growth of carbyne is governed by the experimental conditions (*e.g.* temperature, pressure) as well as the suitability of the host tubes regarding diameter and the presence of enough carbonaceous feedstock to form the carbyne chain.

Confined carbyne is the best known Raman scatterer with a resonant differential Raman cross section per atom in the order of 10^{-22} cm^2 sr^{-1} [26], making Raman spectroscopy the preferred investigative method for CC. The characteristic peak of polyynes can be found at around 2100 cm^{-1} for short chain hydrogen-capped polyynes in liquid [27]. The Raman frequency decreases with increasing chain length [28]. The Raman frequency is also dependent on the matrix, shifting down from chains simulated in vacuum to chains in solution to chains confined inside carbon nanotubes, which appear in the region between 1800 and 1900 cm^{-1} [29]. When comparing Raman spectra of CC, the current state of the art is to compare the area of the CC peaks, which are attributed to the longitudinal optical (LO) mode of the confined carbyne chains in order to access the yield [17]. However, the Raman signal of the carbyne chain inside the CNT hosts is strongly dependent on the geometry of the CNT surrounding it, which explains different frequencies of the CC peaks depending on the chirality of the CNT used as a host tube [30]. Different frequencies of the CC peaks also show starkly different resonance behavior for different laser energies. Estimating the CC yield from the area of the CC peak in Raman is therefore rather complicated, as the resonance behavior has to be considered, which requires access to multi-frequency lasers for the Raman measurements [31].

On the other hand, in the Raman response of the confined carbyne and carbon nanotube host system (CC@CNT), peculiar changes in the G and the 2D mode fine structure can be observed, specifically shoulders on the left and right sides. These shoulders were recently described by anharmonic phonon-phonon interactions as coupled modes between the carbyne chain with the nanotube host and follow the resonance behavior of the surrounding nanotubes and not the highly variable and distinct resonance of CC [32].

Here we present a new model to determine the bulk yield of CC in different nanotube hosts. We show that the additional shoulders in the G and 2D-band can be fitted by coupled modes and act as a fingerprint of the CC yield, circumventing the challenge of the narrow resonance window of the CC modes.

2. Material and methods

For this study we analyzed, SWCNT hosts (eDIPS, semi-conducting arc-discharge) as host tubes to synthesize CC *via* high temperature annealing in high vacuum and also compared them to previously published results on direct growth of CC inside CVD DWCNT hosts [14] and 1.36 nm semi-conducting arc-discharge CNT hosts [32].

For the eDIPS CNT hosts with a mean diameter of around 1.33 nm, different samples of the as grown CNT hosts were annealed once in high vacuum for 1 h at different temperature points, from 1500 °C to 1600 °C in 20 °C steps. To study the influence of repeating the annealing process with oxidation steps in between, one sample was repeatedly annealed at 1500 °C for 1 h at high vacuum, measured with Raman spectroscopy and then oxidized at a pressure of 600 mbar for 2 h at 470 °C and then annealed with the same parameters again.

For the semi-conducting 1.45 nm arc-discharge and the 1.41 nm eDIPS samples, the first step was filling the nanotubes with C_{60} fullerenes under vacuum to create peapods. For the filling, the buckypaper was oxidized for 30 min at 450 °C in air to open the endcaps of the nanotubes and then sealed inside a glass ampule under high vacuum ($< 10^{-6}$ mbar) together with the fullerenes. The sealed ampule was heated to 550 °C for 12 h. From the CNT peapods, inner walls were grown at 1300 °C in ultra high vacuum. Afterwards, the sample was oxidized in air at 500 °C to open the endcaps of the inner tubes and create defects. As a last step, it was annealed again in ultra high vacuum at 1500 °C for 1 h to grow the carbyne chains. For some samples, the process of oxidizing and annealing was repeated multiple times.

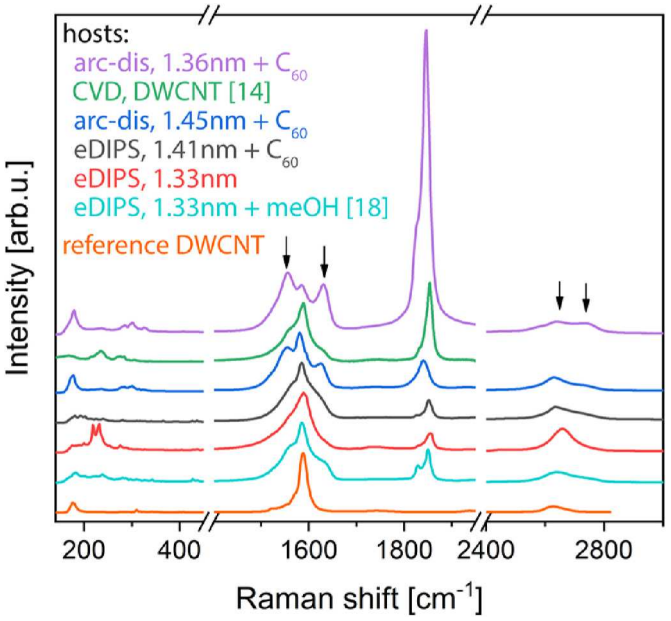

Fig. 1. Spectra of six different types of CNT hosts filled with carbyne measured with 568 nm laser radiation. All spectra show a change in the G-line and the 2D-line indicated by the arrows. For comparison, an arc-discharge DWCNT sample, also measured with the same laser, is shown at the bottom. (A colour version of this figure can be viewed online.)

Raman measurements of the samples were made with a Horiba LabRAM HR spectrometer combined with an Ar+/Kr + laser (Coherent Innova 70C, 458, 488, 514, 532, 568, 647 nm) and a He–Ne laser (633 nm). As detector a liquid nitrogen cooled CCD chip was used.

The optical absorption measurements of the samples were made with a Bruker vertex 70v/80v. For the measurement the nanotubes were sonicated in acetone and then airbrushed on to BaF_2 wedges to create a thin film.

For the fit models we used PeakFit™ v4.06 and their residual model. All structure models were made using VESTA [33].

3. Results and discussion

The Raman spectrum of a DWCNT shows radial breathing modes (RBM) for the inner and outer tube (around 180 cm^{-1} - 400 cm^{-1}), the G mode (around 1600 cm^{-1}) and the 2D-mode (around 2600 cm^{-1}) as shown in Fig. 1. When comparing the Raman spectra of unfilled DWCNT hosts with the Raman spectra of CC@DWCNT, the LO modes of the carbyne chains appear at around 1850 cm^{-1}. Additionally, the nanotube related G-band and the 2D-band reveal strong changes in the fingerprint. These modes, indicated by the arrows in Fig. 1, have been recently successfully explained by anharmonic phonon-phonon interactions [32]. As depicted here, these interaction features are a unique fingerprint of CC@CNT and appear independently of the precursor for all CNT hosts filled with CC.

A more detailed analysis of the G and 2D band by coupled modes is shown in the insets of Fig. 2a. For the G-band, we used a line-shape analysis that has been previously fitted to the DWCNT host tubes of the sample with 4 Voigt peaks to account for the different G^+ and G^- components of the inner and outer nanotubes and 2 additional Voigt peaks. We then describe the extra peaks in the G mode (G_S) with 4 additional Voigtians, where the G_S^+ and G_S^- each consist of 2 Voigtians that are correlated and separated by the same distance as the one between the two main CC modes. For the 2D-band, we used 5 Voigt peaks

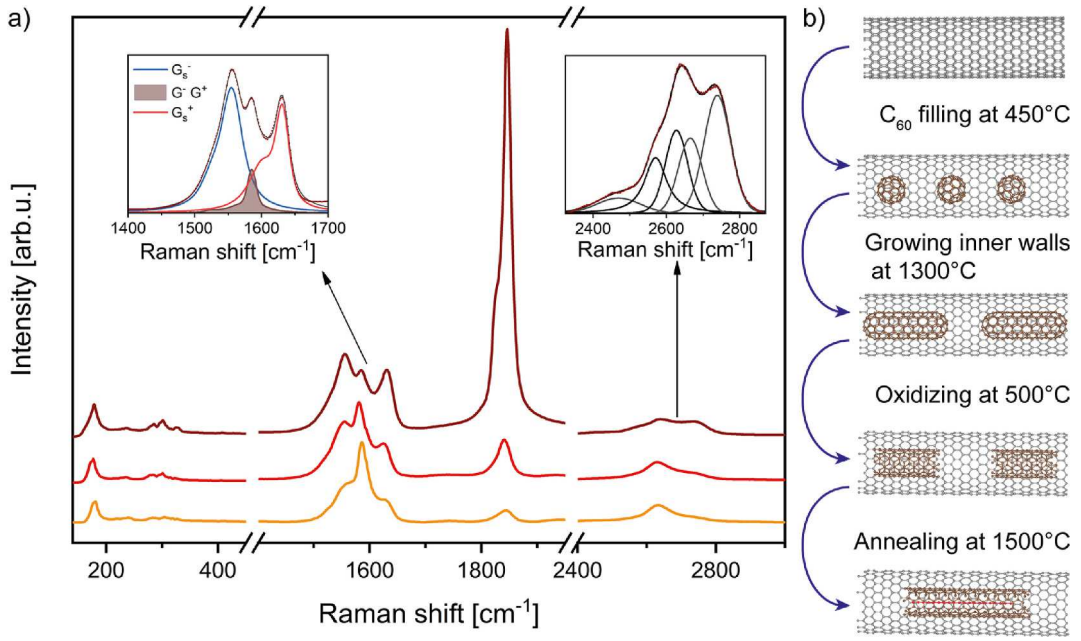

Fig. 2. Synthesis optimization for high temperature annealing of arc-discharge CNT buckypaper. a) Comparison of different CC yields for samples using arc-discharge nanotubes with different diameter distribution (dark red: 1.36 nm, light red and orange: 1.45 nm). The change in the G-line gets more pronounced for higher CC peaks. The insets show the line-shape analysis of the upper spectrum for the G-line together with the shoulders as well as for the 2D-line which also shows extra peaks. b) Schematic synthesis of CC from C_{60} filled CNT hosts. (For interpretation of the references to colour in this figure legend, the reader is referred to the Web version of this article.)

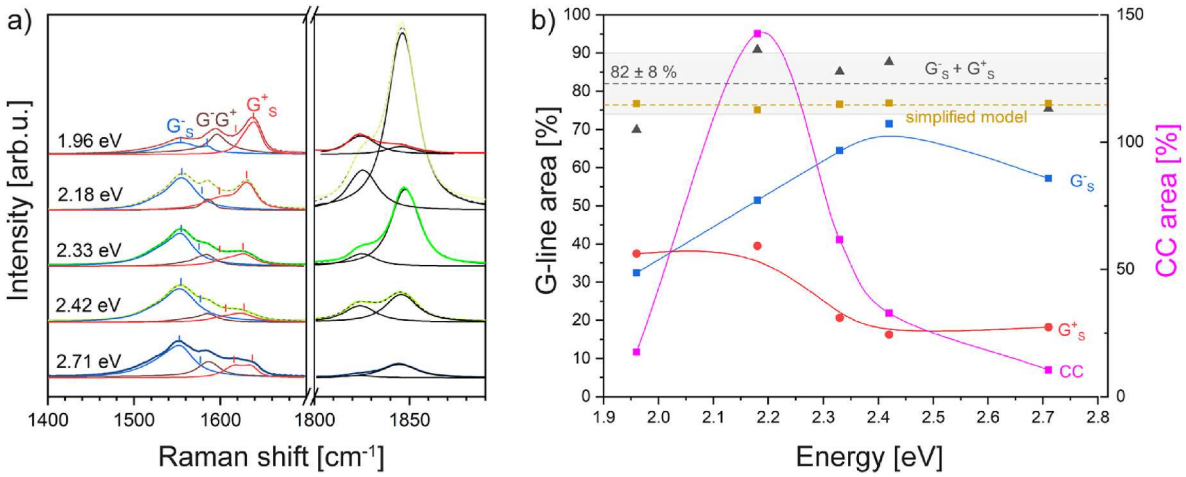

Fig. 3. a) Line-shape analysis of the G-line of the same sample for different laser energies. The center peak (brown) corresponds to the G-line of an unfilled DWCNT sample. The G^- (blue) and G^+ (red) peaks each consist of two Voigt peaks whose distance is determined by the distance of the two main peak components of the CC peak. b) Analysis of the area that the shoulder peaks occupy in relation to the combined G-band as well as the area of the CC peak (pink) in comparison to the combined G-band. While the area occupied by the left (blue) and right (red) shoulders changes for different energies, the combined area is reasonably constant (gray). If instead of using the fit model the area of the DWCNT host tube is subtracted from the G-line of the filled CNT hosts we observe similar values that are also reasonably constant across the studied energy spectrum (dark yellow). (For interpretation of the references to colour in this figure legend, the reader is referred to the Web version of this article.)

to describe the change in the 2D-band. This number of components is based on the analysis of the main components of the anharmonically coupled CC and CNT modes close to the K-point in the Brillouin zone shown in Ref. [32]. A direct comparison of the 2D-line of filled and unfilled samples can be found in the supplementary information highlighting the appearance of several high and low frequency shoulders similar to the spectral fingerprint observed for the G-line. Also depicted in Fig. 2a is how the G and 2D-lines are influenced by the CC yield, which in turn depends on the diameter distribution as well as the available carbon feedstock inside the hosting arc-discharge tube. In Fig. 2b we schematically show how to optimize the CC yield by filling with C_{60} as an example for a carbonaceous precursor. After filling the CNT host with C_{60}, high vacuum annealing at 1300 °C yields inner tubes with narrow diameter distribution. An oxidation step at 500 °C provides additional carbonaceous precursors by opening the endcaps of the inner tubes and introducing defects [19]. In the final high vacuum annealing step at 1500 °C, the precursors are converted to CC. This stepwise growth has sofar achieved the highest yield of CC@CNT.

The detailed line-shape analysis of the G-line and the CC mode described above is shown in Fig. 3a for 5 different laser energies. As

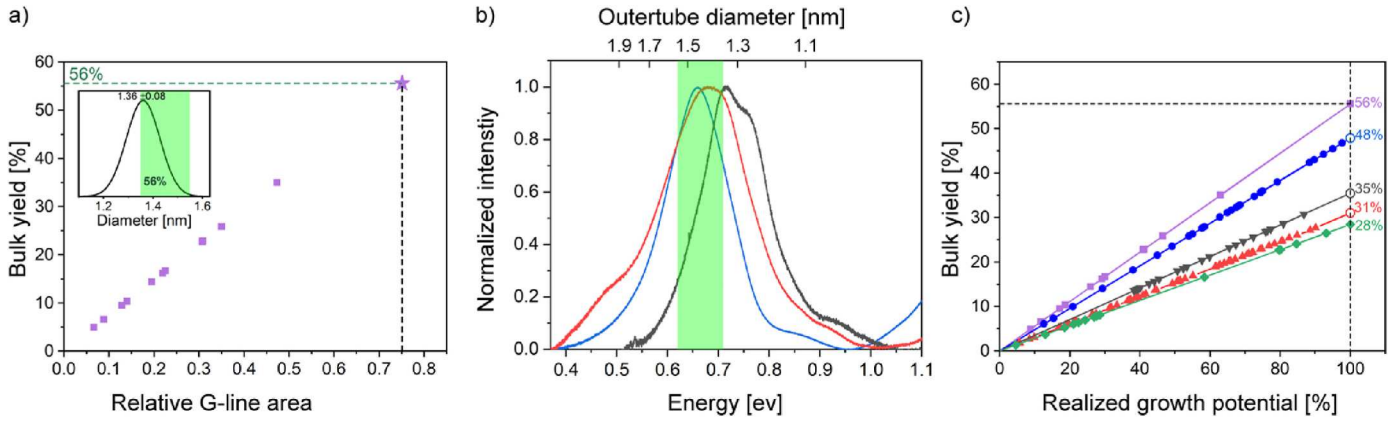

Fig. 4. a) Relative G-line area of the CC filled 1.36 nm arc-discharge samples, diameter distribution shown in the inset. The green area is the range where CC is expected to grow (56 %). We used the highest relative G-line area (indicated by the star) to calibrate the relative G-line area to a specific bulk yield. b) Excitonic E_{11} absorption peak for the different SWCNT host tubes: 1.45 nm arc-discharge (blue), 1.33 nm eDIPS (gray) and 1.41 nm eDIPS (red). The upper x-axis shows the correlated diameters that can be calculated by using the optical absorbance data. The gray labels indicate the expected inner tube diameters [34]. The green area shows the diameter range of inner tubes which are suitable for the CC growth [30]. c) Bulk yield and related realized growth potential for the same CNT hosts shown before for different optimization steps and synthesis conditions: 1.36 nm arc-discharge (lilac), 1.45 nm arc-discharge (blue), 1.41 nm eDIPS (gray), 1.33 nm eDIPS (red) and CVD [14] (green). The empty circles indicate highest possible bulk yield values determined from area integration of the optical spectra (b). (For interpretation of the references to colour in this figure legend, the reader is referred to the Web version of this article.)

shown in Fig. 3b, the area of the CC mode is strongly resonance dependent. However, when we compare the area that each of the shoulders take up of the total G-band we can see that the left and right shoulders (marked as G_S^- and G_S^+) individually have varying percentages of the entire G-band area, but the sum of the G-line area percentage of the two is relatively constant across the visible energy spectrum. In other words, the two shoulders appear on different sides of the resonance window, but the sum of both is independent of the laser energy, making it more robust than the CC peak for the bulk yield determination. This is in good agreement with our previous results showing that the G and 2D-bands of the nanotube host are electronically decoupled but vibronically coupled with the carbon chain [32]. This means the resonance behavior, which is due to the electronic band structure of the individual subsystems (CNT and CC), appears independent. The phononic structure, on the other hand, shows interaction features, which can be explained by correlation effects from phonon-phonon interaction. Therefore the resonance of the coupled modes follows the resonance behavior of the CNT host, which is not strongly dependent on the laser energy in the visible region. In order to check if we can further simplify the analysis without significantly reducing the accuracy of the bulk yield determination, we compared the combined $G_S^+ + G_S^1$ area gained *via* line-shape analysis with a simple area comparison of filled and unfilled tubes. We therefore assessed a simplified model, where the area of the background corrected and then normalized G-band of the empty DWCNT host tube (A_U) is simply subtracted from the area of the total G-band of the CC@CNT sample (A_F) and then divided by the total G-band to obtain the relative G-line area (G_{la}) values (eq. (1)). The Raman spectrum of the CC@CNT sample also needs to be background corrected and then normalized to the G $^{\pm}$ peak, but not the shoulders.

$$G_{la} = \frac{A_F - A_U}{A_F} \tag{1}$$

The result of this analysis is shown as dark yellow dots in Fig. 3b. While the mean G-line area percentage using the line-shape analysis model is 82 ± 8 %, indicated by the light gray box, the simplified model using the areas has mean percentage of 76 % which falls into the uncertainty window of the line-shape analysis model, which highlights that it is accurate enough to assess the bulk yield of CC. Our results also clearly show that the anharmonically coupled modes are only weakly dependent on the laser energy in the visible light region.

Therefore, any single laser in the visible range is enough to assess the bulk yield. In contrast to analyzing the yield from the CC mode, no tunable laser or at least multiple lasers at different laser energies across the CC resonance window, are needed to analyze the bulk yield. The same analysis can also be done for the 2D-bands, however, because the shoulders there are less pronounced and have more components to be analyzed, evaluating the G mode is more reliable.

In order to determine the maximum possible bulk yield for CNT encapsulated CC, we have to consider that CC grows only inside nanotubes with suitable diameter. If the diameter is too big, carbon clusters [14] or even another inner tube will grow, whereas if it is too small, there is no space to grow carbyne. It is not definitively known what the minimum inner tube diameter for carbyne growth is, but the inner tube must be bigger than four times the covalent radius of carbon, because there is no hybridization between the CC and the host tubes.

We rely on previous experimental studies that show carbon growth predominantly for inner tube diameters between $d_{NT} = 0.63 - 0.83$ nm [30]. Since the diameter distribution is dependent on the used CNT host, it is crucial in determining the achievable bulk yield. This diameter distribution can be analyzed using optical absorption data [35–38]. In the inset in Fig. 4a we show the diameter distribution for the 1.36 nm arc-discharge CNT sample, which was modeled assuming 1.36 nm ± 0.08 using a Gaussian peak [32]. Considering that inner and outer tube nanotubes have shown a mean spacing of 0.36 nm, we expect the inner tubes to have a mean diameter of 0.64 ± 0.08 nm [34]. Therefore, for the combined growth of inner tubes and CC inside a SWCNT host, the SWCNT host tubes should have a diameter between 1.35 and 1.55 nm, which is indicated by the green box in the inset (4a and 4 b). Accordingly, the maximum fillability of this host was determined to be 56 %. The main panel of Fig. 4a shows the relation between the bulk yield and the relative G-line area. With the assumption that the.

1.36 nm arc-discharge sample is filled to its maximum and has a bulk yield of 56 % with a corresponding relative G-line area of 0.75, we calibrated all our values so we can estimate the bulk yield of the other samples. The calibration point is indicated by the star. In Fig. 4b we depict optical spectra of the excitonic E_{11} absorption peak for our nanotube hosts (1.45 nm arc-discharge, 1.33 nm eDIPS, 1.41 nm eDIPS). The related tube diameters are shown on the upper axis using the calibration in Wang et al. [37]. Again, the green box indicates the CC growth region. We conclude that the nanotube hosts studied have a maximum fillability of 48, 31 and 35 %, respectively.

In Fig. 4c we show the CC yield for different CNT host tubes. The bulk

yield was calculated from the G-line area values using the simplified model described above. In all different CNT hosts two effects contribute to the carbyne growth as limiting factors: first, the suitable nanotube diameter and second, the available carbonaceous feedstock inside the suitable nanotubes. This can be clearly seen in the growth potential. In some CNT hosts, enoughmcarbonaceous feedstock is available to achieve almost the maximum growth potential under the optimal synthesis conditions. For others, this is not the case and additional filling of carbonaceous precursors, *e.g.* organic solvents or C_{60} [18,19], can lead to improved yield. For the CVD CNT samples from Shi et al., the values obtained with our model indicate a fully realized growth potential which is also in agreement with the previous rough estimation of the bulk yield [14]. Even though the growth potential was fully realized for the CVD nanotubes, the bulk yield is relatively low due to the small fraction of nanotubes with suitable diameters.

4. Conclusions

Different synthesis methods for carbyne confined inside carbon nanotubes were reviewed. The Raman spectra of the CC@CNT systems were analyzed and coupled modes resulting from interactions of the carbyne chain with the surrounding nanotubes were described. Evaluating the area of the coupled G-modes has shown to be a reliable method for determining the bulk yield of confined carbyne, which is not dependent on the laser energy and therefore preferable to the current state of the art which focuses on the LO peak of the CC. A simple model that does not rely on line-shape analysis but rather on the difference in G-line area of a filled and unfilled sample was introduced. The highest bulk yields for carbon nanotubes can be achieved by using CNT hosts with well-suited diameters for the growth of double-walled carbon nanotubes and carbyne as well as filling the host tubes with a carbonaceous precursor. The new fast and robust method for yield determination presented here will simplify and improve systematic approaches to confined carbyne synthesis.

CRediT authorship contribution statement

Christin Schuster: Writing – original draft, Visualization, Methodology, Investigation, Formal analysis. **Clara Freytag:** Writing – original draft, Visualization, Methodology, Investigation, Formal analysis. **Weili Cui:** Investigation. **Lei Shi:** Writing – review & editing, Investigation. **Emil Parth:** Visualization. **Dido Denier van der Gon:** Investigation. **Takeshi Saito:** Resources. **Kazuhiro Yanagi:** Resources. **Thomas Pichler:** Writing – review & editing, Supervision, Funding acquisition.

Declaration of competing interest

The authors declare that they have no known competing financial interests or personal relationships that could have appeared to influence the work reported in this paper.

Acknowledgements

C.S., T.P. and E.P acknowledge funding from the European Research Council (ERC) under the European Union's Horizon 2020 research and innovation programe (MORE-TEM ERC-SYN project, grant agreement No 951215). C.F. acknowledges funding from Doctoral College Advanced Functional Materials (DCAFM) by the Austrian Science Fund (FWF, grant number: DOC 85 doc. funds). D.D. acknowledges funding from the Vienna Doctoral School in Physics (VDSP). L.S. acknowledges the National Natural Science Foundation of China (52472059). W.C. acknowledges the National Natural Science Foundation of China (22401298). K.Y. acknowledges support from JSPS KAKENHI, Grant Nos. JP23H00259, and JP24H01200, and US-JAPAN PIRE, Grant No. JPJSJRP20221202, Japan, and ASPIRE project, Grant No. JPMJAP2310, Japan.

Appendix A. Supplementary data

Supplementary data to this article can be found online at https://doi.org/10.1016/j.carbon.2024.119979.

References

[1] A. Al-Backri, V. Zolyomi, C.J. Lambert, Electronic properties of linear carbon chains: resolving the controversy, J. Chem. Phys. 140 (10) (2014), https://doi.org/10.1063/1.4867635.
[2] C.S. Casari, M. Tommasini, R.R. Tykwinski, A. Milani, Carbon-atom wires: 1-d systems with tunable properties, Nanoscale 8 (8) (2016) 4414–4435, https://doi.org/10.1039/C5NR06175J.
[3] Y. Cui, Q. Wei, H. Park, C.M. Lieber, Nanowire nanosensors for highly sensitive and selective detection of biological and chemical species, Science 293 (5533) (2001) 1289–1292, https://doi.org/10.1126/science.106271.
[4] E. Fazio, F. Neri, S. Patane, L. D'urso, G. Compagnini, Optical limiting effects in linear carbon chains, Carbon 49 (1) (2011) 306–310, https://doi.org/10.1016/j.carbon.2010.09.026.
[5] M. Liu, V.I. Artyukhov, H. Lee, F. Xu, B.I. Yakobson, Carbyne from first principles: chain of c atoms, a nanorod or a nanorope, ACS Nano 7 (11) (2013) 10075–10082, https://doi.org/10.1021/nn404177r.
[6] Y. Wang, Y. Huang, B. Yang, R. Liu, Structural and electronic properties of carbon nanowires made of linear carbon chains enclosed inside zigzag carbon nanotubes, Carbon 44 (3) (2006) 456–462, https://doi.org/10.1016/j.carbon.2005.08.026.
[7] Z. Zanolli, G. Onida, J.-C. Charlier, Quantum spin transport in carbon chains, ACS Nano 4 (9) (2010) 5174–5180, https://doi.org/10.1021/nn100712q.
[8] K. Zhang, Y. Zhang, L. Shi, A review of linear carbon chains, Chin. Chem. Lett. 31 (7) (2020) 1746–1756, https://doi.org/10.1016/j.cclet.2020.03.019.
[9] J.R. Heath, Q. Zhang, S.C. O'Brien, R.F. Curl, H.W. Kroto, R.E. Smalley, The formation of long carbon chain molecules during laser vaporization of graphite, J. Am. Chem. Soc. 109 (2) (1987) 359–363, https://doi.org/10.1021/ja00236a012.
[10] M. Tsuji, T. Tsuji, S. Kuboyama, S.-H. Yoon, Y. Korai, T. Tsuji- moto, K. Kubo, A. Mori, I. Mochida, Formation of hydrogen-capped polyynes by laser ablation of graphite particles suspended in solution, Chem. Phys. Lett. 355 (1–2) (2002) 101–108, https://doi.org/10.1016/s0009-2614(02)00192-6.
[11] F. Cataldo, Simple generation and detection of polyynes in an arc dis- charge between graphite electrodes submerged in various solvents, Carbon 41 (13) (2003) 2671–2674, https://doi.org/10.1016/s0008-6223(03)00345-2.
[12] W.A. Chalifoux, R.R. Tykwinski, Synthesis of polyynes to model the sp-carbon allotrope carbyne, Nat. Chem. 2 (11) (2010) 967–971, https://doi.org/10.1038/nchem.828.
[13] M. Brzhezinskaya, V.E. Zhivulin, Controlled modification of polyvinylidene fluoride as a way for carbyne synthesis, Polym. Degrad. Stabil. 203 (2022) 110054, https://doi.org/10.1016/j.polymdegradstab.2022.110054.
[14] L. Shi, P. Rohringer, K. Suenaga, Y. Niimi, J. Kotakoski, J.C. Meyer, H. Peterlik, M. Wanko, S. Cahangirov, A. Rubio, Z.J. Lapin, L. Novotny, P. Ayala, T. Pichler, Confined linear carbon chains as a route to bulk carbyne, Nat. Mater. 15 (6) (2016) 634–639, https://doi.org/10.1038/nmat4617.
[15] L. Shi, R. Senga, K. Suenaga, H. Kataura, T. Saito, A.P. Paz, A. Rubio, P. Ayala, T. Pichler, Toward confined carbyne with tailored properties, Nano Lett. 21 (2) (2021) 1096–1101, https://doi.org/10.1021/acs.nanolett.0c04482.
[16] L. Shi, R. Senga, K. Suenaga, J. Chimborazo, P. Ayala, T. Pichler, Photothermal synthesis of confined carbyne, Carbon 182 (2021) 348–353, https://doi.org/10.1016/j.carbon.2021.05.058.
[17] Y. Feng, W. Zhang, K. Tang, Y. Chen, J. Zhang, K. Cao, W. Cui, L. Shi, A robust synthesis route of confined carbyne, Nano Res. 17 (7) (2024) 6274–6280, https://doi.org/10.1007/s12274-024-6571-z.
[18] W. Cui, L. Shi, K. Cao, U. Kaiser, T. Saito, P. Ayala, T. Pichler, Isotopic labelling of confined carbyne, Angew. Chem. Int. Ed. 60 (18) (2021) 9897–9901, https://doi.org/10.1002/anie.202017356.
[19] W. Cui, F. Simon, Y. Zhang, L. Shi, P. Ayala, T. Pichler, Ultra-clean isotope engineered double-walled carbon nanotubes as tailored hosts to trace the growth of carbyne, Adv. Funct. Mater. 32 (41) (2022) 2206491, https://doi.org/10.1002/adfm.202206491.
[20] C. Zhao, R. Kitaura, H. Hara, S. Irle, H. Shinohara, Growth of linear carbon chains inside thin double-wall carbon nanotubes, J. Phys. Chem. C 115 (27) (2011) 13166–13170, https://doi.org/10.1021/jp201647m.
[21] X. Zhao, Y. Ando, Y. Liu, M. Jinno, T. Suzuki, Carbon nanowire made of a long linear carbon chain inserted inside a multiwalled carbon nanotube, Phys. Rev. Lett. 90 (18) (2003) 187401, https://doi.org/10.1103/PhysRevLett.90.187401.
[22] T.A. Moura, W.Q. Neves, R.S. Alencar, Y.A. Kim, M. Endo, T.L. Vasconcelos, D. G. Costa, G. Candiotto, R.B. Capaz, P.T. Araujo, et al., Resonance Raman spectroscopy characterization of linear carbon chains encapsulated by multi-walled carbon nanotubes, Carbon 212 (2023) 118123, https://doi.org/10.1016/j.carbon.2023.118123.
[23] L. Shi, P. Rohringer, P. Ayala, T. Saito, T. Pichler, Carbon nanotubes from enhanced direct injection pyrolytic synthesis as templates for long linear carbon chain formation, Phys. Status Solidi 250 (12) (2013) 2611–2615, https://doi.org/10.1002/pssb.201300148.
[24] W. Chang, F. Liu, Y. Liu, T. Zhu, L. Fang, Q. Li, Y. Liu, X. Zhao, Smallest carbon nanowires made easy: long linear carbon chains confined inside single-walled

carbon nanotubes, Carbon 183 (2021) 571–577, https://doi.org/10.1016/j.carbon.2021.07.037.
[25] B.-W. Zhang, X.-Y. Qiu, Y. Ma, Q. Hu, A. Fito-Parera, I. Kohata, Y. Feng, Y. Zheng, C. Zhang, Y. Matsuo, Y. Wang, S. Chiashi, K. Ot-suka, R. Xiang, D.I. Levshov, S. Cambre, W. Wenseleers, S.V. Rotkin, S. Maruyama, Low-temperature Synthesis of Weakly Confined Carbyne inside Single-Walled Carbon Nanotubes, 2024 arXiv: 2411.18899, https://arxiv.org/abs/2411.18899.
[26] C.D. Tschannen, G. Gordeev, S. Reich, L. Shi, T. Pichler, M. Frimmer, L. Novotny, S. Heeg, Raman scattering cross section of confined carbyne, Nano Lett. 20 (9) (2020) 6750–6755, https://doi.org/10.1021/acs.nanolett.0c02632.
[27] H. Tabata, M. Fujii, S. Hayashi, T. Doi, T. Wakabayashi, Raman and surface-enhanced Raman scattering of a series of size-separated polyynes, Carbon 44 (15) (2006) 3168–3176, https://doi.org/10.1016/j.carbon.2006.07.004.
[28] A. Milani, M. Tommasini, M. Del Zoppo, C. Castiglioni, G. Zerbi, Carbon nanowires: phonon and π-electron confinement, Phys. Rev. B 74 (15) (2006) 153418, https://doi.org/10.1103/physrevb.74.153418.
[29] L. Shi, P. Rohringer, M. Wanko, A. Rubio, S. Waßerroth, S. Re- ich, S. Cambre, W. Wenseleers, P. Ayala, T. Pichler, Electronic band gaps of confined linear carbon chains ranging from polyyne to carbyne, Phys. Rev. Mater. 1 (7) (2017) 075601, https://doi.org/10.1103/physrevmaterials.1.075601.
[30] S. Heeg, L. Shi, L.V. Poulikakos, T. Pichler, L. Novotny, Carbon nanotube chirality determines properties of encapsulated linear carbon chain, Nano Lett. 18 (9) (2018) 5426–5431, https://doi.org/10.1021/acs.nanolett.8b01681.
[31] M. Martinati, W. Wenseleers, L. Shi, S.M. Pratik, P. Rohringer, W. Cui, T. Pichler, V. Coropceanu, J.-L. Bredas, S. Cambre, Electronic structure of confined carbyne from joint wavelength-dependent resonant Raman spectroscopy and density functional theory investigations, Carbon 189 (2022) 276–283, https://doi.org/10.1016/j.carbon.2021.12.059.
[32] E. Parth, A. Corradini, W. Cui, W. Romanin, C. Schuster, C. Freytag, L. Shi, K. Yanagi, M. Calandra, T. Pichler, The resonant Raman response of confined carbyne is solely driven by anharmonic interactions, preprint available at Research Square (2024), https://doi.org/10.21203/rs.3.rs-5247129/v1.
[33] K. Momma, F. Izumi, Vesta 3 for three-dimensional visualization of crystal, volumetric and morphology data, J. Appl. Crystallogr. 44 (6) (2011) 1272–1276, https://doi.org/10.1107/s0021889811038970.
[34] M. Abe, H. Kataura, H. Kira, T. Kodama, S. Suzuki, Y. Achiba, K.-i. Kato, M. Takata, A. Fujiwara, K. Matsuda, Y. Maniwa, Structural transformation from single-wall to double-wall carbon nanotube bundles, Phys. Rev. B 68 (4) (2003) 041405, https://doi.org/10.1103/physrevb.68.041405.
[35] T. Saito, S. Ohmori, B. Shukla, M. Yumura, S. Iijima, A novel method for characterizing the diameter of single-wall carbon nanotubes by optical absorption spectra, APEX 2 (9) (2009) 095006, https://doi.org/10.1143/APEX.2.095006.
[36] O. Jost, A. Gorbunov, W. Pompe, T. Pichler, R. Friedlein, M. Knupfer, M. Reibold, H.-D. Bauer, L. Dunsch, M. Golden, et al., Diameter grouping in bulk samples of single-walled carbon nanotubes from optical absorption spectroscopy, Appl. Phys. Lett. 75 (15) (1999) 2217–2219, https://doi.org/10.1063/1.124969.
[37] F. Wang, G. Dukovic, L.E. Brus, T.F. Heinz, The optical resonances in carbon nanotubes arise from excitons, Science 308 (5723) (2005) 838–841, https://doi.org/10.1126/science.1110265.
[38] H. Kataura, Y. Kumazawa, Y. Maniwa, I. Umezu, S. Suzuki, Y. Ohtsuka, Y. Achiba, Optical properties of single-wall carbon nanotubes, Synth. Met. 103 (1–3) (1999) 2555–2558, https://doi.org/10.1016/S0379-6779(98)00278-1.

Appendix A. Supplementary data

Appendix A.1. Lineshape analysis 2D line

Lineshape analysis for the 2D line of the DWCNT host tube and carbyne filled tube of the 1.36 nm arc-discharge CNT host tubes for different laser energies, two Voigt peaks were used for the unfilled DWCNT sample and five Voigt peaks were used for the CC@DWCNT sample, see figures. A.5, A.6, A.7, A.8, A.9.

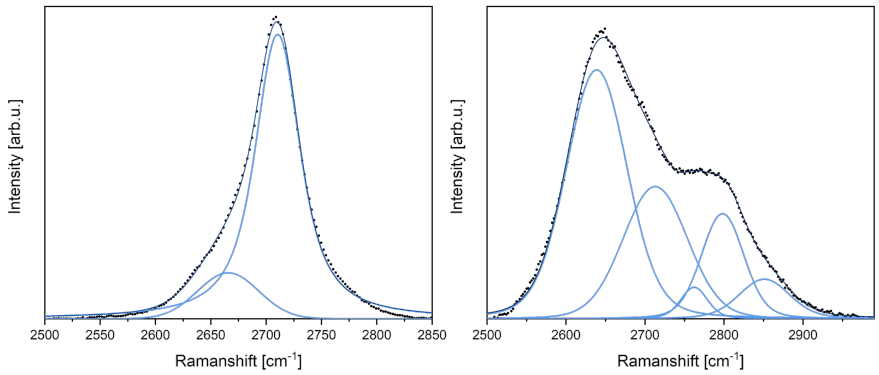

Figure A.5: 2D line of the 1.36 nm arc-discharge sample for an unfilled DWCNT sample (left) and a CC@DWCNT sample (right). Laser energy of 2.71 eV. Fitted with Voigt peaks (blue).

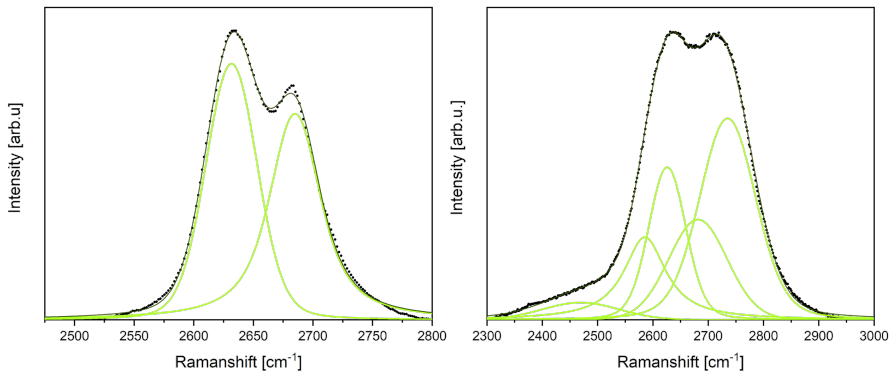

Figure A.6: 2D line of the 1.36 nm arc-discharge sample for an unfilled DWCNT sample (left) and a CC@DWCNT sample (right). Laser energy of 2.42 eV. Fitted with Voigt peaks (green).

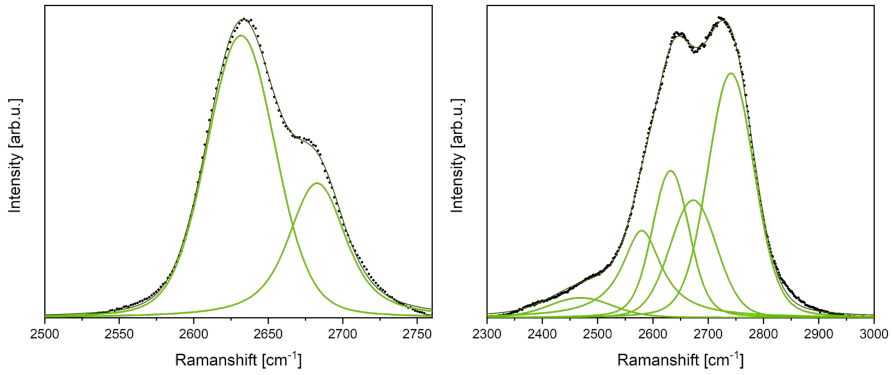

Figure A.7: 2D line of the 1.36 nm arc-discharge sample for unfilled an DWCNT sample (left) and a CC@DWCNT sample (right). Laser energy of 2.33 eV. Fitted with Voigt peaks (green).

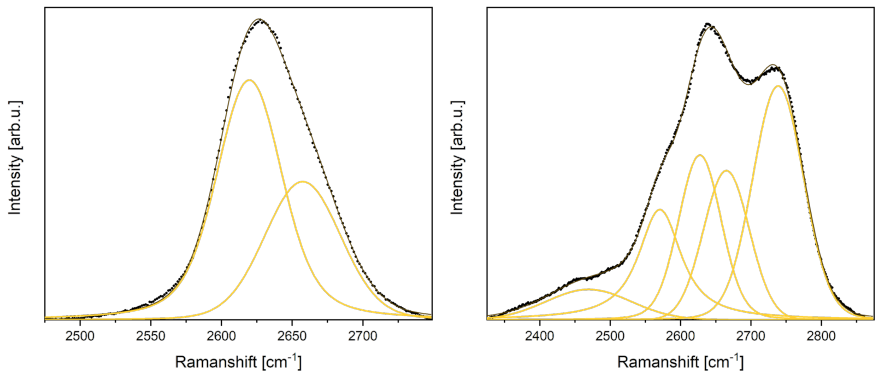

Figure A.8: 2D line of the 1.36 nm arc-discharge sample for an unfilled DWCNT sample (left) and an CC@DWCNT sample (right). Laser energy of 2.18 eV. Fitted with Voigt peaks (yellow).

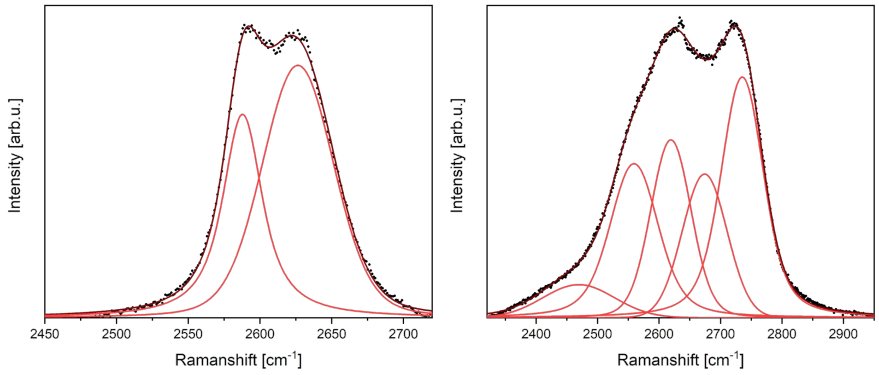

Figure A.9: 2D line of the 1.36 nm arc-discharge sample for unfilled an DWCNT sample (left) and a CC@DWCNT sample (right). Laser energy of 1.96 eV. Fitted with Voigt peaks (red).

Appendix A.2. Optical absorption data

Optical absorption spectrum of the 1.33nm eDIPS SWCNT host tube (fig.A.10). The spectrum was done using a thin film (airbrushed on wedges).

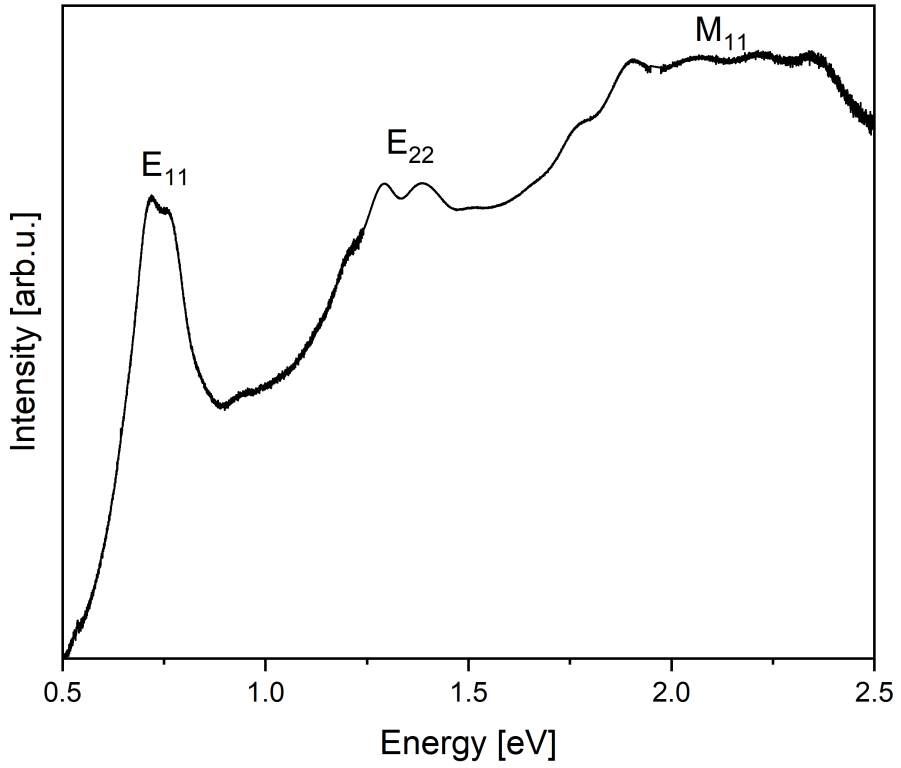

Figure A.10: Optical absorption spectrum of the 1.33nm eDIPs SWCNT host tube. The nanotubes were sonicated in aceton and then airbrushed on BaF_2 wedges. No backround correction.

Appendix A.3. Relative G-line area values

All values depicted in figure 4 in the main article are shown here divided according to host tube. The value for the integrated area is determined by subtracting the background and then normalizing to the G-peak (not the shoulders) and finally integrating the area. The values are rounded and then used to calculate the relative G-line area according to equation 1 of the main article. Values shown in tables A.1, A.2, A.3, A.4, A.5.

Table A.1: Relative G-line area data for the 1.36 nm arc-discharge samples. All but the last value are results of sonication experiments performed on the CC filled sample. The area of the unfilled DWCNT (host tube) is 29.48.

integrated area	G_{la}
55.97	0.47329
45.34	0.3498
42.66	0.30895
38.06	0.22543
42.56	0.30733
37.75	0.21907
36.62	0.19498
34.28	0.14002
33.82	0.12833
31.57	0.0662
32.34	0.08844
118.53	0.75129

Table A.2: Relative G-line area data for the 1.45 nm arc-discharge samples.The area of the unfilled DWCNT (host tube) is 29.48.

integrated area	G_{la}	integrated area	G_{la}
43.25	0.31838	49.66	0.40636
34.08	0.13498	45.32	0.34951
52.32	0.43654	52.97	0.44346
52.54	0.4389	47.03	0.37317
56.89	0.48181	45.78	0.35605
68.92	0.57226	51.51	0.42768
80.12	0.63205	55.61	0.46988
73.31	0.59787	32.73	0.0993
76.54	0.61484	32.11	0.08191
57.32	0.48569	36.38	0.18966
70.39	0.58119	56.84	0.48135
60.51	0.51281	41.6	0.29135
50.86	0.42037	47.38	0.3778
39.1	0.24604		

Table A.3: Relative G-line area data for the 1.33 nm eDIPs samples. The area of the unfilled DWCNT (host tube) is 43.33.

integrated area	G_{la}	integrated area	G_{la}	integrated area	G_{la}
48.66	0.10955	44.34	0.0228	63.62	0.31892
54.47	0.20453	49.92	0.13203	61.45	0.29487
51.16	0.15307	46.97	0.07752	61.77	0.29853
55.12	0.21391	47.65	0.09068	62.66	0.30849
69.24	0.37422	44.4	0.02412	64.99	0.33328
64.22	0.3253	48.64	0.10919	60.08	0.27879
59.44	0.27104	52.17	0.16946	61.89	0.29989
52.38	0.17279	51.58	0.15996	65.93	0.34279
51.18	0.1534	46.68	0.07178	59.02	0.26584
53.18	0.18524	47.1	0.08006	62.83	0.31036
53.08	0.1837	47.48	0.08742	61.27	0.2928
48.91	0.11411	49.79	0.12976	58.18	0.25524
51.83	0.16402	47.19	0.08182	54.82	0.2096
51.61	0.16045	45.18	0.04097	55.50	0.21928
51.28	0.15505	46.57	0.06959	58.23	0.25588
47.58	0.08934	46.94	0.07693	59.51	0.27189
50.31	0.13876	43.99	0.01501	48.69	0.11008
46.94	0.07691	59.65	0.2736	58.18	0.25524
68.50	0.36745	66.87	0.35203	60.79	0.28722
65.14	0.33482	44.91	0.03518	58.51	0.25944
54.96	0.21161	51.06	0.15139	56.18	0.22873
54.88	0.21046	58.62	0.26083	61.28	0.29292

Table A.4: Relative G-line area data for the 1.41 nm eDIPS samples. The area of the unfilled DWCNT (host tube) is 41.22.

integrated area	G_{la}
56.93	0.27595
50.49	0.18359
50.85	0.18937
55.36	0.25541
50.71	0.18714
52.69	0.21768
54.44	0.24283
51.01	0.19192
51.8	0.20424
64.72	0.3631
57.75	0.28623
63.05	0.34623
65.44	0.37011
60.07	0.3138
52.25	0.21109
61.78	0.33279
67.28	0.38733
55.01	0.25068
64.96	0.36545
60.86	0.3227
70.53	0.41556

Table A.5: G-line area data for the CVD CNT samples from [14]. The area of the unfilled DWCNT (host tube) is 37.48.

integrated area	G_{la}
60.898	0.38454
55.57	0.32554
58.4	0.35822
48.32	0.22434
54.17	0.3081
41.36	0.09381
38.15	0.01756
41.024	0.08639
39.46	0.05018
40.35	0.07113
41.95	0.10656
41.8	0.10335
40.78	0.08092
54.04	0.30644
42.1	0.10974

4

Results: Optimizing the synthesis of confined carbyne

In this section, the yield determination model was applied to quantify the influence of key parameters in the confined carbyne synthesis. This work has been published in Small Methods (C. Freytag et al. [238]). The main experimental work of synthesizing the confined carbyne and the data evaluation was performed by me, with support from Christin Schuster. I am the main author of the manuscript. The nanotube host tubes were provided by Dr. Takeshi Saito (eDIPS) and Prof. Kazuhiro Yanagi (arc-discharge). Below, the findings from this paper are summarized.

4.1 Summary: A systematic study on confined carbyne synthesis parameters

The synthesis of confined carbyne from different nanotubes and under different conditions has been studied extensively since the first reports by Shi *et al.* [239] (section 1.5.3. High temperature high vacuum annealing is a common and robust method to make confined carbyne from various precursors and host tubes. However, until recently, there was no reliable method for bulk yield evaluation to quantify the influence of individual parameters in the synthesis. Using the new model described in section 3.1 and published in reference [233], here, important synthesis parameters for confined carbyne synthesis are studied and, for the first time, their influence is quantified. These parameters are filling ratio of carbonaceous precursor, annealing step sequences and annealing temperature. Additionally, for the study of optimal annealing temperature, the results from the bulk yield determination model are compared to the previous state of the art method of evaluating the peak intensities of the confined carbyne peak. Three different types of host tubes were studied: 1.45 nm arc-discharge, 1.41 nm eDIPS and 1.33 nm eDIPS. The realized growth potentials are also discussed. For the host tubes used in my work, the optical absorption spectra are shown in figure 4.1. For the 1.45 nm arc-discharge hosts, 48% of the

host tubes are suitable for confined carbyne growth, for the 1.41 nm eDIPS and 1.33 eDIPS host, 35% and 31% are suitable, respectively. These values were determined by integrating the area in within the boundaries of 1.35 to 1.55 nm. The error of this evaluation can be estimated from the signal-to-noise ratio and is below 1%.

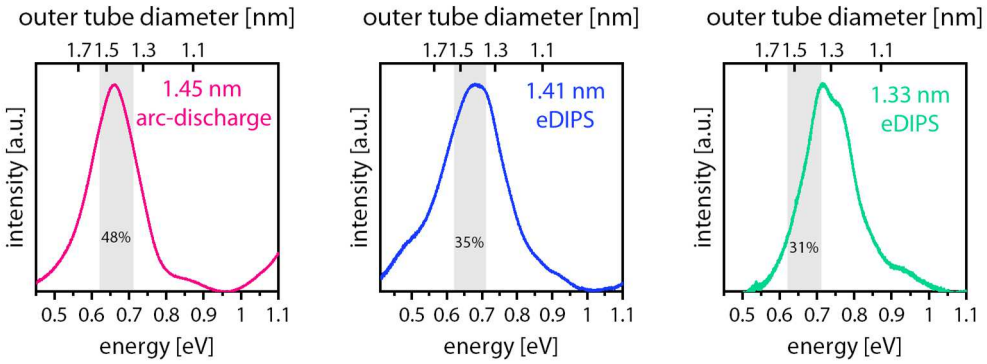

Figure 4.1: Optical absorption spectra of the excitonic E_{11} peak of the studied carbon nanotube hosts: 1.45 nm arc-discharge (left), 1.41 nm eDIPS (middle) and 1.33 nm eDIPS (right).

First, two samples made from 1.45 nm arc-discharge nanotube hosts are compared. One of the samples was filled with C_{60} fullerenes ("F1"), while the other was not filled with any additional carbonaceous material ("U1"). Some amount of carbon is always present inside the nanotubes from their synthesis process, but the samples used are considered very clean. This is why these host tubes for chosen for the comparison here. The bulk yield achieved for these two samples, which were synthesized under the same furnace conditions, was 20% for U1 and 31% for F1. The realized growth potentials, considering the maximum fillability of the 1.45 arc-discharge hosts, are 42% and 65%, respectively. In order to achieve higher bulk yields, one must consider the formation of the inner tubes, which are necessary in order to grow confined carbyne. We assume that all available volume of the suitable nanotubes (1.35 to 1.55 nm) is filled with C_{60} with a center-to-center distance of 0.96 nm between the fullerenes [122]. The interlayer distance between outer and inner tubes is estimated to be 0.36 nm, making the inner tubes in the suitable outer tubes between 0.63 - 0.83 nm. In this case, the number of carbon atoms from the fullerenes can form inner tubes with about 60-70% of the length of the outer wall, depending on diameter and chirality of the inner tubes. Considering that only 48% of the sample fall within this diameter range, a maximum bulk yield of 28%-34% can be expected. This means that in order to increase the yield, one must increase the fraction of outer tubes filled with inner tubes.

Performing two annealing steps with an oxidation step in-between can increase the fraction of inner tubes. During the oxidation step, the single-walled parts are preferentially destroyed, as single-walled carbon nanotubes are less stable than double-walled carbon nanotubes at this temperature [231]. The free carbon from the oxidation can be used to form inner walls and confined carbyne in the remaining parts of the tubes, which further increases the fraction of double-walled carbon nanotubes in the samples. The oxidation step also ensures opening of end-caps of the inner tubes and partial destruction of the double-walled nanotubes and introduces

defects which help the growth of carbyne [222]. While the oxidation step leads to a fracturing of long nanotubes, the resulting segments are still of sufficient length for hosting carbyne. If this were not the case and the chains were significantly shortened, their Raman mode would shift to significantly higher wavenumbers.

Two different pathways were studied in order to quantify the influence of a second annealing step (sample "F2"). In one case, the sample was annealed at 1500°C, then oxidized and then annealed again at 1500°C, so confined carbyne was expected to grow in both steps. In the second case, the first annealing step was performed at only 1300°C, where only inner walls are formed, and in the second step, the annealing temperature was 1500°C. The results from the two-step annealing synthesis showed that in the second annealing step, the yield increased by $\sim 33\%$ from the first to the second step for the 1500°C+1500°C pathway. For the 1300°C+1500°C pathway, a bulk yield of 31% was achieved. It is also interesting to compare the 1300°C+1500°C pathway to the sample that was directly annealed from peapods (F1) in one step discussed above. It shows that forming inner walls as an intermediate does not influence the yield, as very similar values were achieved. The realized growth potentials were 73% and 65% for the 1500°C+1500°C pathway and 1300°C+1500°C pathway, respectively.

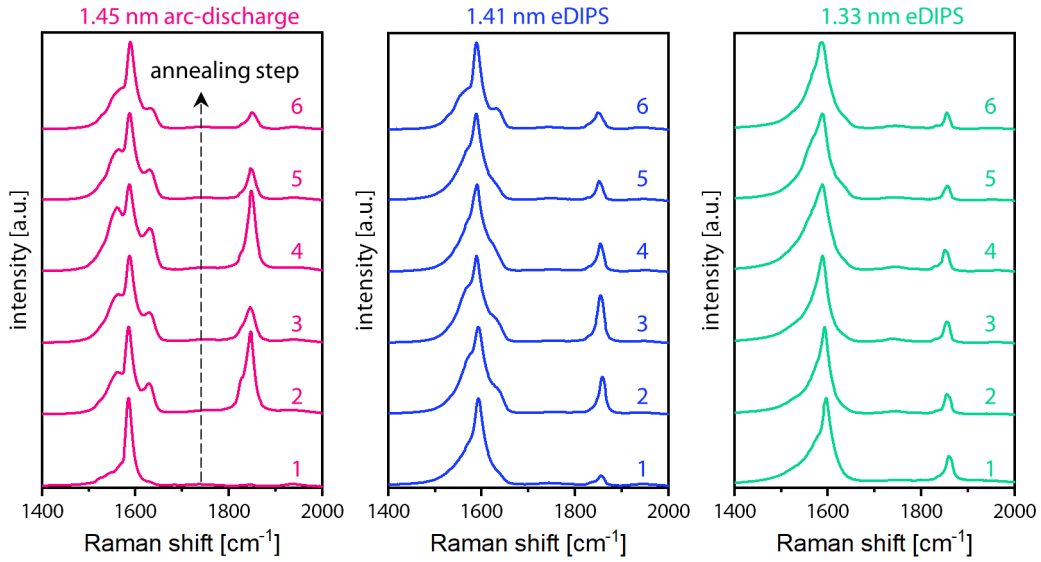

Figure 4.2: Raman spectra of confined carbyne synthesized using multi-step annealing using 1.45 nm arc-discharge (pink), 1.41 nm eDIPS (blue) and 1.33 nm eDIPS (green) host tubes.

Next, more annealing steps were added in order to achieve the full growth potential. In this experiment, all three types of host tubes were used. Sequences of annealing, oxidation and annealing were performed for a total of six annealing steps for each sample (fig. 4.2). For the 1.45 nm arc-discharge hosts and the 1.33 nm eDIPS hosts, the highest bulk yield was achieved after four annealing steps, with 46% and 28%, respectively. For the 1.41 nm eDIPS sample, bulk yields of around 26% and 27% were achieved after two and six steps. For the arc-discharge sample especially, it can be seen that the increase in bulk yield slows after the second annealing step. This is to be expected, since the available carbonaceous feedstock and the amount of single-walled parts of the sample that can be destroyed in the oxidation step decreases. However,

the third and fourth annealing step still increased the bulk yield. After the fourth annealing step, further annealing did not lead to a higher bulk yield.

During the annealing, two processes compete with each other. On one hand, carbyne is formed from carbonaceous precursors inside the double walled carbon nanotubes, increasing the bulk yield. On the other hand, the decrease in bulk yield can be attributed to the destruction of the inner nanotubes at high temperatures due to residual gas in the furnace. Whether the yield will decrease or increase by further annealing depends on the rate at which the two processes occur. As long as enough precursors are inside, the bulk yield can increase, if all precursor material has already been converted to carbyne, the bulk yield can only decrease from destruction. It is however possible that after the destruction of some inner walls, the carbon inside can be used for the formation of more carbyne, which then leads to an increase in yield again. This might be the case for the 1.41 nm eDIPS nanotubes, where the highest bulk yields were measured after two and six steps. The oxidation steps in-between the annealing steps can also play a role, as it can be expected that a certain amount of carbyne will be destroyed in this process. The oxidation stability of confined carbyne inside double-walled carbon nanotubes has been studied and it was shown that the Raman peak of the confined carbyne decreases under oxidation in air, but is very stable in vacuum [240]. This is the reason why the lower pressures were chosen for this step, to avoid destroying too much of the confined carbyne.

When generally comparing the yields of the two different eDIPS host tubes, one can see that the yield was not improved by additional filling with C_{60} fullerenes. A possible explanation is the general availability of amorphous carbon inside the eDIPS carbon nanotubes from the synthesis process, which means that the limiting factor for confined carbyne growth inside eDIPS host tubes is not the carbon source. In comparison, the yield for the more clean arc-discharge host tubes could be significantly improved by filling with C_{60} fullerenes (sample F1/U1). Due to the impurities inside, it is also possible that the filling ratio for the fullerenes is not as high for the eDIPS sample compared to the arc-discharge hosts.

The highest realized growth potentials were 96% for the 1.45 nm arc-discharge sample, 90% for the 1.33 nm eDIPS sample and 77% for the 1.41 nm eDIPS sample. This showed that the synthesis pathway is spot on for the arc-discharge host tubes, but maybe improvements could still me made for the eDIPS sample. Therefore, the optimal synthesis temperature was re-evaluated.

In order to study the optimal synthesis temperature, eDIPS host tubes were annealed at temperatures between 1500°C and 1600°C in steps of 20°C, and multiple spots on the samples were measured in Raman in order to obtain robust averages (fig. 4.3).

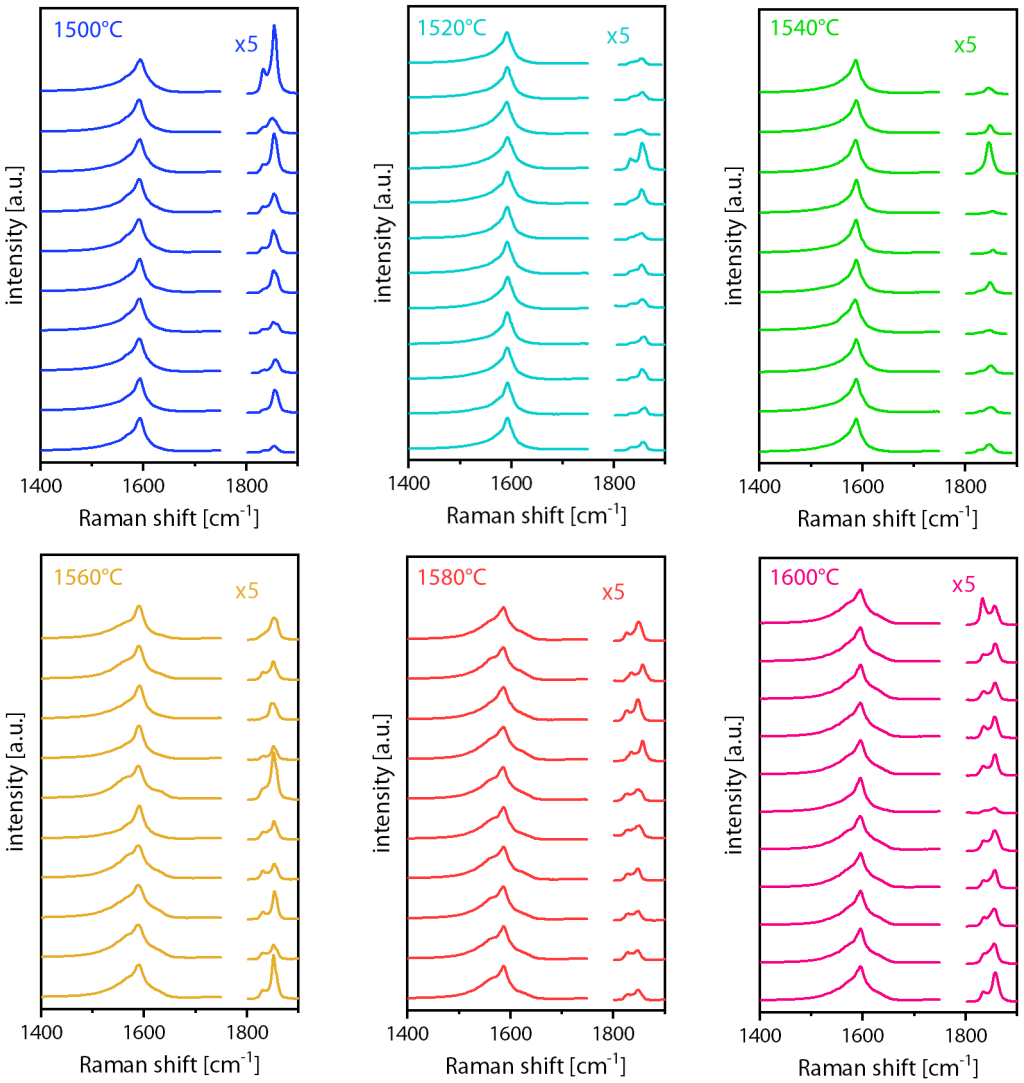

Figure 4.3: Raman spectra of confined carbyne synthesized inside 1.33 nm eDIPS nanotubes at different temperatures from 1500°C to 1600°C in steps of 20°C, measured with a 568 nm laser. The confined carbyne mode at around 1850 cm^{-1} was magnified by a factor of five.

One can immediately see that there is a high variation in the spectra taken from the same sample and the samples are quite inhomogeneous. However, there might still be trends that can be observed when analyzing the bulk yield in detail. Analyzing only the area of the confined carbyne mode, it looked like 1500°C leads to the highest average yield (fig. 4.4a). Using the new area integration model (sec. 3.1) based on the coupled modes, a different trend could be observed where the bulk yields for higher temperatures were higher and the maximum yield could be achieved at 1560°C and the most consistent high yield at 1580°C (fig. 4.4b). This

underlines that the Raman peak of the carbyne chain alone is not a good indicator for the yield, since the Raman mode of the confined carbyne is strongly resonance enhanced. Re-evaluating the optimal synthesis temperature using the new model revealed that higher annealing temperatures lead to a higher bulk yield.

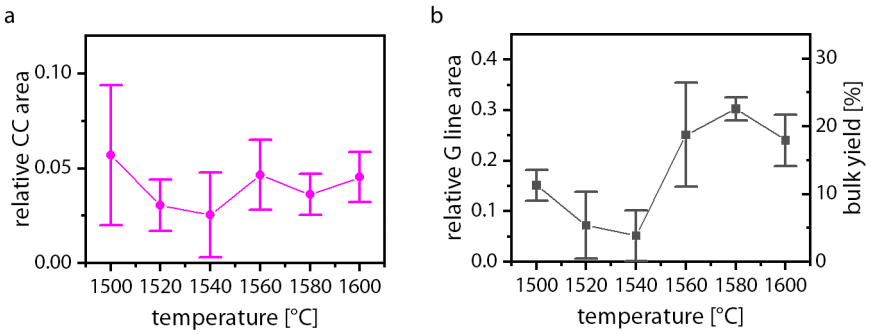

Figure 4.4: Bulk yield of confined carbyne synthesized at different temperatures from 1.33 nm eDIPS host nanotubes: a) relative CC-area at different temperatures between 1500°C and 1600°C from multiple spots on each sample; b) relative G-line area and bulk yield calculation from the same experiment, evaluated using the area integration model.

RESEARCH ARTICLE

small methods
www.small-methods.com

Systematic Optimization of the Synthesis of Confined Carbyne

Clara Freytag, Christin Schuster, Emil Parth, Dido Denier van der Gon, Takeshi Saito, Kazuhiro Yanagi, Paola Ayala, and Thomas Pichler**

Abstract: Confined carbyne, an sp^1-hybridized linear carbon chain inside a carbon nanotube, is a novel material with remarkable properties and potential applications. Among its currently successful synthesis methods, high temperature high vacuum annealing is prevalent. Further optimization could be achieved by tuning the synthesis pathway. Here, a systematic analysis of key synthesis parameters including precursor filling, annealing step sequences, and temperature conditions during high temperature vacuum processing is performed. A novel yield determination model that overcomes previous limitations related to the irregular resonance Raman behavior of carbyne is applied to evaluate bulk yield and realized growth potential. With this refined model, it is possible to make a quantitative assessment of bulk yield optimization potential in multi-step annealing processes. These results provide crucial insights into the fundamental formation mechanisms of confined carbyne, advancing our understanding of this promising hybrid nanomaterial system. It is therefore possible to establish improved protocols for maximizing confined carbyne yields through precise control of synthesis conditions.

1. Introduction

Carbyne is a nanomaterial consisting of an infinite chain of linear sp^{-1}-hybridized carbon atoms. As a true 1D material, it has been predicted to have remarkable optical, electronic and mechanical properties.[1–8] The linear carbon chains can either have continuous double bonds or alternating single-triple bonds with different lengths, which is more stable due to Peierl's distortion.[9] The bond length alternation (BLA), i.e., the difference between the length of the single and triple bond, influences the properties of the carbon chains, such as the bandgap.[10] While the cumulenic structure (double bonds, BLA = 0) is metallic, the polyynic structure (single and triple bonds, BLA ≠ 0) is a semiconductor with a tunable band gap.[11] Many properties of linear carbon chains are length dependent. The term carbyne refers to a material with an "infinitely" long chain, i.e., where the properties become independent of length.[12] The main issue with this material is the lack of stability due to the exothermic collapse of the chain or cross-linking with other chains.[13] End-capping groups can prevent dangling bonds and sterically hinder the collapse of a chain onto itself while spacers impede reaction of chains with each other.

There are many different approaches to synthesize and stabilize linear carbon chains. Polyynes with around 20 carbon atoms end-capped by hydrogen or nitrogen were synthesized by laser vaporization of graphite,[14] in solution using laser ablation of graphite[15,16] and by arc-discharge between graphite electrodes.[17] Organic "bottom-up" synthesis methods have yielded cumulenes with up to 10 carbon atoms[12] and polyynes with up to 44 carbon atoms[18,19] using large organic end-capping groups for stabilization. Recently, with additional stabilization of the chain during synthesis using masking groups and threading the chains through organic macrocycles, even longer chains with up to 68 carbon atoms have been synthesized using this pathway.[20]

Atomic manipulation methods can also lead to interesting structures containing linear carbon. In a transmission electron microscope (TEM), carbon atoms can be removed from a graphene sheet until only a chain remains between two patches of graphene.[21,22] Carbon chains can also be created in situ from graphene flakes by mechanically pulling them apart after electrical contacting to a gold tip inside a TEM.[23] Inside a field ion microscope (FIM), high voltage can be applied to a needle-shaped

C. Freytag, C. Schuster, E. Parth, D. Denier van der Gon, P. Ayala, T. Pichler
University of Vienna
Faculty of Physics
Boltzmanngasse 5, Vienna 1090, Austria
E-mail: clara.freytag@univie.ac.at; thomas.pichler@univie.ac.at
T. Saito
National Institute of Advanced Industrial Science and Technology (AIST)
Nanomaterials Research Institute
1-1-1 Higashi, Tsukuba, Ibaraki 305-8565, Japan
K. Yanagi
Tokyo Metropolitan University
Department of Physics
1-1 Minami-Osawa, Hachioji, Tokyo 192-0397, Japan

The ORCID identification number(s) for the author(s) of this article can be found under https://doi.org/10.1002/smtd.202500075

DOI: 10.1002/smtd.202500075

sample of carbon-based fibers, unraveling chains of carbon from the tip.[24] Recently, a chain with 120 carbon atoms was manufactured in situ using an atomic force microscope (AFM) by demetallization of an organometallic polyyne precursor on a gold surface.[25]

A first pathway to carbyne was found by stabilizing the carbon chain inside small-diameter double-walled carbon nanotubes (DWCNTs).[26] The interaction of the carbyne chain with the host tube stabilizes the chain and sterically prevents the cross-reactions of the chain with itself. In recent years, different synthesis routes for confined carbyne inside carbon nanotubes (CC@CNT) have been developed.[27–30] The most common methods are based on high temperature annealing in high vacuum (HV). Confined carbyne (CC) can grow directly inside as-grown chemical vapor deposition (CVD) DWCNTs[26] or enhanced direct injection pyrolitic synthesis (eDIPS) single-walled carbon nanotubes (SWCNTs).[31] In the case of direct annealing of SWCNT hosts, the inner walls are formed during the annealing, together with the carbyne. The growth of carbyne inside the host CNTs is limited by the availability of carbonaceous precursor. Some amount of carbon feedstock is generally present inside the CNTs from their synthesis, but more can be supplied by filling the host tubes with small organic molecules such as methanol,[30] fullerenes[29] or short chain linear polyynes[32–34] or by oxidizing the DWCNT host to create defects.[35] Photothermal synthesis is an alternative to high temperature annealing in HV.[28] Recently, low temperature annealing has been used to synthesize weakly confined carbyne from surfactant molecules[36] or aromatic hydrocarbons[37] as carbonaceous precursors inside SWCNTs.

In this work, we focus on the quantification of the influence of different parameters in the synthesis of CC. The growth of CC is governed by three main factors: a) availability of carbonaceous precursors inside the host nanotube, b) annealing temperature, and c) residual gas pressure in the furnace. Additionally, the achievable bulk yield is limited by the fraction of carbon nanotube hosts with the appropriate diameter among the diameter distribution of the specific sample.[38] Therefore, it is possible to evaluate the realized growth potential achieved by relating the bulk yield to the fraction of fillable tubes, providing a useful metric to evaluate the success of the synthesis process.

2. Results and Discussion

2.1. Influence of Providing Additional Carbonaceous Precursor via Filling

The growth of confined carbyne is partially governed by the availability of carbonaceous feedstock in the host nanotubes. This led us to evaluate the effect of filling carbonaceous precursors inside small diameter SWCNTs. As an exemplary case study, the CC bulk yield after annealing of unfilled and C_{60} filled 1.45 nm arc-discharge SWCNTs was compared. For filling, the CNTs were first oxidized in air at 450°C for 30 min to open the end-caps. Next, the sample and the fullerenes were placed in a glass ampoule which was then evacuated to HV and placed inside a furnace for 12 h at 550°C to create peapods. Both the peapods and the unfilled sample were placed into a ceramic furnace together for annealing to ensure the same experimental conditions during the annealing step.

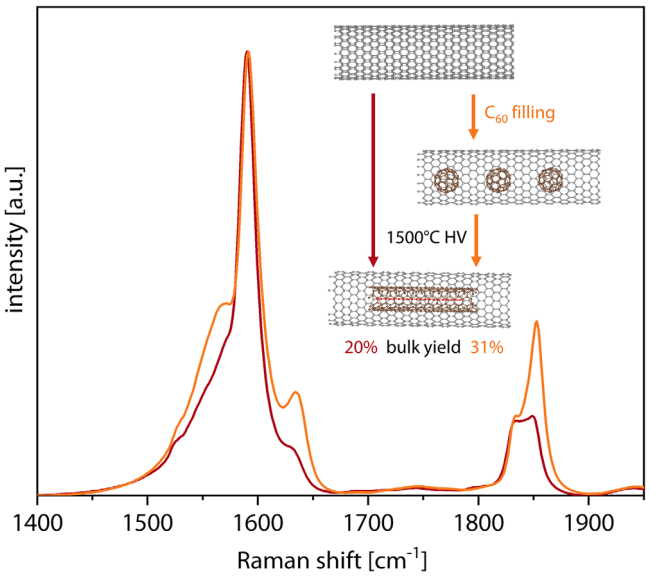

Figure 1. Effects of filling carbon nanotube hosts (1.45 nm arc-discharge) with C_{60} on CC yield: Raman spectra of CC from an unfilled nanotube host (red) and from peapods (orange), measured with a 568 nm laser. The bulk yield increases from 20% to 31%. A schematic of the synthesis process for the filled versus unfilled host tubes is also shown.

In **Figure 1**, Raman spectra of CC@DWCNTs grown from the unfilled and the C_{60} filled hosts are shown. In the Raman spectra, changes in the peak attributed to the CC at around 1850 cm^{-1} and to the G-line of the host DWCNT can be observed. The CC-peak is made up of multiple components according to the geometry of the surrounding inner host tube.[39] Depending on the growth rate inside the different inner tubes, combined with the narrow resonance window and strong resonance enhancement of the CC-mode, the components may appear with different intensities. This demonstrates the unreliability of using the CC-mode for yield determination. The growing left and right shoulders in the G-lines were recently explained by anharmonic phonon-phonon interaction as coupled modes between the host nanotube and the carbyne chain.[40] While the CC-peak is strongly resonance dependent, the G-line shoulders follow the more stable resonance behavior of the chain and can therefore be reliably used to determine the bulk yield. The coupled mode evaluation model is described in detail in Section 4 and the work of Schuster *et al.*[38] Using this method, an improvement in the bulk yield from 20% to 31% was determined when filling the SWCNT hosts with C_{60} as a carbonaceous feedstock.

2.2. Improving the Yield via a Multi-Step Annealing Process

Two-step annealing processes have previously shown to improve the CC yield.[29,35] To quantify the influence of a second annealing step and the introduction of a double-walled intermediate, peapods made from 1.45 nm arc-discharge CNTs were used as hosts for two different synthesis pathways. One half of the original sample was annealed in HV for 1 h at 1500°C to immediately grow CC. The other half was annealed in HV for 2 h at 1300°C

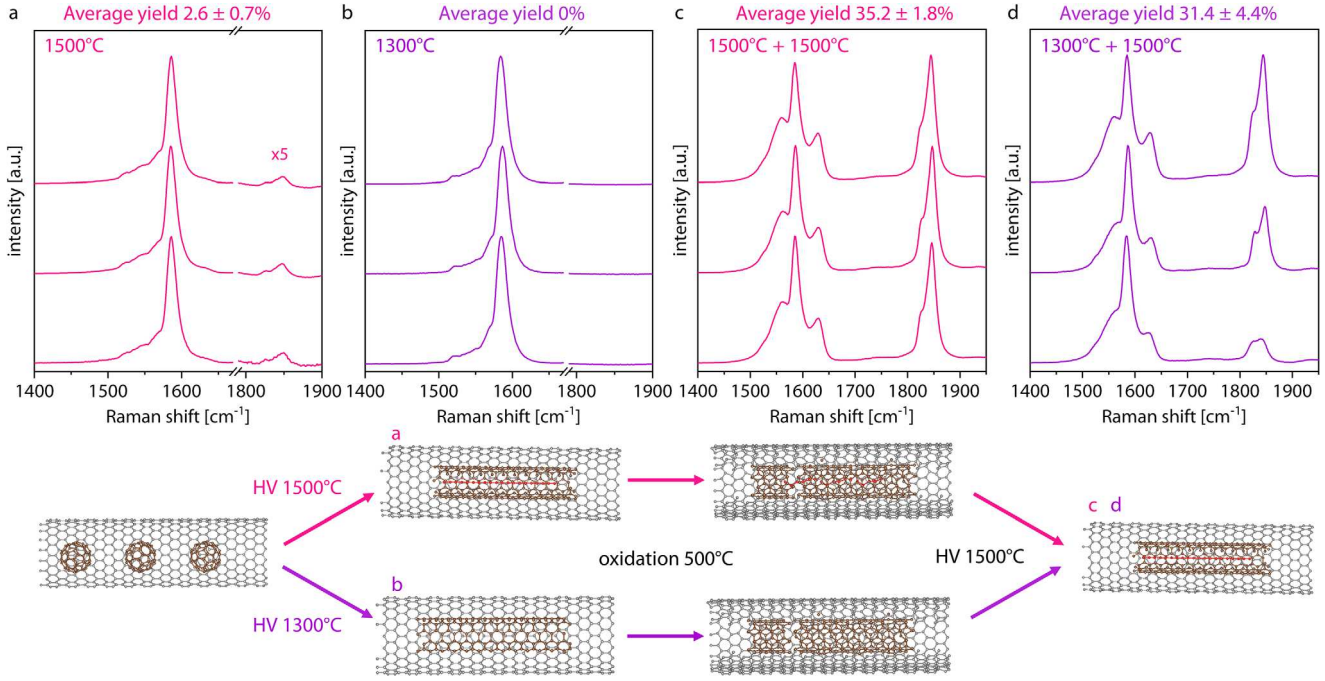

Figure 2. Two-step synthesis process for CC grown from 1.45 nm arc-discharge peapods: Raman spectra of 3 spots on the sample after a) annealing once at 1500°C; b) annealing once at 1300°C; c) annealing twice at 1500° C with an oxidation step in-between; d) annealing first at 1300° C and then at 1500° C with an oxidation step in-between. All Raman spectra were measured with a 568 nm laser. Below, the process of carbyne growth from peapods is shown schematically.

in order to first only grow DWCNTs as an intermediate. In both cases, the maximum length of CNTs where inner walls (and CC) can be grown is around two thirds, governed by the amount of fullerenes inside. In the following step, both halves were placed in a furnace and oxidized at 500°C for 1 h at 600 mbar of air, where the single-walled parts are preferentially destroyed, as SWCNTs are less stable than DWCNTs at this temperature.[41] The free carbon from etching can be used to form inner walls and CC in the remaining parts of the tubes, which further increases the fraction of DWCNTs in the samples. The oxidation step also ensures opening of the end-caps of the inner tubes and partial destruction of the DWCNTs and introduces defects which help the growth of carbyne.[35] While the oxidation step leads to a fracturing of long nanotubes, the resulting segments are still of sufficient length for hosting carbyne. In the second annealing step, both halves of the sample were annealed at 1500°C for 1 hour in HV to grow carbyne.

Raman spectra were taken after the first and second annealing step for both pathways (**Figure 2**). After the first annealing step, there is only a very small peak visible for CC (Figure 2a) and the G-line very closely resembles the G-line area of the DWCNTs made by annealing once at 1300°C (Figure 2b). After the second annealing step, both samples showed strong CC peaks and the characteristic G-line shoulders resulting from coupled modes appear for both samples. The evaluation of the G-line area and subsequent calculation of bulk yield showed that both samples have a similar average bulk yield of 35% for the 1500°C+1500°C pathway and 31% for the 1300°C+1500°C pathway. The fraction of theoretically fillable host nanotubes of the 1.45 nm arc-discharge CNTs was calculated to be 48% from optical absorption data (see Supporting Information S3). The realized growth potential, relating the bulk yield to this maximum fillabilty of the host nanotubes, was determined to be 73% and 65% for the two pathways, respectively, with the two-step method of annealing from peapods.

2.3. Analysis of Multiple Annealing Steps: How Close Can We Get to The Maximum Fillability

Since it was shown that two annealing steps with oxidation in-between can improve the bulk yield of CC, it was tested if more repetitions will further improve the yield. This experiment was conducted with three types of CNT hosts: 1.45 nm arc-discharge nanotubes, 1.33 nm eDIPS nanotubes and 1.41 nm eDIPS nanotubes. The 1.45 nm arc-discharge and 1.41 nm eDIPs nanotubes were filled with C_{60} fullerenes prior to the first annealing step. All samples were then annealed a total of six times in HV for 1 hour at 1500° C, with an oxidation step at 500° C for 1 h at 600 mbar of air between annealing. Raman spectra were taken after each annealing step for each of the CNT hosts (**Figure 3**).

For the 1.45 nm arc-discharge and the 1.33 nm eDIPS CNT hosts, the highest bulk yield was achieved after four annealing steps, with 46% and 28%, respectively (Figure 3a). Further annealing did not lead to a higher bulk yield as during annealing, two processes compete with each other. On one hand, carbyne is formed from carbonaceous precursors inside the DWCNTs, increasing the bulk yield. On the other hand, the residual gas inside the furnace destroys the inner nanotubes and the carbyne chains, leading to a decrease in the bulk yield (Figure 3d).

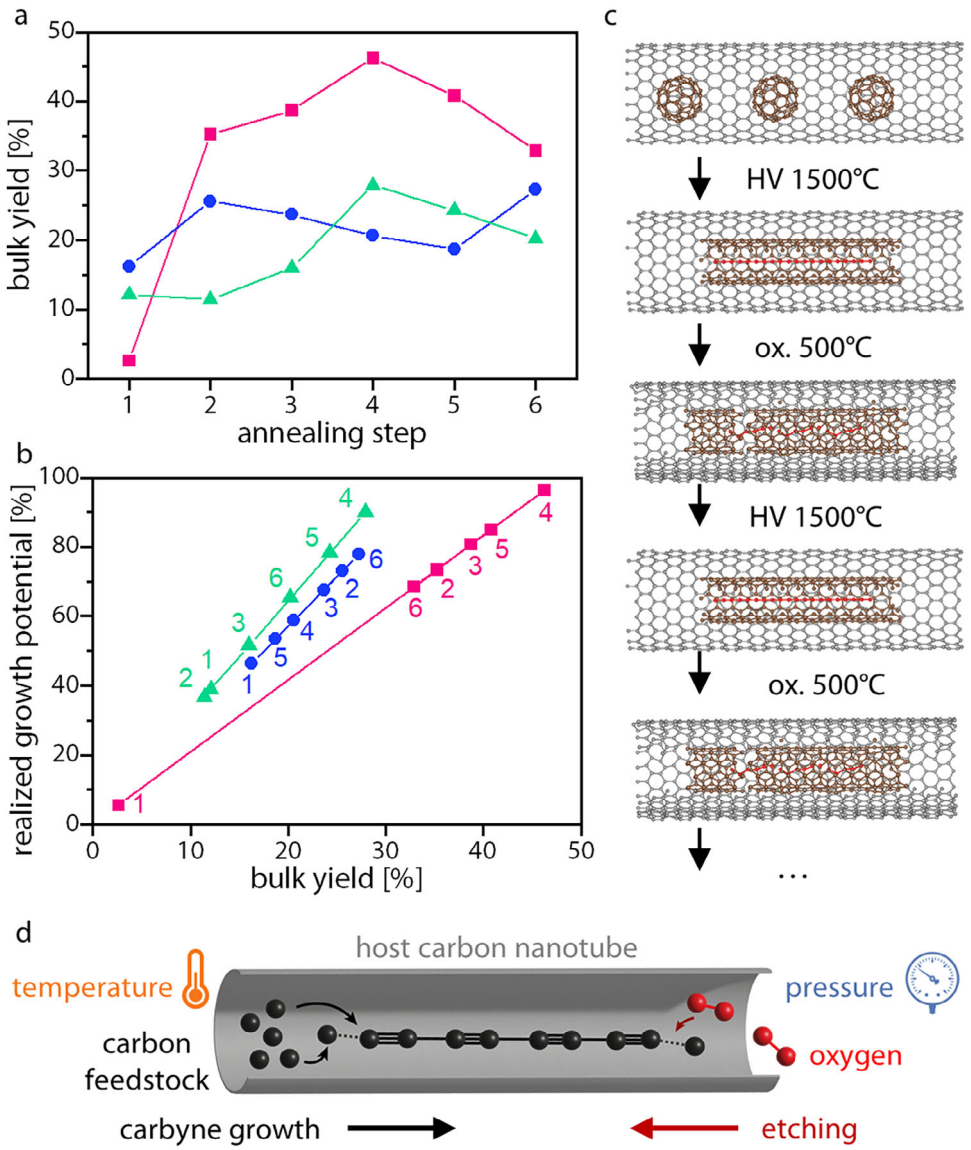

Figure 3. Multi-step synthesis of CC inside different CNT hosts: a) bulk yield of CC inside 1.45 nm arc-discharge (pink square), 1.33 nm eDIPS (green triangle) and 1.41 nm eDIPS (blue circle); b) realized growth potential for the different CNT hosts; c) schematic of the multi-step annealing process from peapods; d) growth model for CC: two processes compete with each other - formation of the carbyne chain, which is governed by the temperature and availability of carbonaceous feedstock, and etching/destruction of the carbyne chain due to residual gas in the furnace (i.e., pressure).

Whether the yield will increase or decrease by further annealing depends on the rate at which the two processes occur. As long as enough precursors are inside, more carbyne is formed, while carbyne is etched, i.e., broken down after most precursor has already been converted to inner nanotubes or carbyne. After the etching of some inner walls and chains, the resulting carbon inside can be used as new precursor for the formation of more carbyne, leading to an increase in yield once more. This might be the case for the 1.41 nm eDIPS nanotubes, where the highest bulk yields of around 26% and 27% were measured after two and six steps. In Figure 3b, the realized growth potential for each nanotube host type is plotted, based on the CNT hosts containing only a certain fraction of tubes with the appropriate diameter for carbyne growth. Maximum fillabilties of 48%, 31% and 35% were determined from optical absorption (see Supporting Information S1–S3) for the 1.45 nm arc-discharge, the 1.33 nm eDIPS and for the 1.41 eDIPS hosts, respectively. For the 1.45 nm arc-discharge peapods, with 96%, almost the full growth potential could be achieved while 90% of the growth potential was realized for the 1.33 nm sample. For the 1.41 nm eDIPS sample, 77% realized growth was accomplished.

The yield results from a complex interplay between etching and growth of inner walls and carbyne chains. Therefore, the knowledge of the realized growth potential is essential to determine the optimal number of annealing and oxidation steps. When comparing the two different eDIPS host tubes, the bulk yield is not improved by additional filling with C_{60} fullerenes. A possible explanation is the general availability of amorphous

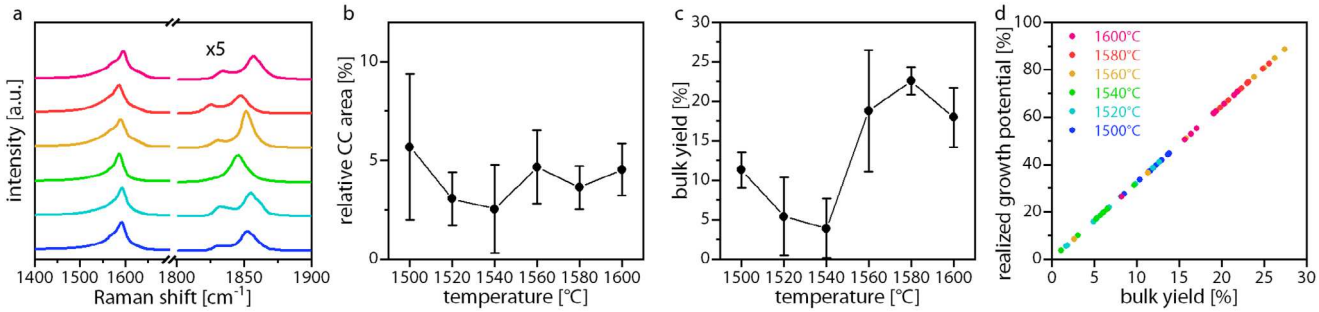

Figure 4. Temperature optimization for CC synthesis: a) Raman spectra of CC synthesized from 1.33 nm eDIPS nanotube hosts at different temperatures from 1500°C (bottom) to 1600°C (top) in steps of 20°C, measured using a 568 nm laser. The mode of the CC at around 1850 cm^{-1} was magnified by a factor of five; b) relative area of the LO-peak of CC at different temperatures between 1500 and 1600°C from multiple spots on each sample; c) bulk yield calculated using the coupled mode evaluation model from the same experiment; d) bulk yield and realized growth potential calculated for all spectra.

carbon inside eDIPS CNTs from their synthesis process, indicating that the limiting factor for CC growth inside eDIPS host tubes is not the carbon source. In comparison, the yield for the "cleaner" arc-discharge host tubes was significantly improved by filling with C_{60} fullerenes, as discussed in Section 2.1.

2.4. Re-Evaluating the Optimal Synthesis Temperature

In previous studies, temperatures of 1500°C or slightly below were used for high temperature annealing.[26,29–31,35] Since it was shown in Section 2.3 that the full growth potential was not yet realized for the eDIPS host tubes, it was investigated if higher annealing temperatures could improve the yield. Additionally, the novel method for yield determination (coupled mode evaluation model) was compared to the established practice of comparing the areas of the CC-peaks at around 1850 cm^{-1}.[29] For this experiment, eDIPS CNTs with a mean diameter of 1.33 nm were used as host tubes. The nanotube samples were annealed in HV for 1 h with annealing temperatures between 1500 and 1600°C in steps of 20°C. The eDIPS nanotubes were shown to have enough carbon inside from the synthesis process so carbyne can grow without filling with a carbonaceous precursor. The associated Raman spectra are shown in **Figure 4**. For each sample, at least 10 spots were measured to determine the average bulk yield (see Supporting Information S4).

From the analysis of the CC-mode alone (Figure 4b) one might conclude that higher temperatures do not significantly improve the CC yield. However, the relative CC-peak area is not directly related to the bulk yield. The CC-mode intensity strongly varies among different spots, as the signal is dependent on the amount of carbyne chains in resonance with the specific laser. Therefore, using our newly developed model which is independent of the resonance behavior of CC, we could determine the actual trend of the bulk yield (Figure 4c). Our results show that the optimal temperature for the synthesis of CC inside 1.33 nm eDIPS hosts is around 1580°C, with an average bulk yield of 23% and an average realized growth potential of 73% (Figure 4d).

3. Conclusion

Several parameters for the synthesis of carbyne confined inside different CNT hosts and their influence on the bulk yield were quantitatively evaluated utilizing a novel method of yield determination.[38] Filling the CNT hosts with a carbonaceous precursor strongly improves the yield for arc-discharge CNT hosts. Repeating the annealing step with an oxidation step in-between also increases the bulk yield. Whether only DWCNTs are grown in the first step (1300°C) or there is inner wall and carbyne growth (1500°C) at the same time was not found relevant. When testing a multi-step procedure with more repetitions of high temperature annealing, the highest yields were observed after four steps for some samples, with additional steps leading to lowering of the yield. For another sample, the highest yields were observed after two and six steps, with lower yields observed for the steps in-between. Therefore, we propose a mechanism of concomitant carbyne growth from carbon feedstock and destruction of the carbyne due to residual gas inside the furnace. The availability of carbon feedstock limits the growth and the interplay of the two mechanisms determines whether the yield increases or decreases. Using the new model for yield quantification, it was determined that the optimal temperature for high temperature HV annealing for the eDIPS host tubes is around 1580°C. These findings show that the optimal synthesis temperature and number of annealing steps may vary when using different host nanotubes. For comparability, here, the same oxidation and annealing experimental conditions were applied to all three of the samples. However, each sample has different optimal conditions depending on the carbonaceous material inside and the diameter distribution. During the oxidation process, the stability of the CC@DWCNTs strongly depends on the diameter/chirality of the inner and outer tubes, which is dependent on the synthesis and separation methods used to prepare the SWCNT hosts. This underlines the importance of reliable methods for yield determination and the usefulness of the realized growth potential as a metric for the success of the synthesis and allows optimization of the synthesis pathway for individual samples. Here, optimizing the relative fraction of the carbonaceous precursors by stepwise re-oxidation and annealing is a suitable pathway to achieve the growth of CC@DWCNT with close to 100% growth efficiency.

4. Experimental Section

The CC@DWCNT samples were prepared using a ceramic furnace set-up with ultra-high vacuum at room temperature and high vacuum (<10^{-5} mbar) at the annealing temperatures. The details of the synthe-

sis are discussed in the relevant sections in the results chapter. The yield was determined using the coupled mode evaluation model, based on the changes in the G-mode of CC@DWCNT samples compared to unfilled DWCNTs.[38] The area of the G-mode of the DWCNTs is subtracted from the G-line area of the CC@DWCNT sample and then divided by the G-line area of the CC@DWCNT sample in order to obtain the relative area percentage of the G-mode contributed by the carbyne chain. This was then calibrated to obtain absolute bulk yield values. The realized growth potential referenced in the results section refers to the yield related to the amount of CNT hosts with a suitable diameter for carbyne growth. The diameter distribution of all samples were determined using optical absorption spectroscopy (see Supporting Information S1–S3). The optical absorption measurements were made with a Bruker vertex 80v spectrometer. The measurements were performed on thin films on BaF_2 wedges.

The challenges of systematic investigations into carbyne synthesis parameters are the inhomogeneity of the samples and the lack of exact control over some of the parameters, such as the pressure inside the furnace during the high temperature HV annealing. The issue of inhomogeneity was mitigated by measuring multiple spots depending on the size of the sample in order to obtain robust averages. For example, for the temperature evaluation, at least 10 spots were measured on each sample (see Supporting Information). For the evaluation of the optimal number of annealing steps, the same spot on the sample was measured after each step to ensure comparability. Additionally, samples can be put into the furnace together to ensure the same external parameters, such as temperature and pressure, for optimal comparability.

The Raman measurements of all samples were made with a Horiba LabRAM HR spectrometer combined with an Ar^+/Kr^+ laser (Coherent Innova 70C). All spectra were measured with a wavelength of 568 nm. As detector, a liquid nitrogen cooled CCD chip was used.

All structure models were made using VESTA.[42]

Statistical Analysis: The Raman spectra were normalized to the intensity of the G-line. Average values from different spots on the samples (Figure 2) correspond to the mean ± the standard deviation. In Figure 4b,c, the sample sizes were 10 to 12 (see Supporting Information S4). Mean values are plotted, the standard deviation is shown as error bars. For the area estimations in the optical absorption spectra (Supporting Information S1–S3), a linear background subtraction was performed.[43]

Supporting Information

Supporting Information is available from the Wiley Online Library or from the author.

Acknowledgements

This work was in part funded by the Austrian Science Fund (FWF), Doctoral College Advanced Functional Materials-Hierarchical Design of Hybrid Systems (10.55776/DOC85) (C.F., P.A. and T.P.). C.S., T.P., and E.P. received funding from the European Research Council (ERC) under the European Union's Horizon 2020 research and innovation program (MORETEM ERC-SYN project, grant agreement No. 951215). D. D. acknowledges funding from the Vienna Doctoral school in Physics. P.A. acknowledges the COST Action EsSENce CA119, supported by COST (European Cooperation in Science and Technology). K.Y. acknowledges support from JSPS KAKENHI, Grant Nos. JP23H00259, and JP24H01200, and US-JAPAN PIRE, Grant No. JPJSJRP20221202, Japan, and ASPIRE project, Grant No. JPMJAP2310, Japan.

Conflict of Interest

The authors declare no conflict of interest.

Data Availability Statement

The data that support the findings of this study are available from the corresponding author upon reasonable request.

Keywords

carbyne, confined carbyne, carbon nanotubes, Raman spectroscopy, synthesis

Received: January 13, 2025
Revised: March 7, 2025
Published online:

[1] A. Al-Backri, V. Zólyomi, C. J. Lambert, *J. Chem. Phys.* **2014**, *140*, 10.
[2] Y. Cui, Q. Wei, H. Park, C. M. Lieber, *science* **2001**, *293*, 1289.
[3] E. Fazio, F. Neri, S. Patanè, L. D'urso, G. Compagnini, *Carbon* **2011**, *49*, 306.
[4] M. Liu, V. I. Artyukhov, H. Lee, F. Xu, B. I. Yakobson, *ACS nano* **2013**, *7*, 10075.
[5] Y. Wang, Y. Huang, B. Yang, R. Liu, *Carbon* **2006**, *44*, 456.
[6] Z. Zanolli, G. Onida, J.-C. Charlier, *ACS nano* **2010**, *4*, 5174.
[7] K. Zhang, Y. Zhang, L. Shi, *Chin. Chem. Lett.* **2020**, *31*, 1746.
[8] S. Kotrechko, I. Mikhailovskij, T. Mazilova, E. Sadanov, A. Timoshevskii, N. Stetsenko, Y. Matviychuk, *Nanoscale Res. Lett.* **2015**, *10*, 1.
[9] R. E. Peierls, *Quantum theory of solids*, Clarendon Press, **1996**.
[10] F. Banhart, *ChemTexts* **2019**, *6*, 1.
[11] C. S. Casari, M. Tommasini, R. R. Tykwinski, A. Milani, *Nanoscale* **2016**, *8*, 4414.
[12] J. A. Januszewski, R. R. Tykwinski, *Chem. Soc. Rev.* **2014**, *43*, 3184.
[13] R. B. Heimann, *The Nature of Carbyne- Pros and Cons*, Springer Netherlands, ISBN 9789401147422, **1999**, pp. 7–15.
[14] J. R. Heath, Q. Zhang, S. C. O'Brien, R. F. Curl, H. W. Kroto, R. E. Smalley, *J. Am. Chem. Soc.* **1987**, *109*, 359.
[15] M. Tsuji, T. Tsuji, S. Kuboyama, S.-H. Yoon, Y. Korai, T. Tsujimoto, K. Kubo, A. Mori, I. Mochida, *Chem. Phys. Lett.* **2002**, *355*, 101.
[16] P. Marabotti, S. Peggiani, S. Melesi, B. Rossi, A. Gessini, A. L. Bassi, V. Russo, C. S. Casari, *Small* **2024**, *20*, 49.
[17] F. Cataldo, *Carbon* **2003**, *41*, 2671.
[18] W. A. Chalifoux, R. R. Tykwinski, *Comptes Rendus. Chimie* **2008**, *12*, 341.
[19] W. A. Chalifoux, R. R. Tykwinski, *Nat. Chem.* **2010**, *2*, 967.
[20] C. W. Patrick, Y. Gao, P. Gupta, A. L. Thompson, A. W. Parker, H. L. Anderson, *Nat. Chem.* **2023**, *16*, 193.
[21] A. Chuvilin, J. C. Meyer, G. Algara-Siller, U. Kaiser, *New J. Phys.* **2009**, *11*, 083019.
[22] C. Jin, H. Lan, L. Peng, K. Suenaga, S. Iijima, *Phys. Rev. Lett.* **2009**, *102*, 205501.
[23] O. Cretu, A. R. Botello-Mendez, I. Janowska, C. Pham-Huu, J.-C. Charlier, F. Banhart, *Nano Lett.* **2013**, *13*, 3487.
[24] I. M. Mikhailovskij, N. Wanderka, V. A. Ksenofontov, T. I. Mazilova, E. V. Sadanov, O. A. Velicodnaja, *Nanotechnology* **2007**, *18*, 475705.
[25] W. Gao, W. Zheng, L. Sun, F. Kang, Z. Zhou, W. Xu, *Natl. Sci. Rev.* **2024**, *11*, 3.
[26] L. Shi, P. Rohringer, K. Suenaga, Y. Niimi, J. Kotakoski, J. C. Meyer, H. Peterlik, M. Wanko, S. Cahangirov, A. Rubio, Z. J. Lapin, L. Novotny, P. Ayala, T. Pichler, *Nat. Mater.* **2016**, *15*, 634.
[27] L. Shi, R. Senga, K. Suenaga, H. Kataura, T. Saito, A. P. Paz, A. Rubio, P. Ayala, T. Pichler, *Nano Lett.* **2021**, *21*, 1096.
[28] L. Shi, R. Senga, K. Suenaga, J. Chimborazo, P. Ayala, T. Pichler, *Carbon* **2021**, *182*, 348.

[29] Y. Feng, W. Zhang, K. Tang, Y. Chen, J. Zhang, K. Cao, W. Cui, L. Shi, *Nano Res.* **2024**, *17*, 6274.
[30] W. Cui, L. Shi, K. Cao, U. Kaiser, T. Saito, P. Ayala, T. Pichler, *Angew. Chem., Int. Ed.* **2021**, *60*, 9897.
[31] L. Shi, P. Rohringer, P. Ayala, T. Saito, T. Pichler, *Phys. Status Solidi B* **2013**, *250*, 2611.
[32] C. Zhao, R. Kitaura, H. Hara, S. Irle, H. Shinohara, *J. Phys. Chem. C* **2011**, *115*, 13166.
[33] W. Chang, F. Liu, Y. Liu, T. Zhu, L. Fang, Q. Li, Y. Liu, X. Zhao, *Carbon* **2021**, *183*, 571.
[34] K. Tang, Y. Li, Y. Chen, W. Cui, Z. Lin, Y. Zhang, L. Shi, *Nanomaterials* **2024**, *14*, 966.
[35] W. Cui, F. Simon, Y. Zhang, L. Shi, P. Ayala, T. Pichler, *Adv. Funct. Mater.* **2022**, *32*, 2206491.
[36] B.-W. Zhang, X.-Y. Qiu, Y. Ma, Q. Hu, A. Fitó-Parera, I. Kohata, Y. Feng, Y. Zheng, C. Zhang, Y. Matsuo, Y. Wang, S. Chiashi, K. Otsuka, R. Xiang, D. I. Levshov, S. Cambré, W. Wenseleers, S. V. Rotkin, S. Maruyama, *arXiv* **2024**.
[37] Y. Chen, K. Tang, W. Zhang, H. Cao, H. Zhang, Y. Feng, W. Cui, Y. Hu, L. Shi, G. Yang, *arXiv* **2024**.
[38] C. Schuster, C. Freytag, W. Cui, L. Shi, E. Parth, D. Denier van der Gon, T. Saito, K. Yanagi, T. Pichler, *Carbon* **2025**, *234*, 119979.
[39] S. Heeg, L. Shi, L. V. Poulikakos, T. Pichler, L. Novotny, *Nano Lett.* **2018**, *18*, 5426.
[40] E. Parth, A. Corradini, W. Cui, W. Romanin, C. Schuster, C. Freytag, L. Shi, K. Yanagi, M. Calandra, T. Pichler, *preprint available at Research Square* **2024**.
[41] H. Muramatsu, T. Hayashi, Y. Kim, D. Shimamoto, Y. Kim, K. Tantrakarn, M. Endo, M. Terrones, M. Dresselhaus, *Chem. Phys. Lett.* **2005**, *414*, 444.
[42] K. Momma, F. Izumi, *J. Appl. Crystallogr.* **2011**, *44*, 1272.
[43] O. Jost, A. Gorbunov, W. Pompe, T. Pichler, R. Friedlein, M. Knupfer, M. Reibold, H.-D. Bauer, L. Dunsch, M. Golden, J. Fink, *Appl. Phys. Lett.* **1999**, *75*, 2217.

5

Results: Introducing heteroatoms into the confined carbyne system

5.1 Summary: Hybrid systems with nitrogen

Nitrogen was introduced into the confined carbyne system by using doped fullerenes as carbonaceous precursors. The preliminary work on this was done by Dr. Weili Cui and Prof. Lei Shi, which is shown in figure 2 in the attached paper. They demonstrated the feasibility of growing confined carbyne from the doped precursor. I then repeated the experiment with support from Christin Schuster and performed line-shape analyses on the meticulously calibrated spectra, shown in figures 3 and 4 in the paper. I was the main author of the manuscript. The nanotube host tubes were provided by Prof. Kazuhiro Yanagi and the doped fullerenes were provided by Dr. Nikos Tagmatarchis and Dr. Rubén Cantón-Vitoria. The manuscript was submitted to The Journal of Physical Chemistry Letters (submission date: 08.04.2025).

The second part of my work was the introduction of heteroatoms into the confined carbyne system. One possible method to dope the nanotubes and the carbyne chain is to fill a specifically doped precursor into the host tubes. In this case, azafullerenes (C_{59})N) were used, which should behave similarly to the well studied C_{60} fullerenes as precursors. For comparison, the experiment was performed under the same conditions for the doped and undoped peapods using the same host tubes. First, inner walls were grown from the peapods and the Raman spectra were evaluated. This showed a downshift of the components of the G-mode and 2D-mode of the double-walled carbon nanotubes, which confirms the incorporation of nitrogen into the system. Due to the higher mass of nitrogen compared to carbon, the Raman frequency is expected to be lower for nitrogen doped nanotubes. Additionally, downshifts can be attributed to strain.

Next, confined carbyne was grown from the undoped and doped double-walled carbon nanotubes. Shifts could also be observed for the components of the confined carbyne mode, but

interestingly, these components shift towards higher wavenumbers. This also confirms the presence of nitrogen, but the shifts must be coming from a different effect on the Raman frequency. Increases or decreases in the surface electron concentration lead to increases in the Raman frequency. While this effect is not dominant for the nanotubes, as the level of additional charge is very low, the confinement to a linear chain increases the effect to the point were net upshifts in the Raman frequencies are observed for the nitrogen doped carbyne.

Regarding the position of the nitrogen in the chains, it is likely that nitrogen atoms would preferentially terminate fragments of carbyne chains, as nitrogen generally forms three covalent bonds. The carbon atoms in the middle of the chain all have four covalent bonds (alternating single and triple bonds), which means the chain end would be ideal for a three-valent atom, preventing dangling bonds at the end of the carbyne chain (fig. 5.1a). Another theoretical possibility for nitrogen to be incorporated into the chain is in a pyridinic way, which would mean a single bond to one carbon atom and a double bond to another carbon atom (fig. 5.1b). Due to the lone electron pair of the nitrogen, this would however not lead to a completely linear geometry, but introduce a kink into the chain. Due to the strong confinement in the small-diameter inner nanotubes, this is considered impossible and would likely lead to a splitting of the chain into two parts. Additionally, due to the double bond, this type of substitution would impose a cumulenic structure on one side, which is generally considered less stable than a polyynic structure.

To my knowledge, there are no computational studies on the positions of heteroatoms in carbyne chains yet. However, a study on the incorporation of nitrogen in graphene nanoribbons showed the preferential formation of the nanoribbons for specific sites of the nitrogen [241]. The nitrogen preferred to distribute along the edges, where less bonds to other carbons exist. It was also shown that the distribution of the non-bonding electrons of nitrogen differs for different bonding sites.

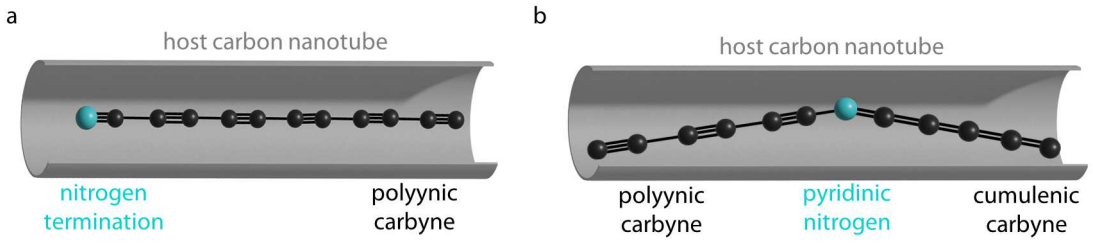

Figure 5.1: Models for hybrid chains with nitrogen: a) likely nitrogen termination; b) ruled out pyridinic-type doping.

Nitrogen doping of confined carbyne

Clara Freytag,*,† Christin Schuster,† Weili Cui,‡ Nikos Tagmatarchis,¶ Rubén Cantón-Vitoria,¶ Lei Shi,‡ Emil Parth,† Kazuhiro Yanagi,§ Paola Ayala,† and Thomas Pichler*,†

†*University of Vienna, Faculty of Physics, Boltzmanngasse 5, 1090 Vienna, Austria*
‡*State Key Laboratory of Optoelectronic Materials and Technologies, Guangdong Basic Research Center of Excellence for Functional Molecular Engineering, Nanotechnology Research Center, School of Materials Science and Engineering, Sun Yat-sen University, Guangzhou 510275, China*
¶*National Hellenic Research Foundation, Theoretical and Physical Chemistry Institute, 48, Vasileos Constantinou Ave., 11635 Athens, Greece*
§*Department of Physics, Tokyo Metropolitan University, 192-0397 Tokyo, Japan*

E-mail: clara.freytag@univie.ac.at; thomas.pichler@univie.ac.at

Abstract

Low-dimensional carbon allotropes belong to the most revolutionary materials of the last decades. Confined carbyne, a linear chain of sp^1-hybridized carbon encapsulated inside a small-diameter carbon nanotube host, is one extraordinary nano-engineering example. Inspired by these hybrid structures, we demonstrate the feasibility to synthesize nitrogen-doped confined carbyne by using azafullerenes ($C_{59}N$) encapsulated in nanotubes ("peapods") as precursors for the growth of confined carbyne. Resonance Raman spectroscopy as a site selective local probe has served to identify the changes in the spectra of nitrogen-doped *versus* pristine carbon peapods and confined carbyne. We are able to disentangle frequency changes due to charge transfer from changes due to the difference in mass for both the nanotube and the carbyne, where different effects dominate. This study demonstrates a suitable pathway to achieve controlled doping of carbyne chains *via* using specifically doped precursors.

Carbyne is a material consisting of an infinitely long linear chain of sp^1-hybridized carbon atoms with extraordinary predicted electronic, optical and mechanical properties.[1–7] In general, linear chains of carbon can have two different bonding geometries, either exhibiting continuous double bonds (cumulenic structure) or alternating single and triple bonds (polyynic structure), with the latter being more energetically favorable due to Peierl's distortion.[8] A linear carbon chain is only considered infinite when the properties of the chain become independent of the chain length, otherwise, they are referred to as polyynes or cumulenes, depending on the bonding situation.[9] Free-standing carbyne is unstable due to exothermic collapse of the chain or cross-linking with other chains.[10] This explains the breakthrough in stabilizing carbyne chains by synthesizing them directly inside double-walled carbon nanotubes (DWCNT).[11] The interaction of the chain with the surrounding CNT stabilizes it and prevents cross-linking or collapse of the chain onto it-

self. Hereafter, we will refer to the hybrid material of carbyne inside carbon nanotube hosts as confined carbyne (CC). The main synthesis method of CC involves high temperature high vacuum annealing of CNTs.[12–14] However, low temperature annealing[15–17] and photothermal synthesis[18] have also been successfully applied. Investigations into the growth mechanisms have shown that CC grows from carbonaceous precursors inside the nanotube hosts that exist from the CNT synthesis process and can be increased by filling the nanotubes with e.g. small organic molecules,[19] short chain polyynes[20] or fullerenes.[14] Through isotopic labeling of C_{60} filled into ultra-clean single-walled carbon nanotubes (SWCNT), it was shown that the inner tube and the chain grow from the fullerenes, and there is also an exchange of carbon atoms between the inner and outer tube and the chain.[21] Furthermore, the possibility to encapsulate azafulleneres into SWCNTs has been demonstrated previously[22] and opens more possibilities exploiting the incorporation of nitrogen as a dopant into nanotubes and confined carbyne.

The primary method to study CC is Raman spectroscopy, since carbyne is an exceptional Raman scatterer.[23] Additionally, shifts in the Raman frequency can be observed for doped CNTs,[24] making it the ideal technique to study doped CC. There are two concomitant effects which contribute to a shift in the Raman frequency of CNTs. First, the change in mass of the dopant influences the frequency according to equation 1, where ν is the frequency of the doped nanotube, ν_0 the frequency of the undoped nanotube, m_0 and m_x are the atomic masses of carbon and the dopant, and c is the relative concentration of the dopant.[25]

$$\frac{\nu_0 - \nu}{\nu_0} = 1 - \sqrt{\frac{m_0}{m_0 + (m_x - m_0)c}} \qquad (1)$$

Additionally, changes in the electronic structure due to charge transfer lead to shifts in the Raman frequency of the G-band in graphene to higher wavenumbers, regardless of p-type or n-type doping. Both the increase and decrease of the surface electron concentration leads to an upshift of the G-band frequency, which has

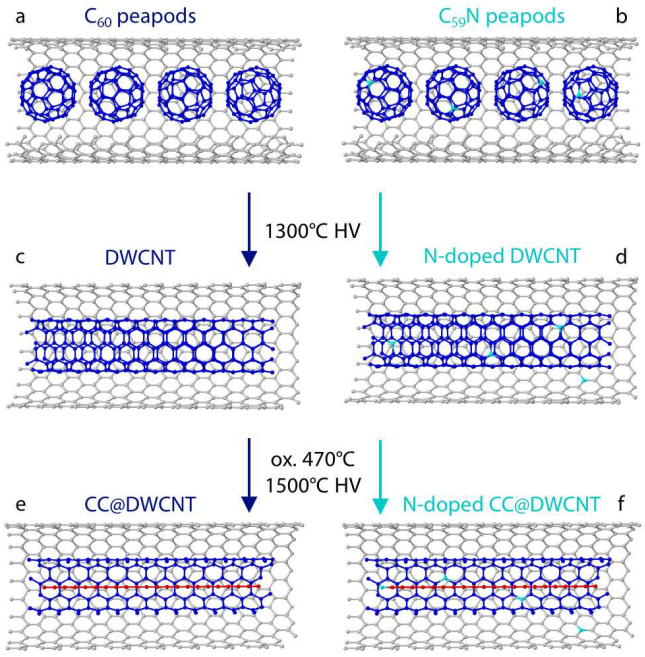

Figure 1: Synthesis of undoped (left) and nitrogen-doped (right) confined carbyne: a) C_{60} inside a SWCNT; b) $C_{59}N$ inside a SWCNT; c) undoped DWCNT; d) nitrogen-doped DWCNT; e) undoped CC@DWCNT; f) nitrogen-doped CC@DWCNT.

been demonstrated theoretically and experimentally.[26,27] This has been attributed to nonadiabitic effects and the breakdown of the Born-Oppenheimer approximation. Upshifts in the G-mode of graphite have also been observed for graphite intercalation compounds for moderate levels of intercalant.[28] Further, for intercalated graphite, downshifts of the frequency of G-mode and 2D-mode were attributed to strain in the lattice. For the 2D-mode, only the downshift effect from the strain is observed, as this mode originates, as opposed to the G-band, from the K-point rather than the Γ-point, where the charge transfer effects the band structure. Downshifts in the 2D-mode were also observed for nitrogen-doped graphene in moderate concentrations.[29] It is hard to disentangle these effects quantitatively, especially as they lead to a shift of the Raman frequency in different directions. Despite the difficulties to quantify the doping-related effects on the Raman response of these hybrid materials, it is clearly feasible

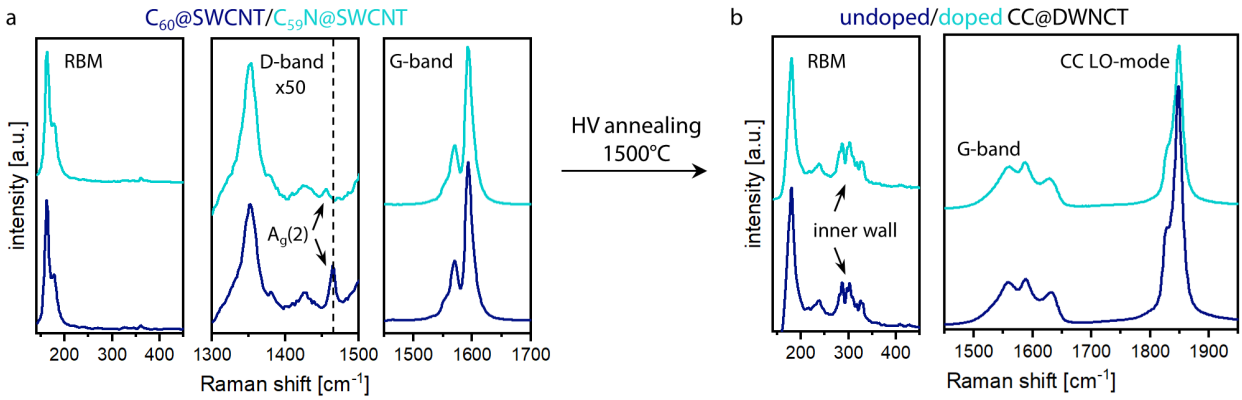

Figure 2: a) Raman spectra of C_{60} (dark blue) and $C_{59}N$ (teal) peapods, measured with a 488 nm laser, the shift of the $A_g(2)$-mode is highlighted; b) Raman spectra of doped/undoped CC@DWCNTs, measured with a 568 nm laser.

to pinpoint the predominant effects related to the net change of the Raman shift.

For the experiments, semi-conducting arc-discharge CNTs (diameter 1.36±0.08 nm) were used as SWCNT hosts. These host tubes were filled with C_{60} and $C_{59}N$ fullerenes, respectively, in vacuum to create the doped and undoped peapods. The peapods were then annealed at high temperature in high vacuum to create DWCNTs and, in a second high temperature high vacuum annealing step, CC@DWCNTs. Raman spectra were taken after making the DWCNTs and after the final annealing step. The synthesis pathway is schematically shown in Fig.1, the exact experimental conditions for each step are described in the Supporting Information.

The presence of the respective fullerenes inside the SWCNTs after filling was confirmed using Raman spectroscopy, where the $A_g(2)$-modes of the C_{60} and $C_{59}N$ at $\sim$ 1468 cm^{-1} and $\sim$ 1459 cm^{-1}, respectively, were observed (Fig.2a). The spectrum of the doped fullerene peapods shows a significant downshift in the Raman frequency, confirming the presence of the doped species inside the SWCNTs.

As an intermediate step, DWCNTs were grown from the C_{60} and $C_{59}N$ peapods and Raman spectra were recorded (Fig.3). The Raman spectra of the G-mode at $\sim$ 1595 cm^{-1} of the doped and undoped samples were compared. A small downshift can be observed for the sample grown from the doped fullerenes. In order to make an estimation of the shifts for the double-walled carbon nanotubes grown from C_{60} and $C_{59}N$ fullerenes, a line-shape analysis was performed. It was observed that for the nitrogen-doped system, for the G-mode (Fig.3a and c), almost all peaks are shifted towards lower wavenumbers by 1 to 3 cm^{-1}, as it would be expected for doping with an atom with a higher mass. The increase in surface electron concentration from the nitrogen concentration in the fullerenes would not lead to strong shifts in the Raman frequency according to the calculation in Pisana *et al.*,[26] which means that in this case, the effect of the mass is dominant. For the 2D-peak of the DWCNTs, even larger downshifts of 6 to 10 cm^{-1} were observed for the doped DWCNTs (Fig.3b and d). The shift in the 2D-line is expected to result only from the mass effect and strain.[28] Similar shifts in the 2D-mode have been previously observed for double-walled carbon nanotubes grown from $C_{59}N$ peapeds .[30]

After the synthesis of CC, the LO-mode assigned to the CC at $\sim$ 1850 cm^{-1} is observed in the Raman spectra for both the doped and the undoped sample (Fig.2b) with similar intensity. Additionally, the changes in the G-mode, which have recently been described by anharmonic phonon-phonon interactions of the CC with the hosting DWCNT,[31] confirm the presence of CC.

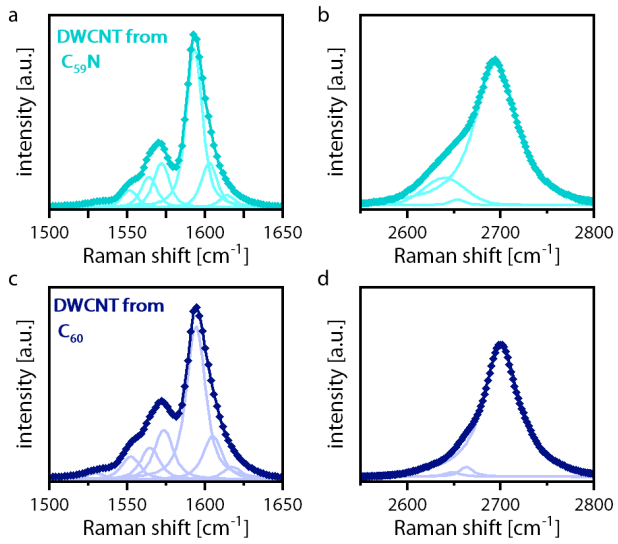

Figure 3: Raman spectra of DWCNT grown from C_{60} (dark blue) and $C_{59}N$ (teal) peapods: a) line-shape analysis of the G-mode of doped DWCNTs; b) line-shape analysis of the 2D-mode of doped DWCNTS; c) line-shape analysis of the G-mode of undoped DWCNTs; d) line-shape analysis of the 2D-mode of undoped DWCNTs.

The CC-mode can be fitted with multiple components due to the different Raman frequency of CC present in the sample, depending on the host nanotube geometry.[32] According to the estimations made in the work of Heeg *et al.*, the predominant inner tube chiralities and diameters in this samples were assigned to (6,5/0.75 nm), (7,4/0.76 nm), (8,3/0.78 nm) and (9,2/0.80 nm). Since the same single-walled hosts were used for both samples, the same inner tube chiralities can be expected to grow and the peak positions of the components can be compared in order to analyze shifts due to doping. The line-shape analysis for the CC-modes of the undoped and doped sample are shown in Fig.4a. The Raman shifts of the four components relative to the undoped sample are plotted in Fig.4b. Multiple spots were measured on each sample. The components of the undoped sample are all at very similar Raman shifts, with only a small deviation (4 spots measured). The shifts in the frequency of the CC-peaks of the doped sample are shifted to higher wavenumbers by an average of around 3 cm^{-1}, and show a higher variance (10 spots measured). The higher variance is to be expected as the nitrogen is not necessarily homogeneously distributed in the sample.

To interpret the shifts observed for the Raman frequency of the CC, we must consider the above-mentioned two effects of mass change and charge transfer that contribute to shifts in the Raman frequency. On one hand, the frequency of a vibration is inversely proportional to the masses involved, leading to an increase in the frequency for lower masses and a decrease for higher masses. On the other hand, electronic doping leads to upwards shifts in the Raman frequency, regardless of whether the structure is depleted of electrons (p-type doping) or electrons are added (n-type doping). In the case of graphene according to the estimations made in Pisana *et al.*[26] and Lazzeri *et al.*,[27] the small amount of doping achieved in our case would not lead to significant shifts in the Raman frequency of the G-mode. We can, however, assume that due to the confinement to one dimension compared to graphene, the effect of additional charges in the system is stronger. Disentangling the two effects and evaluating the dopant concentration is not trivial. In our case, the effect from charge transfer dominates the effect of the mass on the Raman frequency, since only shifts to higher frequencies were observed.

The nitrogen bonding configuration within the chain has multiple possibilities. Assuming that nitrogen would form three covalent bonds, it could be expected that it would terminate fragments of CC. The carbon atoms in the middle of the chain all have four covalent bonds (alternating single and triple bonds), which means the chain end would be ideal for a three-valent atom, preventing dangling bonds at the end of the carbyne chain. Short chain nitrogen-capped polyynes have been successfully isolated before by introducing nitrogen in the carrier gas during laser vaporization of graphite, showing that such a structure would be stable.[33] Another theoretical possibility would be for the nitrogen to be coordinated in a pyridinic way, with two carbons bonded on either side, one with a double bond and one with a single bond. This would however disrupt the more stable polyynic

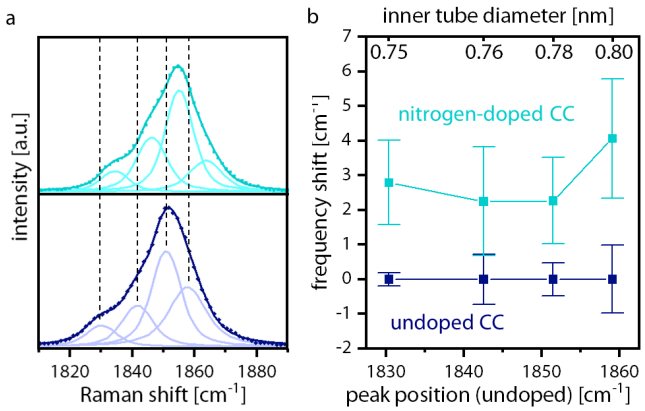

Figure 4: Analysis of CC grown from nitrogen-doped fullerenes (teal) and undoped fullerenes (dark blue): a) line-shape analysis of the CC-mode of the undoped sample compared to the doped sample; b) average frequency shifts of components of the doped sample (10 different spots measured) compared to the undoped sample (4 different spots measured).

character (alternating single and triple bonds) of the chain and impose a cumulenic structure (continuous double bonds) on one side. Additionally, due to the lone electron pair of the nitrogen, the bonding geometry would not be linear, but introduce a kink into the chain. Due to the strong spatial confinement in the small-diameter host tubes, this is unlikely.

In conclusion, nitrogen atoms were successfully introduced into the carbyne/nanotube system by means of filling the carbon nanotube host tubes with a nitrogen doped precursor. The presence of nitrogen atoms in the chain was indirectly confirmed by shifts in the Raman frequency of the peaks related to the carbyne chain. Different effects dominate the shift in the Raman frequencies of the chain and the surrounding host tubes. To the best of our knowledge, this is the first report of introducing heteroatoms into confined carbyne structures.

Acknowledgement This work was in part funded by the Austrian Science Fund (FWF), Doctoral College Advanced Functional Materials-Hierarchical Design of Hybrid Systems (10.55776/DOC85) (C.F., P.A., T.P.). C.S., T.P., C.F. and E.P. acknowledge funding from the European Research Council (ERC) under the European Union's Horizon 2020 research and innovation program (MORE-TEM ERC-SYN project, grant agreement No 951215). R.C.-V. and N.T. acknowledge COST Action CA21126 – Carbon molecular nanostructures in space (NanoSpace), supported by COST (European Cooperation in Science and Technology). L.S. acknowledges the National Natural Science Foundation of China (52472059). W.C. acknowledges the National Natural Science Foundation of China (22401298). P.A. acknowledges the COST Action EsSENce CA119, supported by COST (European Cooperation in Science and Technology). K.Y. acknowledges support from JSPS KAKENHI, Grant Nos. JP23H00259, and JP24H01200, and US-JAPAN PIRE, Grant No. JPJSJRP20221202, Japan, and ASPIRE project, Grant No. JPMJAP2310, Japan.

Supporting Information Available

Experimental details, tables containing peak positions from the line-shape analysis of the G-mode and 2D-mode of doped and undoped DWCNTs.

References

(1) Al-Backri, A.; Zólyomi, V.; Lambert, C. J. Electronic properties of linear carbon chains: Resolving the controversy. *The Journal of chemical physics* **2014**, *140*.

(2) Casari, C. S.; Tommasini, M.; Tykwinski, R. R.; Milani, A. Carbon-atom wires: 1-D systems with tunable properties. *Nanoscale* **2016**, *8*, 4414–4435.

(3) Fazio, E.; Neri, F.; Patanè, S.; D'urso, L.; Compagnini, G. Optical limiting effects in linear carbon chains. *Carbon* **2011**, *49*, 306–310.

(4) Liu, M.; Artyukhov, V. I.; Lee, H.; Xu, F.; Yakobson, B. I. Carbyne from first principles: chain of C atoms, a nanorod or a nanorope. *ACS nano* **2013**, *7*, 10075–10082.

(5) Wang, Y.; Huang, Y.; Yang, B.; Liu, R. Structural and electronic properties of carbon nanowires made of linear carbon chains enclosed inside zigzag carbon nanotubes. *Carbon* **2006**, *44*, 456–462.

(6) Zanolli, Z.; Onida, G.; Charlier, J.-C. Quantum spin transport in carbon chains. *ACS nano* **2010**, *4*, 5174–5180.

(7) Zhang, K.; Zhang, Y.; Shi, L. A review of linear carbon chains. *Chinese Chemical Letters* **2020**, *31*, 1746–1756.

(8) Peierls, R. E. *Quantum theory of solids*; Clarendon Press, 1996.

(9) Januszewski, J. A.; Tykwinski, R. R. Synthesis and properties of long [n]cumulenes (n$\geq$ 5). *Chem. Soc. Rev.* **2014**, *43*, 3184–3203.

(10) Heimann, R. B. *Carbyne and Carbynoid Structures*; Springer Netherlands, 1999; pp 7–15.

(11) Shi, L.; Rohringer, P.; Suenaga, K.; Niimi, Y.; Kotakoski, J.; Meyer, J. C.; Peterlik, H.; Wanko, M.; Cahangirov, S.; Rubio, A.; Lapin, Z. J.; Novotny, L.; Ayala, P.; Pichler, T. Confined linear carbon chains as a route to bulk carbyne. *Nature Materials* **2016**, *15*, 634–639.

(12) Shi, L.; Rohringer, P.; Ayala, P.; Saito, T.; Pichler, T. Carbon nanotubes from enhanced direct injection pyrolytic synthesis as templates for long linear carbon chain formation. *physica status solidi (b)* **2013**, *250*, 2611–2615.

(13) Shi, L.; Senga, R.; Suenaga, K.; Kataura, H.; Saito, T.; Paz, A. P.; Rubio, A.; Ayala, P.; Pichler, T. Toward confined carbyne with tailored properties. *Nano Letters* **2021**, *21*, 1096–1101.

(14) Feng, Y.; Zhang, W.; Tang, K.; Chen, Y.; Zhang, J.; Cao, K.; Cui, W.; Shi, L. A robust synthesis route of confined carbyne. *Nano Research* **2024**, *17*, 6274–6280.

(15) Zhang, B.-W. et al. Low-Temperature Synthesis of Weakly Confined Carbyne inside Single-Walled Carbon Nanotubes. 2024; `https://arxiv.org/abs/2411.18899`.

(16) Chang, W.; Liu, F.; Liu, Y.; Zhu, T.; Fang, L.; Li, Q.; Liu, Y.; Zhao, X. Smallest carbon nanowires made easy: Long linear carbon chains confined inside single-walled carbon nanotubes. *Carbon* **2021**, *183*, 571–577.

(17) Chen, Y.; Tang, K.; Zhang, W.; Cao, H.; Zhang, H.; Feng, Y.; Cui, W.; Hu, Y.; Shi, L.; Yang, G. A Universal Method to Transform Aromatic Hydrocarbon Molecules into Confined Carbyne inside Single-Walled Carbon Nanotubes. 2024; `https://arxiv.org/abs/2412.20394`.

(18) Shi, L.; Senga, R.; Suenaga, K.; Chimborazo, J.; Ayala, P.; Pichler, T. Photothermal synthesis of confined carbyne. *Carbon* **2021**, *182*, 348–353.

(19) Cui, W.; Shi, L.; Cao, K.; Kaiser, U.; Saito, T.; Ayala, P.; Pichler, T. Isotopic labelling of confined carbyne. *Angewandte Chemie International Edition* **2021**, *60*, 9897–9901.

(20) Zhao, C.; Kitaura, R.; Hara, H.; Irle, S.; Shinohara, H. Growth of linear carbon chains inside thin double-wall carbon nanotubes. *The Journal of Physical Chemistry C* **2011**, *115*, 13166–13170.

(21) Cui, W.; Simon, F.; Zhang, Y.; Shi, L.; Ayala, P.; Pichler, T. Ultra-Clean Isotope Engineered Double-Walled Carbon Nanotubes as Tailored Hosts to Trace the Growth of Carbyne. *Advanced Functional Materials* **2022**, *32*, 2206491.

(22) Pagona, G.; Rotas, G.; Khlobystov, A. N.; Chamberlain, T. W.; Porfyrakis, K.; Tagmatarchis, N. Azafullerenes encapsulated within single-walled carbon nanotubes. *Journal of the American Chemical Society* **2008**, *130*, 6062–6063.

(23) Tschannen, C. D.; Gordeev, G.; Reich, S.; Shi, L.; Pichler, T.; Frimmer, M.; Novotny, L.; Heeg, S. Raman scattering cross section of confined carbyne. *Nano letters* **2020**, *20*, 6750–6755.

(24) Yang, Q.-H.; Hou, P.-X.; Unno, M.; Yamauchi, S.; Saito, R.; Kyotani, T. Dual Raman Features of Double Coaxial Carbon Nanotubes with N-Doped and B-Doped Multiwalls. *Nano Letters* **2005**, *5*, 2465–2469.

(25) Simon, F.; Kramberger, C.; Pfeiffer, R.; Kuzmany, H.; Zólyomi, V.; Kürti, J.; Singer, P. M.; Alloul, H. Isotope Engineering of Carbon Nanotube Systems. *Physical Review Letters* **2005**, *95*, 017401.

(26) Pisana, S.; Lazzeri, M.; Casiraghi, C.; Novoselov, K. S.; Geim, A. K.; Ferrari, A. C.; Mauri, F. Breakdown of the adiabatic Born–Oppenheimer approximation in graphene. *Nature Materials* **2007**, *6*, 198–201.

(27) Lazzeri, M.; Mauri, F. Nonadiabatic Kohn Anomaly in a Doped Graphene Monolayer. *Physical Review Letters* **2006**, *97*, 266407.

(28) Chacon-Torres, J. C.; Wirtz, L.; Pichler, T. Manifestation of charged and strained graphene layers in the Raman response of graphite intercalation compounds. *ACS nano* **2013**, *7*, 9249–9259.

(29) Podila, R.; Chacón-Torres, J.; Spear, J. T.; Pichler, T.; Ayala, P.; Rao, A. M. Spectroscopic investigation of nitrogen doped graphene. *Applied Physics Letters* **2012**, *101*.

(30) Kuzmany, H.; Plank, W.; Pfeiffer, R.; Simon, F. Raman scattering from double-walled carbon nanotubes. *Journal of Raman Spectroscopy* **2007**, *39*, 134–140.

(31) Parth, E.; Corradini, A.; Cui, W.; Romanin, W.; Schuster, C.; Freytag, C.; Shi, L.; Yanagi, K.; Calandra, M.; Pichler, T. The Resonant Raman Response of Confined Carbyne Is Solely Driven by Anharmonic Interactions. *preprint available at Research Square* **2024**,

(32) Heeg, S.; Shi, L.; Poulikakos, L. V.; Pichler, T.; Novotny, L. Carbon Nanotube Chirality Determines Properties of Encapsulated Linear Carbon Chain. *Nano Letters* **2018**, *18*, 5426–5431.

(33) Heath, J. R.; Zhang, Q.; O'Brien, S. C.; Curl, R. F.; Kroto, H. W.; Smalley, R. E. The formation of long carbon chain molecules during laser vaporization of graphite. *Journal of the American Chemical Society* **1987**, *109*, 359–363.

Supporting Information

Experimental details

The doped and undoped CC@DWCNT samples shown in Figure 2 (main text) were synthesized using the following procedure. The synthesis began with the oxidation of semiconducting arc-discharge nanotubes in air at 450 °C for 30 minutes to open their caps. Subsequently, the C_{60} or the $C_{59}N$ powder was combined with the cap-opened nanotubes and sealed under vacuum (10^{-7} mbar) within a glass tube. The sealed glass tube was then heated to 500 °C for 72 hours to obtain the C_{60} and the $C_{59}N$ peapods. Following the vapor filling, the C_{60} and the $C_{59}N$ peapods were subjected to high vacuum annealing at 1300 °C to grow inner tubes. This was followed by an additional heating step at 1600 °C to facilitate the formation of confined carbyne inside the inner tubes.

For the analysis performed in Figures 3 and 4 (main text), the samples were synthesized using the following procedure. Before filling with fullerenes, the nanotubes were oxidized in air at 450°C for 30 minutes to open the end caps. The C_{60} and the $C_{59}N$ fullerenes were each sublimated for 30 minutes at 550°C inside a glass ampoule. For the doped fullerenes, the dimer $(C_{59}N)_2$ was used in the process and this material is sublimed in monomeric form, as a $C_{59}N^{\cdot}$ radical, while the C_{60} is already a monomer in the starting material. The CNT samples were then sealed into glass ampoules under high vacuum with the doped fullerenes or undoped fullerenes. In order to fill the fullerenes into the nanotubes, the ampoules were placed in a two-zone furnace for 72 hours. The temperature at the fullerene side was 560°C for the $C_{59}N$ and 600°C for the C_{60} fullerenes and 370°C on the side of the carbon nanotubes for both ampoules. The next step was annealing the nanotube samples at 1300°C in high vacuum in order to grow double-walled carbon nanotubes (DWCNT). Both samples were annealed at 1500°C in high vacuum for 1 hour, oxidized at 470°C for 1 hour at 600 mbar of air and then annealed again at 1500°C in high vacuum for 1 hour.

The Raman measurements of all samples were made with a Horiba LabRAM HR spectrometer combined with an Ar^+/Kr^+ laser (Coherent Innova 70C). As detector, a liquid nitrogen cooled CCD chip was used. The spectra were calibrated using a Neon lamp.

Analysis of doped and undoped DWCNTs

Table 1: Raman frequencies of components of the G-mode fitted for double-walled carbon nanotubes made from undoped and doped precursors. The peaks marked with * are attributed to the G^- peak of the outer nanotube, the peaks marked with † are attributed to the G^+ peak of the outer nanotube.

C_{60} [cm^{-1}]	$C_{59}N$ [cm^{-1}]	Difference [cm^{-1}]
1529.80	1530.76	+0.96
1552.19	1551.48	-0.71
1564.59	1563.88	-0.71
1573.46*	1571.88*	-1.58
1594.04†	1592.95†	-1.09
1604.85	1602.66	-2.19
1617.33	1614.19	-3.17

Table 2: Raman frequencies of components of the 2D-mode fitted for double-walled carbon nanotubes made from undoped and doped precursors.

C_{60} [cm^{-1}]	$C_{59}N$ [cm^{-1}]	Difference [cm^{-1}]
2647.28	2639.62	-7.66
2663.22	2653.59	-9.63
2700.28	2694.39	-5.89

5.3 Hybrid systems with boron nitride

For this experiment, the first idea was to form a coaxial boron nitride nanotube around the single-walled carbon nanotubes using chemical vapor deposition (CVD), following a synthesis process from the work of Xiang *et al.* [164]. A piece of carbon nanotube bucky paper (semiconducting 1.45 arc-discharge) was placed into a CVD furnace with ammonia borane (H_3NBH_3) as a boron nitride precursor. The ammonia borane is heated to 90°C and transported in the furnace with a flow of Ar/H_2 to the carbon nanotubes, which are heated to 1000-1100°C (fig. 5.2). The annealing time was 6 hours.

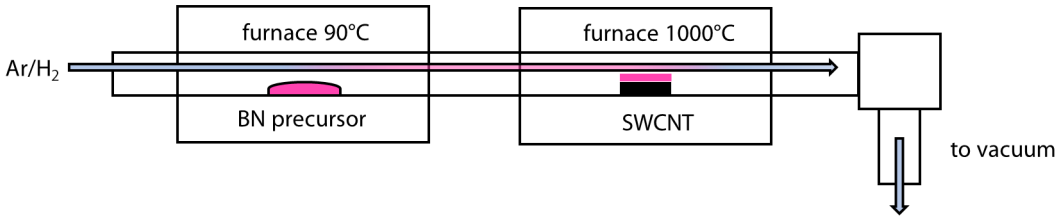

Figure 5.2: Schematic of the CVD furnace set-up used for the synthesis of boron nitride hybrid systems.

Raman spectra were taken after the experiment (fig. 5.3). In the work by Xiang *et al.*, a downshift of 10 cm^{-1} in the G-line of the carbon-boron nitride nanotube (SWNCT-BNNT) coaxial system was observed which was tentatively attributed to thermal strain [164]. Generally, the SWCNT-BNNT coaxial structure has Raman modes from vibrations attributed to boron-nitride bonds at 1370 cm^{-1} from in-plane B-N stretching and at 795 cm^{-1} from out-of-plane B-N-B bending [242].

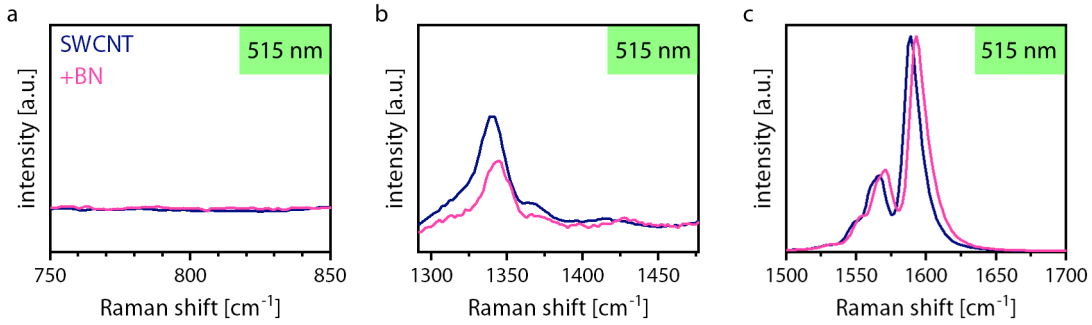

Figure 5.3: Raman spectra of the carbon/boron nitride hybrid system (pink) compared to a pure carbon nanotube sample (blue) measured with a 515 nm laser: a) spectral range where out-of-plane B-N-B stretching would be observed; b) spectral range of the D-mode of the carbon nanotube and the in-plane B-N stretching; c) spectral range of the G-line.

In the Raman spectra in figure 5.3, none of the characteristic boron-nitride vibrations appear. In contrast to the observations from literature, a shift to higher wavenumbers of the G-line and the D-mode were observed. Such a shift in the frequency can arise from the lower mass of boron compared to carbon. From the shift, using equation 1.13, it can be calculated that a 6% doping could account for the upshift, assuming that no electronic effects play a part in the shift.

As a next step, the sample was annealed at 1500°C for 1 hour in high vacuum in order to grow carbyne chains and the sample was then measured using Raman spectroscopy. The Raman spectrum of the annealed boron doped sample in comparison to a pure carbon confined carbyne sample is shown in figure 5.4a, which shows the same shift in the G-mode of the confined carbyne sample observed in the same sample before the annealing process (fig. 5.3c).

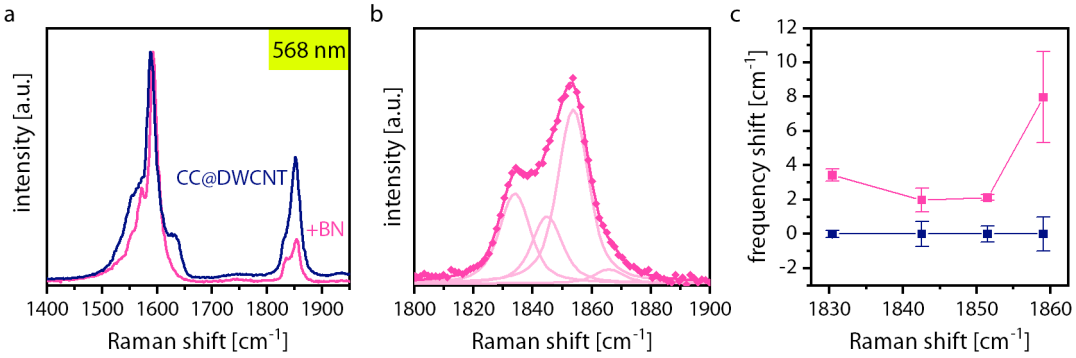

Figure 5.4: Confined carbyne inside the carbon/boron nitride hybrid system, measured with a 568 nm laser: a) Raman spectrum of pure carbyne inside double-walled carbon nanotubes (CC@DWCNT) (blue) compared to the spectrum of the carbyne grown from the doped host tubes (pink); b) line-shape analysis of the Raman mode attributed to the carbyne; c) peak positions of the main components of the doped confined carbyne (pink) compared to undoped confined carbyne (blue).

A small peak attributed to the confined carbyne was observed as well. For this peak, a line-shape analysis was performed in order to evaluate shifts in the confined carbyne peaks compared to an undoped sample (fig. 5.4b). Three different spots on the sample were analyzed. For all spots, an upshift of between 2 and 4 cm^{-1} was observed for the main components of the peak (fig. 5.4c). The small uncertainties of the components of the peaks of the carbyne chains indicate a rather homogeneous sample. This would correspond to a concentration of 2.5-5% of boron inside the chain, again under the assumption that the shift is only due to changes in the mass. Since the depletion of electrons would also lead to a upshift in the Raman spectrum, this effect cannot be separated from the mass effect in the case of boron doping.

It is not trivial to predict in which way boron atoms would incorporate into a chain of linear carbon. While it is a three-valent atom similar to nitrogen, the most common bonding geometry for boron atoms is trigonal planar, which means it has three single bonds in the same plane with an angle of 120°, which is not compatible with the geometry of carbyne. However, boron has been shown to form double bonds to other boron atoms, leading to a linear bonding geometry for the third bond [243]. This could be incorporated into a carbyne chain, with a single bond on one side of the boron and a double bond on the other side. This would lead to a cumulenic structure on the side of the double bond. The possibility for boron to form a triple bond has also been demonstrated [244], [245]. It would therefore be possible for the boron to terminate a carbyne chain with a triple bond. A model for a boron including and a boron terminated chain is shown in figure 5.5. The interpretation of the shifts in the Raman frequency is, however, quite complex as it cannot be ruled out that nitrogen from the boron nitride precursor plays a role.

We assume the surrounding nanotubes are doped with boron, as for nitrogen, the double-walled spectra showed a downshift for the double walled carbon nanotubes. For this system, the G-band of the double-walled carbon nanotubes is clearly shifted to higher frequencies. For the confined carbyne, upshifts could also be observed from doping with nitrogen (sec. 5.1). Therefore, it cannot be definitively ruled out that nitrogen was incorporated into the carbyne chain.

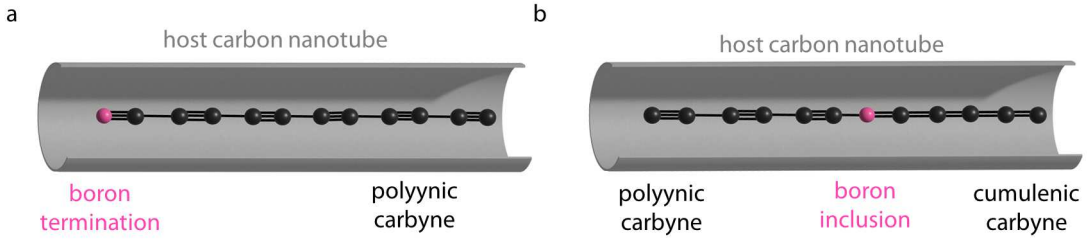

Figure 5.5: Models for the incorporation of boron into carbyne chains: a) boron termination of the chain with a triple bond; b) inclusion of the boron into the chain with a single and a double bond.

5.4 Outlook for hybrid chains

Hybrid chains were successfully synthesized. The shifted Raman peaks of the chains are a reliable indicator for the synthesis of carbyne derivatives. The comparison can only be made if the starting material, the single-walled carbon nanotube hosts, are the same. The interaction of the chain with the inner tube is dependent on the structure of the tube and leads to shifts in the chain frequency [176]. Therefore, only samples with the same diameter single-walled nanotubes and a narrow diameter distribution are suitable to compare the small shifts caused by doping due to mass effect and charge transfer, as the same type of inner tubes can be assumed to grow. A good indicator for the fact that this is the case for the samples studied here is that the carbyne peak has very similar shapes and always four main components at very similar Raman frequencies.

The biggest challenge is to quantify the level of doping, since there are multiple entangled effects influencing the Raman frequency of the studied peaks. The effect arising from different masses participating in the vibration can be described with a simple formula, but the effect from electronic doping is more complex. Detailed calculations of the confined carbyne hybrid system are necessary to quantify the dependence of the Raman frequency on the electron concentrations, similarly to the work on graphene by Lazzeri *et al.* [128].

The binding energy of the nitrogen is observable in x-ray photoelectron spectroscopy (XPS), but this would not allow the differentiation between nitrogen in the nanotube and the chain. High-resolution transmission electron microscopy (HR-TEM) is needed for the direct observation of the nitrogen atoms in the chain as well as the surrounding nanotubes. As outlook, HR-TEM using core level electron energy loss spectroscopy (EELS) of the N_{1s} edge will be needed to finally prove the nitrogen bonding environment and confirm the position of the incorporated nitrogen atoms.

Due to the strong resonance enhancement and different signals of the sp^2-hybridized and sp^1-hybridized carbon, Raman spectroscopy is the fastest and most suited way to fingerprint heteroatom incorporation into the system.

6

Conclusion

The main focus of this thesis was to find a reliable and efficient synthesis pathway for confined carbyne. Confined carbyne was synthesized from single-walled carbon nanotubes (e.g. arc-discharge or eDIPS) using high temperature annealing in high vacuum. Additional steps include filling the host tubes with fullerenes as a carbonaceous precursor and multiple steps of annealing and oxidizing. In order to optimize the synthesis, first, a robust way to determine the bulk yield and realized growth potential needed to be developed. The state-of-the-art method to determine the yield was from the intensity or area of the LO peak attributed to the carbyne chain. However, this is not a good metric for bulk yield, since the signal of carbyne is highly enhanced and its resonance profile is irregular.

Therefore, a new model was developed for yield determination, based on recent *ab-initio* calculations describing the effects of anharmonic coupling between the carbyne chain and the host nanotube on the Raman response of the confined carbyne system. Coupled modes that arise from the interactions between the chain and the surrounding host tube appear in the Raman spectrum of confined carbyne. These modes appear together with the G-mode and the 2D-mode as shoulders. These peaks follow the stable resonance behavior of the nanotube host and can therefore be used to determine the bulk yield. The new model compares the areas of the G-modes of double-walled carbon nanotubes and confined carbyne inside double-walled carbon nanotubes in order to assess the bulk yield. Furthermore, the realized growth potential was established as a quantitative metric to determine the success of the synthesis. The bulk yield is set in relation to the fraction of the nanotube host starting material with the appropriate diameter to grow carbyne.

With these analysis tools, the bulk yield and realized growth potential, the influence of various parameters on the synthesis was quantified. The optimal synthesis temperature for eDIPS host nanotubes was re-evaluated and determined to be 1580°C, which is higher than the previously used temperatures of 1400°C to 1500°C. Filling the single-walled host tubes with fullerenes as a carbon source for carbyne growth can increase the yield. This step is mainly important for carbon nanotube hosts which do not have a lot of carbonaceous precursor inside from their synthesis, such as arc-discharge carbon nanotubes. For eDIPS carbon nanotubes, additional filling does

not increase the yield, which indicates that there is enough carbonaceous precursor inside the hosts already. Repeating the high temperature high vacuum annealing step with an oxidation step in-between increases the yield. For the arc-discharge nanotube hosts, annealing a second time increased the yield by 33%. Adding more annealing steps with oxidation steps in between increased the bulk yield for the arc-discharge hosts to 46%, which corresponds to a realized growth potential of 96% after four annealing steps. Additional annealing steps lead to a decrease in the bulk yield. This can be attributed to the destruction of carbyne and inner nanotubes by the residual gas in the furnace during annealing. For one of the eDIPS hosts, an interesting phenomenon was observed. The highest bulk yield was achieved after the second annealing step, the bulk yield then decreased in the next three steps and then increased again. This is explained by the interplay of carbyne growth from carbonaceous precursor and destruction due to the residual gas etching. When the maximum yield has been achieved and there is no more precursor, the bulk yield can only decrease. However, the destroyed carbyne and inner tubes can be used as new precursor for more growth. The optimal number of annealing steps is different for different hosts and the bulk yield is limited by the availability of carbonaceous precursor. The realized growth potential is useful to estimate whether an additional annealing step should be performed. The vacuum should be as good as possible during the high temperature annealing in order to prevent destruction of the sample.

The second part of this work concerned the introduction of heteroatoms into the confined carbyne system. The first approach used nitrogen doped fullerenes as precursors. The doped fullerenes were filled into the single-walled carbon nanotube precursors to create doped peapods. From the doped peapods, double-walled nanotubes were grown and then, using two annealing steps, carbyne. The Raman spectra of a doped and undoped sample were compared. The carbyne peak showed shifts in the Raman frequency for the doped sample compared to the undoped reference sample, which can be attributed to the incorporation of nitrogen into the carbyne chain. Due to the bonding geometry of nitrogen, I propose the incorporation of nitrogen as a termination for carbyne chains.

The second approach of incorporating heteroatoms into the chain was chemical vapor deposition of a boron nitride precursor onto the carbon nanotube hosts. From the doped nanotubes, carbyne was grown using high temperature high vacuum annealing. The peaks of the carbyne grown from the doped samples are shifted towards higher wavenumbers, indicating a possible substitutional doping by boron or electronic doping from either boron or nitrogen. In the case of substitutional doping by boron, either a termination by boron of the chain or the incorporation into the chain with a single and a double bond to the neighboring carbon atoms would be expected. Since both the mass and charge transfer have an effect on the Raman frequency in different directions, unraveling the meaning of shifts in the Raman frequencies is complex and invites further investigation.

7

Outlook

Carbyne confined inside carbon nanotubes is the ultimate one dimensional material. The carbon nanotube host provides a unique environment for novel one dimensional polymerization reactions, including the formation of carbyne, graphene nanoribbons, and equivalent structures made from sulfur [246], arsenic [247] and phosphorous [248]. These are not only interesting model systems to study, but also have potential applications in e.g. cathode materials for batteries (Li-S rechargeable batteries) and energy generation.

Filling carbon nanotubes with molecules or nanocrystals can be used to tune their electronic and magnetic properties, highlighting the possibility to manufacture electrodes and apply the modified structures in quantum computing elements, nano-mechatronics and spintronics [137]. Other applications of filled nanotubes are proposed in the fields of biology, medicine (e.g. drug delivery), industrial catalysis, single-molecule sensing, environmental remediation (e.g. wastewater treatment), batteries, nano-optoelectronics, and gas sensors. The possibility to combine different types of structures at the nanoscale and encapsulate them in nanotubes offers a wide range of potential novel functionalities and miniaturization of devices. Many such interesting structures can be made from abundant and non-toxic elements such as carbon, sulfur and cheap metals and may provide alternatives to existing technologies using rare earths or toxic elements, paving the way to more sustainable alternative solutions.

For linear carbon chains and confined carbyne, some possible applications have been demonstrated. For example, chemically modified polyynes have been used for multiplexed bio-imaging [249]. Confined carbyne can, due to its high scattering cross-section, be used for nanoscale thermometry [250]. Due to its tunable band gap, it is also a suitable candidate for nano-electronic devices. Such applications require excellent uniformity of the materials and reliable, high yield synthesis. My work is a small piece of this puzzle - partly focusing on the synthesis of the material and demonstrating the possibility to modify carbyne to create new, tailored structures.

This work also showcases the use of carbon nanotubes as nanoreactors for chemical reactions, which is useful for stabilizing structures and exotic phases that would otherwise not exist in a free-standing form.

Appendix

Table 1: Bulk yield achieved during the multi-step annealing synthesis of confined carbyne in different nanotube hosts.

	Bulk yield 1.45 nm arc-discharge [%]	Bulk yield 1.33 nm eDIPS [%]	Bulk yield 1.41 nm eDIPS [%]
Annealing 1	2.6	12.1	16.2
Annealing 2	35.2	11.4	25.6
Annealing 3	38.7	15.9	23.7
Annealing 4	46.2	27.9	20.6
Annealing 5	40.8	24.3	18.7
Annealing 6	32.9	20.2	27.3

Table 2: Relative area of the CC-mode (compared to the normalized G-mode) of confined carbyne inside 1.33 nm eDIPS carbon nanotube hosts synthesized at different temperatures. Ten to twelve spots were measured on each sample. One value is missing from the 1540°C column, since the gratings move during the measurement and for one spectrum, the cutoff led to an irregular background.

ECC area 1500°C	ECC area 1520°C	ECC area 1540°C	ECC area 1560°C	ECC area 1580°C	ECC area 1600°C
0.016	0.026	0.026	0.069	0.025	0.060
0.049	0.025	0.018	0.029	0.026	0.054
0.031	0.027	0.022	0.039	0.025	0.044
0.030	0.025	0.031	0.034	0.026	0.038
0.055	0.024	0.017	0.052	0.032	0.051
0.15	0.030	0.007	0.056	0.044	0.014
0.051	0.023	0.082	0.028	0.047	0.045
0.085	0.039	0.016	0.035	0.050	0.045
0.051	0.067	0.008	0.041	0.051	0.039
0.052	0.018		0.084	0.038	0.044
	0.041				0.063
	0.021				

Table 3: Bulk yield of confined carbyne inside 1.33 nm eDIPS carbon nanotube hosts synthesized at different temperatures. Ten to twelve spots were measured on each sample. Negative values arise from very small yields and small errors from the area integration model. One value is missing from the 1540°C column, since the gratings move during the measurement and for one spectrum, the cutoff led to an irregular background.

Yield [%] 1500°C	Yield [%] 1520°C	Yield [%] 1540°C	Yield [%] 1560°C	Yield [%] 1580°C	Yield [%] 1600°C
12.9	1.7	6.5	20.4	22.0	19.1
11.5	-3.4	9.7	27.4	22.3	15.7
13.8	9.9	6.1	26.3	23.0	16.4
13.7	-0.8	3.1	25.0	24.9	19.1
8.5	4.9	5.2	2.6	20.8	20.3
12.2	6.8	-0.4	15.8	22.4	8.2
11.9	1.8	1.1	11.3	25.6	19.1
11.6	8.2	5.7	15.7	19.9	21.4
6.7	12.7	-2.1	19.5	23.2	19.4
10.3	11.9		23.8	21.9	17.1
	5.4				21.9
	5.9				

Table 4: Raman frequencies of components of the CC-mode of undoped confined carbyne, four different spots on the sample were measured. The average values and standard deviation are plotted in figure 5.4 and in section 5.2.

	Component 1 [cm^{-1}]	Component 2 [cm^{-1}]	Component 3 [cm^{-1}]	Component 4 [cm^{-1}]
Spot 1	1830.64	1842.47	1851.43	1859.61
Spot 2	1830.10	1841.67	1850.93	1857.78
Spot 3	1830.42	1843.42	1852.06	1852.90
Spot 4	1830.36	1840.77	1852.07	1860.35

Table 5: Raman frequencies of components of the CC-mode of boron doped confined carbyne, three different spots on the sample were measured. The average values and standard deviation are plotted in section 5.3, figure 5.4.

	Component 1 [cm^{-1}]	Component 2 [cm^{-1}]	Component 3 [cm^{-1}]	Component 4 [cm^{-1}]
Spot 1	1833.90	1844.81	1853.68	1865.74
Spot 2	1834.13	1844.99	1853.69	1870.08
Spot 3	1833.42	1843.72	1853.41	1865.34

Table 6: Raman frequencies of components of the CC-mode of nitrogen doped confined carbyne, ten different spots on the sample were measured. The average values and standard deviation are shown in section 5.2.

	Component 1 [cm^{-1}]	Component 2 [cm^{-1}]	Component 3 [cm^{-1}]	Component 4 [cm^{-1}]
Spot 1	1833.88	1846.36	1855.17	1865.44
Spot 2	1834.12	1846.08	1854.89	1863.45
Spot 3	1830.72	1843.23	1851.87	1861.36
Spot 4	1834.19	1845.07	1854.22	1864.33
Spot 5	1834.62	1846.33	1855.06	1864.88
Spot 6	1834.08	1846.05	1854.95	1864.94
Spot 7	1833.00	1844.63	1853.33	1862.23
Spot 8	1832.60	1844.09	1853.13	1862.77
Spot 9	1831.04	1840.77	1851.24	1859.22
Spot 10	1833.56	1845.08	1853.55	1862.62

List of Figures

List of Tables

Bibliography

[1] I.-S. Kim, C.-E. Shim, S. W. Kim, C.-S. Lee, J. Kwon, K.-E. Byun, and U. Jeong, "Amorphous Carbon Films for Electronic Applications", *Advanced Materials*, vol. 35, no. 43, Nov. 2022, ISSN: 1521-4095. DOI: 10.1002/adma.202204912.

[2] D. B. Boyd and Z. Slanina, "Introduction and foreword to the special issue commemorating the thirtieth anniversary of Eiji Osawa's C_{60} paper", *Journal of Molecular Graphics and Modelling*, vol. 19, no. 2, pp. 181–184, Apr. 2001, ISSN: 1093-3263. DOI: 10.1016/s1093-3263(00)00106-6.

[3] H. W. Kroto, J. R. Heath, S. C. O'Brien, R. F. Curl, and R. E. Smalley, "C_{60}: Buckminsterfullerene", *Nature*, vol. 318, no. 6042, pp. 162–163, Nov. 1985, ISSN: 1476-4687. DOI: 10.1038/318162a0.

[4] W. Krätschmer, L. D. Lamb, K. Fostiropoulos, and D. R. Huffman, "Solid C_{60}: A new form of carbon", *Nature*, vol. 347, no. 6291, pp. 354–358, Sep. 1990, ISSN: 1476-4687. DOI: 10.1038/347354a0.

[5] S. Iijima, "Helical microtubules of graphitic carbon", *Nature*, vol. 354, no. 6348, pp. 56–58, Nov. 1991, ISSN: 1476-4687. DOI: 10.1038/354056a0.

[6] A. Oberlin, M. Endo, and T. Koyama, "Filamentous growth of carbon through benzene decomposition", *Journal of Crystal Growth*, vol. 32, no. 3, pp. 335–349, Mar. 1976, ISSN: 0022-0248. DOI: 10.1016/0022-0248(76)90115-9.

[7] M. L. Lieberman, C. R. Hills, and C. J. Miglionico, "Growth of graphite filaments", *Carbon*, vol. 9, no. 5, pp. 633–635, Oct. 1971, ISSN: 0008-6223. DOI: 10.1016/0008-6223(71)90085-6.

[8] S. Iijima and T. Ichihashi, "Single-shell carbon nanotubes of 1-nm diameter", *Nature*, vol. 363, no. 6430, pp. 603–605, Jun. 1993, ISSN: 1476-4687. DOI: 10.1038/363603a0.

[9] D. S. Bethune, C. H. Kiang, M. S. de Vries, G. Gorman, R. Savoy, J. Vazquez, and R. Beyers, "Cobalt-catalysed growth of carbon nanotubes with single-atomic-layer walls", *Nature*, vol. 363, no. 6430, pp. 605–607, Jun. 1993, ISSN: 1476-4687. DOI: 10.1038/363605a0.

[10] K. S. Novoselov, A. K. Geim, S. V. Morozov, D. Jiang, Y. Zhang, S. V. Dubonos, I. V. Grigorieva, and A. A. Firsov, "Electric Field Effect in Atomically Thin Carbon Films", *Science*, vol. 306, no. 5696, pp. 666–669, Oct. 2004, ISSN: 1095-9203. DOI: 10.1126/science.1102896.

[11] M. Davenport, "Contention Over Carbyne", *Chem. Eng. News*, vol. 93, p. 46, 2015. [Online]. Available: https://cen.acs.org/articles/93/i46/Contention-Over-Carbyne.html.

[12] G. Maduraiveeran and W. Jin, "Carbon nanomaterials: Synthesis, properties and applications in electrochemical sensors and energy conversion systems", *Materials Science and Engineering: B*, vol. 272, p. 115 341, Oct. 2021, ISSN: 0921-5107. DOI: 10.1016/j.mseb.2021.115341.

[13] R. Heimann, S. Evsvukov, and Y. Koga, "Carbon allotropes: a suggested classification scheme based on valence orbital hybridization", *Carbon*, vol. 35, no. 10–11, pp. 1654–1658, 1997, ISSN: 0008-6223. DOI: 10.1016/s0008-6223(97)82794-7.

[14] A. Baeyer, "Ueber Polyacetylenverbindungen", *Berichte der deutschen chemischen Gesellschaft*, vol. 18, no. 2, pp. 2269–2281, Jul. 1885, ISSN: 0365-9496. DOI: 10.1002/cber.18850180296.

[15] M. Anchel, "IDENTIFICATION OF AN ANTIBIOTIC POLYACETYLENE FROM CLITOCYBE DIATRETA AS A SUBERAMIC ACID ENE-DIYNE*", *Journal of the American Chemical Society*, vol. 75, no. 18, pp. 4621–4622, Sep. 1953, ISSN: 1520-5126. DOI: 10.1021/ja01114a536.

[16] F. Bohlmann, "Naturally-occurring acetylenes", *Chemistry and biology of naturally-occurring acetylenes and related compounds (NOARC)*, pp. 1–19, 1988.

[17] J. D. Bu'Lock, "Acetylenic compounds as natural products", *Quarterly Reviews, Chemical Society*, vol. 10, no. 4, p. 371, 1956, ISSN: 0009-2681. DOI: 10.1039/qr9561000371.

[18] E. Jones, H. Lee, and M. Whiting, "Researches on acetylenic compounds. Part LXIV. The preparation of conjugated octa-and deca-acetylenic compounds", *Journal of the Chemical Society (Resumed)*, pp. 3483–3489, 1960.

[19] S. Szafert and J. A. Gladysz, "Carbon in One Dimension: Structural Analysis of the Higher Conjugated Polyynes", *Chemical Reviews*, vol. 103, no. 11, pp. 4175–4206, Oct. 2003, ISSN: 1520-6890. DOI: 10.1021/cr030041o.

[20] W. A. Chalifoux and R. R. Tykwinski, "Synthesis of polyynes to model the sp-carbon allotrope carbyne", *Nature Chemistry*, vol. 2, no. 11, pp. 967–971, Sep. 2010, ISSN: 1755-4349. DOI: 10.1038/nchem.828.

[21] A. El Goresy and G. Donnay, "A New Allotropic Form of Carbon from the Ries Crater", *Science*, vol. 161, no. 3839, pp. 363–364, Jul. 1968, ISSN: 1095-9203. DOI: 10.1126/science.161.3839.363.

[22] A. M. Sladkov and Y. P. Kudryavtsev, "Diamond, graphite, carbyne - Allotropic forms of carbon", *Priroda*, vol. vol.5, pp. 37–44, 1969.

[23] A. G. Whittaker, "Carbon: A New View of Its High-Temperature Behavior", *Science*, vol. 200, no. 4343, pp. 763–764, May 1978, ISSN: 1095-9203. DOI: 10.1126/science.200.4343.763.

[24] C. T. Pillinger, "Elemental carbon as interstellar dust", *Philosophical Transactions of the Royal Society of London. Series A: Physical and Engineering Sciences*, vol. 343, no. 1667, pp. 73–86, Apr. 1993, ISSN: 2054-0299. DOI: 10.1098/rsta.1993.0042.

[25] P. Smith and P. R. Buseck, "Carbyne forms of carbon: do they exist?", *Science*, vol. 216, no. 4549, pp. 984–986, 1982.

[26] R. B. Heimann, "The Nature of Carbyne- Pros and Cons", in *Carbyne and Carbynoid Structures*. Springer Netherlands, 1999, pp. 7–15, ISBN: 9789401147422. DOI: 10.1007/978-94-011-4742-2_2.

[27] H. Kroto, "Carbyne and other myths about carbon", *Chemistry World*, vol. 7, no. 11, pp. 37–37, 2010.

[28] R. H. Baughman, "Dangerously Seeking Linear Carbon", *Science*, vol. 312, no. 5776, pp. 1009–1110, May 2006, ISSN: 1095-9203. DOI: 10.1126/science.1125999.

[29] B. Pan, J. Xiao, J. Li, P. Liu, C. Wang, and G. Yang, "Carbyne with finite length: The one-dimensional sp carbon", *Science Advances*, vol. 1, no. 9, Oct. 2015, ISSN: 2375-2548. DOI: 10.1126/sciadv.1500857.

[30] P. Tarakeshwar, P. R. Buseck, and H. W. Kroto, "Pseudocarbynes: Charge-Stabilized Carbon Chains", *The Journal of Physical Chemistry Letters*, vol. 7, no. 9, pp. 1675–1681, Apr. 14, 2016, ISSN: 1948-7185. DOI: 10.1021/acs.jpclett.6b00671.

[31] J. R. Heath, Q. Zhang, S. C. O'Brien, R. F. Curl, H. W. Kroto, and R. E. Smalley, "The formation of long carbon chain molecules during laser vaporization of graphite", *Journal of the American Chemical Society*, vol. 109, no. 2, pp. 359–363, Jan. 1987, ISSN: 1520-5126. DOI: 10.1021/ja00236a012.

[32] M. Tsuji, T. Tsuji, S. Kuboyama, S.-H. Yoon, Y. Korai, T. Tsujimoto, K. Kubo, A. Mori, and I. Mochida, "Formation of hydrogen-capped polyynes by laser ablation of graphite particles suspended in solution", *Chemical Physics Letters*, vol. 355, no. 1–2, pp. 101–108, Mar. 2002, ISSN: 0009-2614. DOI: 10.1016/s0009-2614(02)00192-6.

[33] F. Cataldo, "Simple generation and detection of polyynes in an arc discharge between graphite electrodes submerged in various solvents", *Carbon*, vol. 41, no. 13, pp. 2671–2674, 2003, ISSN: 0008-6223. DOI: 10.1016/s0008-6223(03)00345-2.

[34] A. Chuvilin, J. C. Meyer, G. Algara-Siller, and U. Kaiser, "From graphene constrictions to single carbon chains", *New Journal of Physics*, vol. 11, no. 8, p. 083 019, Aug. 19, 2009, ISSN: 1367-2630. DOI: 10.1088/1367-2630/11/8/083019.

[35] O. Cretu, A. R. Botello-Mendez, I. Janowska, C. Pham-Huu, J.-C. Charlier, and F. Banhart, "Electrical Transport Measured in Atomic Carbon Chains", *Nano Letters*, vol. 13, no. 8, pp. 3487–3493, Jul. 23, 2013, ISSN: 1530-6992. DOI: 10.1021/nl4018918.

[36] I. M. Mikhailovskij, N. Wanderka, V. A. Ksenofontov, T. I. Mazilova, E. V. Sadanov, and O. A. Velicodnaja, "Preparation and characterization of monoatomic C-chains: unraveling and field emission", *Nanotechnology*, vol. 18, no. 47, p. 475 705, Oct. 19, 2007, ISSN: 1361-6528. DOI: 10.1088/0957-4484/18/47/475705.

[37] X. Zhao, Y. Ando, Y. Liu, M. Jinno, and T. Suzuki, "Carbon Nanowire Made of a Long Linear Carbon Chain Inserted Inside a Multiwalled Carbon Nanotube", *Physical Review Letters*, vol. 90, no. 18, p. 187 401, May 6, 2003, ISSN: 1079-7114. DOI: 10.1103/physrevlett.90.187401.

[38] D. Nishide, H. Dohi, T. Wakabayashi, E. Nishibori, S. Aoyagi, M. Ishida, S. Kikuchi, R. Kitaura, T. Sugai, M. Sakata, and H. Shinohara, "Single-wall carbon nanotubes encaging linear chain $C_{10}H_2$ polyyne molecules inside", *Chemical Physics Letters*, vol. 428, no. 4–6, pp. 356–360, Sep. 2006, ISSN: 0009-2614. DOI: 10.1016/j.cplett.2006.07.016.

[39] C. Zhao, R. Kitaura, H. Hara, S. Irle, and H. Shinohara, "Growth of Linear Carbon Chains inside Thin Double-Wall Carbon Nanotubes", *The Journal of Physical Chemistry C*, vol. 115, no. 27, pp. 13 166–13 170, Jun. 7, 2011, ISSN: 1932-7455. DOI: 10.1021/jp201647m.

[40] L. Shi, P. Rohringer, K. Suenaga, Y. Niimi, J. Kotakoski, J. C. Meyer, H. Peterlik, M. Wanko, S. Cahangirov, A. Rubio, Z. J. Lapin, L. Novotny, P. Ayala, and T. Pichler, "Confined linear carbon chains as a route to bulk carbyne", *Nature Materials*, vol. 15, no. 6, pp. 634–639, Apr. 2016, ISSN: 1476-4660. DOI: 10.1038/nmat4617.

[41] M. Peplow, "The Record Breakers", *ACS Central Science*, vol. 2, no. 8, pp. 489–492, Aug. 2016, ISSN: 2374-7951. DOI: 10.1021/acscentsci.6b00211.

[42] A. Jorio, M. S. Dresselhaus, R. Saito, and G. Dresselhaus, *Raman spectroscopy in graphene related systems*. John Wiley & Sons, 2011.

[43] H. Kuzmany, *Solid-State Spectroscopy: An Introduction*. Springer Berlin Heidelberg, 2009, ISBN: 9783642014796. DOI: 10.1007/978-3-642-01479-6.

[44] A. Smekal, "Zur Quantentheorie der Dispersion", *Die Naturwissenschaften*, vol. 11, no. 43, pp. 873–875, Oct. 1923, ISSN: 1432-1904. DOI: 10.1007/bf01576902.

[45] C. V. Raman and K. S. Krishnan, "A New Type of Secondary Radiation", *Nature*, vol. 121, no. 3048, pp. 501–502, Mar. 1928, ISSN: 1476-4687. DOI: 10.1038/121501c0.

[46] H. Poulet and J. P. Mathieu, *Vibration Spectra and Symmetry of Crystals*. Gordon and Breach, 1976.

[47] F. Simon, C. Kramberger, R. Pfeiffer, H. Kuzmany, V. Zólyomi, J. Kürti, P. M. Singer, and H. Alloul, "Isotope Engineering of Carbon Nanotube Systems", *Physical Review Letters*, vol. 95, no. 1, p. 017 401, Jun. 2005, ISSN: 1079-7114. DOI: 10.1103/physrevlett.95.017401.

[48] M. Dresselhaus, G. Dresselhaus, and R. Saito, "Physics of carbon nanotubes", *Carbon*, vol. 33, no. 7, pp. 883–891, 1995, ISSN: 0008-6223. DOI: 10.1016/0008-6223(95)00017-8.

[49] N. Wang, Z. K. Tang, G. D. Li, and J. S. Chen, "Single-walled 4 Åcarbon nanotube arrays", *Nature*, vol. 408, no. 6808, pp. 50–51, Nov. 2000, ISSN: 1476-4687. DOI: 10.1038/35040702.

[50] M. Monthioux, P. Serp, B. Caussat, E. Flahaut, M. Razafinimanana, F. Valensi, C. Laurent, A. Peigney, D. Mesguich, A. Weibel, W. Bacsa, and J.-M. Broto, "Carbon Nanotubes", in *Springer Handbooks*. Springer Berlin Heidelberg, 2017, pp. 193–247, ISBN: 9783662543573. DOI: 10.1007/978-3-662-54357-3_8.

[51] J. Tersoff and R. S. Ruoff, "Structural Properties of a Carbon-Nanotube Crystal", *Physical Review Letters*, vol. 73, no. 5, pp. 676–679, Aug. 1994, ISSN: 0031-9007. DOI: 10.1103/physrevlett.73.676.

[52] R. Zhang, Y. Zhang, Q. Zhang, H. Xie, W. Qian, and F. Wei, "Growth of Half-Meter Long Carbon Nanotubes Based on Schulz–Flory Distribution", *ACS Nano*, vol. 7, no. 7, pp. 6156–6161, Jul. 2013, ISSN: 1936-086X. DOI: 10.1021/nn401995z.

[53] R. E. Peierls, *Quantum theory of solids*. Clarendon Press, 1996.

[54] M. Baldo, "Peierls and Spin-Density Instability: From Polyacetylene to Graphene", in *Correlations in Condensed Matter under Extreme Conditions*. Springer International Publishing, 2017, pp. 151–166, ISBN: 9783319536644. DOI: 10.1007/978-3-319-53664-4_11.

[55] Á. Kukovecz, G. Kozma, and Z. Kónya, "Multi-Walled Carbon Nanotubes", in *Springer Handbook of Nanomaterials*. Springer Berlin Heidelberg, 2013, pp. 147–188, ISBN: 9783642205958. DOI: 10.1007/978-3-642-20595-8_5.

[56] J. H. Warner, N. P. Young, A. I. Kirkland, and G. A. D. Briggs, "Resolving strain in carbon nanotubes at the atomic level", *Nature Materials*, vol. 10, no. 12, pp. 958–962, Oct. 2011, ISSN: 1476-4660. DOI: 10.1038/nmat3125.

[57] A. Zettl, "Nanotubes: an experimental overview", in *Contemporary Concepts of Condensed Matter Science*. Elsevier, 2008, pp. 1–27, ISBN: 9780444532763. DOI: 10.1016/s1572-0934(08)00001-2.

[58] E. A. Laird, F. Kuemmeth, G. A. Steele, K. Grove-Rasmussen, J. Nygård, K. Flensberg, and L. P. Kouwenhoven, "Quantum transport in carbon nanotubes", *Reviews of Modern Physics*, vol. 87, no. 3, pp. 703–764, Jul. 2015, ISSN: 1539-0756. DOI: 10.1103/revmodphys.87.703.

[59] J.-C. Charlier, X. Blase, and S. Roche, "Electronic and transport properties of nanotubes", *Reviews of Modern Physics*, vol. 79, no. 2, pp. 677–732, May 2007, ISSN: 1539-0756. DOI: 10.1103/revmodphys.79.677.

[60] S. G. Louie, "Electronic Properties, Junctions, and Defects of Carbon Nanotubes", in *Carbon Nanotubes*. Springer Berlin Heidelberg, 2001, pp. 113–145, ISBN: 9783540410867. DOI: 10.1007/3-540-39947-x_6.

[61] R. Saito, G. Dresselhaus, and M. S. Dresselhaus, "Trigonal warping effect of carbon nanotubes", *Physical Review B*, vol. 61, no. 4, pp. 2981–2990, Jan. 2000, ISSN: 1095-3795. DOI: 10.1103/physrevb.61.2981.

[62] H. Kataura, Y. Kumazawa, Y. Maniwa, I. Umezu, S. Suzuki, Y. Ohtsuka, and Y. Achiba, "Optical properties of single-wall carbon nanotubes", *Synthetic Metals*, vol. 103, no. 1–3, pp. 2555–2558, Jun. 1999, ISSN: 0379-6779. DOI: 10.1016/s0379-6779(98)00278-1.

[63] J. Lefebvre, J. M. Fraser, P. Finnie, and Y. Homma, "Photoluminescence from an individual single-walled carbon nanotube", *Physical Review B*, vol. 69, no. 7, p. 075 403, Feb. 2004, ISSN: 1550-235X. DOI: 10.1103/physrevb.69.075403.

[64] Y. Miyauchi, "Photoluminescence studies on exciton photophysics in carbon nanotubes", *Journal of Materials Chemistry C*, vol. 1, no. 40, p. 6499, 2013, ISSN: 2050-7534. DOI: 10.1039/c3tc00947e.

[65] M. Jones, C. Engtrakul, W. K. Metzger, R. J. Ellingson, A. J. Nozik, M. J. Heben, and G. Rumbles, "Analysis of photoluminescence from solubilized single-walled carbon nanotubes", *Physical Review B*, vol. 71, no. 11, p. 115 426, Mar. 2005, ISSN: 1550-235X. DOI: 10.1103/physrevb.71.115426.

[66] S. Hasegawa, "Surface one-dimensional structures", *Chinese Journal of Physics*, vol. 45, no. 4, pp. 385–411, 2007.

[67] P. Delaney, H. Joon Choi, J. Ihm, S. G. Louie, and M. L. Cohen, "Broken symmetry and pseudogaps in ropes of carbon nanotubes", *Physical Review B*, vol. 60, no. 11, pp. 7899–7904, Sep. 1999, ISSN: 1095-3795. DOI: 10.1103/physrevb.60.7899.

[68] A. A. Balandin, "Phononics of Graphene and Related Materials", *ACS Nano*, vol. 14, no. 5, pp. 5170–5178, Apr. 2020, ISSN: 1936-086X. DOI: 10.1021/acsnano.0c02718.

[69] S. Piscanec, M. Lazzeri, F. Mauri, A. C. Ferrari, and J. Robertson, "Kohn Anomalies and Electron-Phonon Interactions in Graphite", *Physical Review Letters*, vol. 93, no. 18, p. 185 503, Oct. 2004, ISSN: 1079-7114. DOI: 10.1103/physrevlett.93.185503.

[70] A. Grüneis, J. Serrano, A. Bosak, M. Lazzeri, S. L. Molodtsov, L. Wirtz, C. Attaccalite, M. Krisch, A. Rubio, F. Mauri, and T. Pichler, "Phonon surface mapping of graphite: Disentangling quasi-degenerate phonon dispersions", *Physical Review B*, vol. 80, no. 8, p. 085 423, Aug. 2009, ISSN: 1550-235X. DOI: 10.1103/physrevb.80.085423.

[71] T. Mueller, M. Kinoshita, M. Steiner, V. Perebeinos, A. A. Bol, D. B. Farmer, and P. Avouris, "Efficient narrow-band light emission from a single carbon nanotube p–n diode", *Nature Nanotechnology*, vol. 5, no. 1, pp. 27–31, Nov. 2009, ISSN: 1748-3395. DOI: 10.1038/nnano.2009.319.

[72] M. Schroter, M. Claus, P. Sakalas, M. Haferlach, and D. Wang, "Carbon Nanotube FET Technology for Radio-Frequency Electronics: State-of-the-Art Overview", *IEEE Journal of the Electron Devices Society*, vol. 1, no. 1, pp. 9–20, Jan. 2013, ISSN: 2168-6734. DOI: 10.1109/jeds.2013.2244641.

[73] J. Wang, "Carbon-Nanotube Based Electrochemical Biosensors: A Review", *Electroanalysis*, vol. 17, no. 1, pp. 7–14, Jan. 2005, ISSN: 1521-4109. DOI: 10.1002/elan.200403113.

[74] D. A. Walters, L. M. Ericson, M. J. Casavant, J. Liu, D. T. Colbert, K. A. Smith, and R. E. Smalley, "Elastic strain of freely suspended single-wall carbon nanotube ropes", *Applied Physics Letters*, vol. 74, no. 25, pp. 3803–3805, Jun. 1999, ISSN: 1077-3118. DOI: 10.1063/1.124185.

[75] B. Demczyk, Y. Wang, J. Cumings, M. Hetman, W. Han, A. Zettl, and R. Ritchie, "Direct mechanical measurement of the tensile strength and elastic modulus of multiwalled carbon nanotubes", *Materials Science and Engineering: A*, vol. 334, no. 1–2, pp. 173–178, Sep. 2002, ISSN: 0921-5093. DOI: 10.1016/s0921-5093(01)01807-x.

[76] E. Pavlina and C. Van Tyne, "Correlation of Yield Strength and Tensile Strength with Hardness for Steels", *Journal of Materials Engineering and Performance*, vol. 17, no. 6, pp. 888–893, Dec. 2008, ISSN: 1544-1024. DOI: 10.1007/s11665-008-9225-5.

[77] M. M. J. Treacy, T. W. Ebbesen, and J. M. Gibson, "Exceptionally high Young's modulus observed for individual carbon nanotubes", *Nature*, vol. 381, no. 6584, pp. 678–680, Jun. 1996, ISSN: 1476-4687. DOI: 10.1038/381678a0.

[78] B. I. Yakobson and P. Avouris, "Mechanical Properties of Carbon Nanotubes", in *Carbon Nanotubes*. Springer Berlin Heidelberg, 2001, pp. 287–327, ISBN: 9783540410867. DOI: 10.1007/3-540-39947-x_12.

[79] W. Lu, M. Zu, J.-H. Byun, B.-S. Kim, and T.-W. Chou, "State of the Art of Carbon Nanotube Fibers: Opportunities and Challenges", *Advanced Materials*, vol. 24, no. 14, pp. 1805–1833, Mar. 2012, ISSN: 1521-4095. DOI: 10.1002/adma.201104672.

[80] A. Jorio, M. A. Pimenta, A. G. S. Filho, R. Saito, G. Dresselhaus, and M. S. Dresselhaus, "Characterizing carbon nanotube samples with resonance Raman scattering", *New Journal of Physics*, vol. 5, pp. 139–139, Oct. 2003, ISSN: 1367-2630. DOI: 10.1088/1367-2630/5/1/139.

[81] P. Corio, A. G. Souza Filho, A. P. Santos, C. A. Furtado, A. Jorio, F. Plentz, and M. A. Pimenta, "Spectroscopic Characterization of carbon nanotubes", *Chemistry of Carbon Nanotubes (American Scientific Publishers, 2008) v*, vol. 3, pp. 142–171, 2008.

[82] A. Jorio, R. Saito, J. H. Hafner, C. M. Lieber, M. Hunter, T. McClure, G. Dresselhaus, and M. S. Dresselhaus, "Structural (n,m) Determination of Isolated Single-Wall Carbon Nanotubes by Resonant Raman Scattering", *Physical Review Letters*, vol. 86, no. 6, pp. 1118–1121, Feb. 2001, ISSN: 1079-7114. DOI: 10.1103/physrevlett.86.1118.

[83] A. G. Souza Filho, A. Jorio, J. H. Hafner, C. M. Lieber, R. Saito, M. A. Pimenta, G. Dresselhaus, and M. S. Dresselhaus, "Electronic transition energy E_{ii} for an isolated(n,m)single-wall carbon nanotube obtained by anti-Stokes/Stokes resonant Raman intensity ratio", *Physical Review B*, vol. 63, no. 24, p. 241 404, Jun. 2001, ISSN: 1095-3795. DOI: 10.1103/physrevb.63.241404.

[84] M. Dresselhaus, A. Jorio, and R. Saito, "Characterizing Graphene, Graphite, and Carbon Nanotubes by Raman Spectroscopy", *Annual Review of Condensed Matter Physics*, vol. 1, no. 1, pp. 89–108, Aug. 2010, ISSN: 1947-5462. DOI: 10.1146/annurev-conmatphys-070909-103919.

[85] V. N. Popov and L. Henrard, "Breathinglike phonon modes of multiwalled carbon nanotubes", *Physical Review B*, vol. 65, no. 23, p. 235 415, May 2002, ISSN: 1095-3795. DOI: 10.1103/physrevb.65.235415.

[86] C. Thomsen and S. Reich, "Raman Scattering in Carbon Nanotubes", in *Light Scattering in Solid IX*. Springer Berlin Heidelberg, 2007, pp. 115–234, ISBN: 9783540344353. DOI: 10.1007/978-3-540-34436-0_3.

[87] R. Pfeiffer, C. Kramberger, F. Simon, H. Kuzmany, V. N. Popov, and H. Kataura, "Interaction between concentric tubes in DWCNTs", *The European Physical Journal B*, vol. 42, no. 3, pp. 345–350, Dec. 2004, ISSN: 1434-6036. DOI: 10.1140/epjb/e2004-00389-0.

[88] M. Lazzeri, S. Piscanec, F. Mauri, A. C. Ferrari, and J. Robertson, "Phonon linewidths and electron-phonon coupling in graphite and nanotubes", *Physical Review B*, vol. 73, no. 15, p. 155 426, Apr. 2006, ISSN: 1550-235X. DOI: 10.1103/physrevb.73.155426.

[89] T. Michel, M. Paillet, A. Zahab, D. Nakabayashi, V. Jourdain, R. Parret, and J.-L. Sauvajol, "About the indexing of the structure of single-walled carbon nanotubes from resonant Raman scattering", *Advances in Natural Sciences: Nanoscience and Nanotechnology*, vol. 1, no. 4, p. 045 007, Dec. 2010, ISSN: 2043-6262. DOI: 10.1088/2043-6262/1/4/045007.

[90] C. Thomsen and S. Reich, "Double Resonant Raman Scattering in Graphite", *Physical Review Letters*, vol. 85, no. 24, pp. 5214–5217, Dec. 2000, ISSN: 1079-7114. DOI: 10.1103/physrevlett.85.5214.

[91] M. Lucchese, F. Stavale, E. M. Ferreira, C. Vilani, M. Moutinho, R. B. Capaz, C. Achete, and A. Jorio, "Quantifying ion-induced defects and Raman relaxation length in graphene", *Carbon*, vol. 48, no. 5, pp. 1592–1597, Apr. 2010, ISSN: 0008-6223. DOI: 10.1016/j.carbon.2009.12.057.

[92] H. Dai, "Nanotube Growth and Characterization", in *Carbon Nanotubes*. Springer Berlin Heidelberg, 2001, pp. 29–53, ISBN: 9783540410867. DOI: 10.1007/3-540-39947-x_3.

[93] T. W. Ebbesen and P. M. Ajayan, "Large-scale synthesis of carbon nanotubes", *Nature*, vol. 358, no. 6383, pp. 220–222, Jul. 1992, ISSN: 1476-4687. DOI: 10.1038/358220a0.

[94] C. Journet, W. K. Maser, P. Bernier, A. Loiseau, M. L. de la Chapelle, S. Lefrant, P. Deniard, R. Lee, and J. E. Fischer, "Large-scale production of single-walled carbon nanotubes by the electric-arc technique", *Nature*, vol. 388, no. 6644, pp. 756–758, Aug. 1997, ISSN: 1476-4687. DOI: 10.1038/41972.

[95] T. Guo, P. Nikolaev, A. G. Rinzler, D. Tomanek, D. T. Colbert, and R. E. Smalley, "Self-Assembly of Tubular Fullerenes", *The Journal of Physical Chemistry*, vol. 99, no. 27, pp. 10 694–10 697, Jul. 1995, ISSN: 1541-5740. DOI: 10.1021/j100027a002.

[96] T. Guo, P. Nikolaev, A. Thess, D. Colbert, and R. Smalley, "Catalytic growth of single-walled nanotubes by laser vaporization", *Chemical Physics Letters*, vol. 243, no. 1–2, pp. 49–54, Sep. 1995, ISSN: 0009-2614. DOI: 10.1016/0009-2614(95)00825-o.

[97] M. José-Yacamán, M. Miki-Yoshida, L. Rendón, and J. G. Santiesteban, "Catalytic growth of carbon microtubules with fullerene structure", *Applied Physics Letters*, vol. 62, no. 6, pp. 657–659, Feb. 1993, ISSN: 1077-3118. DOI: 10.1063/1.108857.

[98] J. Kong, A. M. Cassell, and H. Dai, "Chemical vapor deposition of methane for single-walled carbon nanotubes", *Chemical Physics Letters*, vol. 292, no. 4–6, pp. 567–574, Aug. 1998, ISSN: 0009-2614. DOI: 10.1016/s0009-2614(98)00745-3.

[99] W. Z. Li, S. S. Xie, L. X. Qian, B. H. Chang, B. S. Zou, W. Y. Zhou, R. A. Zhao, and G. Wang, "Large-Scale Synthesis of Aligned Carbon Nanotubes", *Science*, vol. 274, no. 5293, pp. 1701–1703, Dec. 1996, ISSN: 1095-9203. DOI: 10.1126/science.274.5293.1701.

[100] P. G. Collins and P. Avouris, "Nanotubes for Electronics", *Scientific American*, vol. 283, no. 6, pp. 62–69, Dec. 2000, ISSN: 0036-8733. DOI: 10.1038/scientificamerican1200-62.

[101] T. Saito, S. Ohshima, T. Okazaki, S. Ohmori, M. Yumura, and S. Iijima, "Selective Diameter Control of Single-Walled Carbon Nanotubes in the Gas-Phase Synthesis", *Journal of Nanoscience and Nanotechnology*, vol. 8, no. 11, pp. 6153–6157, Nov. 2008, ISSN: 1533-4880. DOI: 10.1166/jnn.2008.sw23.

[102] P.-X. Hou, C. Liu, and H.-M. Cheng, "Purification of carbon nanotubes", *Carbon*, vol. 46, no. 15, pp. 2003–2025, Dec. 2008, ISSN: 0008-6223. DOI: 10.1016/j.carbon.2008.09.009.

[103] D. E. Luzzi and B. W. Smith, "Carbon cage structures in single wall carbon nanotubes: a new class of materials", *Carbon*, vol. 38, no. 11–12, pp. 1751–1756, 2000, ISSN: 0008-6223. DOI: 10.1016/s0008-6223(00)00088-9.

[104] M. S. Arnold, A. A. Green, J. F. Hulvat, S. I. Stupp, and M. C. Hersam, "Sorting carbon nanotubes by electronic structure using density differentiation", *Nature Nanotechnology*, vol. 1, no. 1, pp. 60–65, Oct. 2006, ISSN: 1748-3395. DOI: 10.1038/nnano.2006.52.

[105] M. S. Arnold, S. I. Stupp, and M. C. Hersam, "Enrichment of Single-Walled Carbon Nanotubes by Diameter in Density Gradients", *Nano Letters*, vol. 5, no. 4, pp. 713–718, Mar. 2005, ISSN: 1530-6992. DOI: 10.1021/nl050133o.

[106] J. Lu, S. Nagase, X. Zhang, D. Wang, M. Ni, Y. Maeda, T. Wakahara, T. Nakahodo, T. Tsuchiya, T. Akasaka, Z. Gao, D. Yu, H. Ye, W. N. Mei, and Y. Zhou, "Selective Interaction of Large or Charge-Transfer Aromatic Molecules with Metallic Single-Wall Carbon Nanotubes: Critical Role of the Molecular Size and Orientation", *Journal of the American Chemical Society*, vol. 128, no. 15, pp. 5114–5118, Mar. 2006, ISSN: 1520-5126. DOI: 10.1021/ja058214+.

[107] S. Ghosh, S. M. Bachilo, and R. B. Weisman, "Advanced sorting of single-walled carbon nanotubes by nonlinear density-gradient ultracentrifugation", *Nature Nanotechnology*, vol. 5, no. 6, pp. 443–450, May 2010, ISSN: 1748-3395. DOI: 10.1038/nnano.2010.68.

[108] A. A. Green, M. C. Duch, and M. C. Hersam, "Isolation of single-walled carbon nanotube enantiomers by density differentiation", *Nano Research*, vol. 2, no. 1, pp. 69–77, Jan. 2009, ISSN: 1998-0000. DOI: 10.1007/s12274-009-9006-y.

[109] H. Gui, H. Chen, C. Y. Khripin, B. Liu, J. A. Fagan, C. Zhou, and M. Zheng, "A facile and low-cost length sorting of single-wall carbon nanotubes by precipitation and applications for thin-film transistors", *Nanoscale*, vol. 8, no. 6, pp. 3467–3473, 2016, ISSN: 2040-3372. DOI: 10.1039/c5nr07329d.

[110] Y. Chen, Y. Xu, K. Perry, A. P. Sokolov, K. More, and Y. Pang, "Achieving Diameter-Selective Separation of Single-Walled Carbon Nanotubes by Using Polymer Conformation-Confined Helical Cavity", *ACS Macro Letters*, vol. 1, no. 6, pp. 701–705, May 2012, ISSN: 2161-1653. DOI: 10.1021/mz3001308.

[111] F. Lemasson, N. Berton, J. Tittmann, F. Hennrich, M. M. Kappes, and M. Mayor, "Polymer Library Comprising Fluorene and Carbazole Homo- and Copolymers for Selective Single-Walled Carbon Nanotubes Extraction", *Macromolecules*, vol. 45, no. 2, pp. 713–722, Dec. 2011, ISSN: 1520-5835. DOI: 10.1021/ma201890g.

[112] K. Akazaki, F. Toshimitsu, H. Ozawa, T. Fujigaya, and N. Nakashima, "Recognition and One-Pot Extraction of Right- and Left-Handed Semiconducting Single-Walled Carbon Nanotube Enantiomers Using Fluorene-Binaphthol Chiral Copolymers", *Journal of the American Chemical Society*, vol. 134, no. 30, pp. 12 700–12 707, Jul. 2012, ISSN: 1520-5126. DOI: 10.1021/ja304244g.

[113] J. A. Fagan, "Aqueous two-polymer phase extraction of single-wall carbon nanotubes using surfactants", *Nanoscale Advances*, vol. 1, no. 9, pp. 3307–3324, 2019, ISSN: 2516-0230. DOI: 10.1039/c9na00280d.

[114] G. S. Duesberg, M. Burghard, J. Muster, and G. Philipp, "Separation of carbon nanotubes by size exclusion chromatography", *Chemical Communications*, no. 3, pp. 435–436, 1998, ISSN: 1364-548X. DOI: 10.1039/a707465d.

[115] T. Tanaka, Y. Urabe, D. Nishide, and H. Kataura, "Continuous Separation of Metallic and Semiconducting Carbon Nanotubes Using Agarose Gel", *Applied Physics Express*, vol. 2, no. 12, p. 125 002, Nov. 2009, ISSN: 1882-0786. DOI: 10.1143/apex.2.125002.

[116] H. Liu, T. Tanaka, Y. Urabe, and H. Kataura, "High-Efficiency Single-Chirality Separation of Carbon Nanotubes Using Temperature-Controlled Gel Chromatography", *Nano Letters*, vol. 13, no. 5, pp. 1996–2003, Apr. 2013, ISSN: 1530-6992. DOI: 10.1021/nl400128m.

[117] M. Zheng and E. D. Semke, "Enrichment of Single Chirality Carbon Nanotubes", *Journal of the American Chemical Society*, vol. 129, no. 19, pp. 6084–6085, Apr. 2007, ISSN: 1520-5126. DOI: 10.1021/ja071577k.

[118] X. Li, X. Tu, S. Zaric, K. Welsher, W. S. Seo, W. Zhao, and H. Dai, "Selective Synthesis Combined with Chemical Separation of Single-Walled Carbon Nanotubes for Chirality Selection", *Journal of the American Chemical Society*, vol. 129, no. 51, pp. 15 770–15 771, Dec. 2007, ISSN: 1520-5126. DOI: 10.1021/ja077886s.

[119] H. Li, G. Gordeev, S. Wasserroth, V. S. K. Chakravadhanula, S. K. C. Neelakandhan, F. Hennrich, A. Jorio, S. Reich, R. Krupke, and B. S. Flavel, "Inner- and outer-wall sorting of double-walled carbon nanotubes", *Nature Nanotechnology*, vol. 12, no. 12, pp. 1176–1182, Oct. 2017, ISSN: 1748-3395. DOI: 10.1038/nnano.2017.207.

[120] T. Tanaka, H. Jin, Y. Miyata, and H. Kataura, "High-Yield Separation of Metallic and Semiconducting Single-Wall Carbon Nanotubes by Agarose Gel Electrophoresis", *Applied Physics Express*, vol. 1, p. 114 001, Nov. 2008, ISSN: 1882-0786. DOI: 10.1143/apex.1.114001.

[121] D. Janas, "Towards monochiral carbon nanotubes: a review of progress in the sorting of single-walled carbon nanotubes", *Materials Chemistry Frontiers*, vol. 2, no. 1, pp. 36–63, 2018, ISSN: 2052-1537. DOI: 10.1039/c7qm00427c.

[122] M. Monthioux, *Carbon meta-nanotubes: Synthesis, properties and applications*. John Wiley & Sons, 2011.

[123] C. Kramberger, H. Rauf, M. Knupfer, H. Shiozawa, D. Batchelor, A. Rubio, H. Kataura, and T. Pichler, "Potassium-intercalated single-wall carbon nanotube bundles: Archetypes for semiconductor/metal hybrid systems", *Physical Review B*, vol. 79, no. 19, p. 195 442, May 2009, ISSN: 1550-235X. DOI: 10.1103/physrevb.79.195442.

[124] C. Kröckel, M. R. Preciado-Rivas, V. A. Torres-Sánchez, D. J. Mowbray, S. Reich, F. Hauke, J. C. Chacón-Torres, and A. Hirsch, "Understanding the Electron-Doping Mechanism in Potassium-Intercalated Single-Walled Carbon Nanotubes", *Journal of the American Chemical Society*, vol. 142, no. 5, pp. 2327–2337, Jan. 2020, ISSN: 1520-5126. DOI: 10.1021/jacs.9b11370.

[125] J. Chacón-Torres, S. Dzsaber, S. Vega-Diaz, J. Akbarzadeh, H. Peterlik, J. Kotakoski, G. Argentero, J. Meyer, T. Pichler, F. Simon, M. Terrones, and S. Reich, "Potassium intercalated multiwalled carbon nanotubes", *Carbon*, vol. 105, pp. 90–95, Aug. 2016, ISSN: 0008-6223. DOI: 10.1016/j.carbon.2016.04.016.

[126] J. C. Chacón-Torres, L. Wirtz, and T. Pichler, "Manifestation of Charged and Strained Graphene Layers in the Raman Response of Graphite Intercalation Compounds", *ACS Nano*, vol. 7, no. 10, pp. 9249–9259, Sep. 2013, ISSN: 1936-086X. DOI: 10.1021/nn403885k.

[127] S. Pisana, M. Lazzeri, C. Casiraghi, K. S. Novoselov, A. K. Geim, A. C. Ferrari, and F. Mauri, "Breakdown of the adiabatic Born–Oppenheimer approximation in graphene", *Nature Materials*, vol. 6, no. 3, pp. 198–201, Feb. 2007, ISSN: 1476-4660. DOI: 10.1038/nmat1846.

[128] M. Lazzeri and F. Mauri, "Nonadiabatic Kohn Anomaly in a Doped Graphene Monolayer", *Physical Review Letters*, vol. 97, no. 26, p. 266 407, Dec. 2006, ISSN: 1079-7114. DOI: 10.1103/physrevlett.97.266407.

[129] S. Yuan, Q. Zhang, Y. You, Z.-X. Shen, D. Shimamoto, and M. Endo, "Correlation between in Situ Raman Scattering and Electrical Conductance for an Individual Double-Walled Carbon Nanotube", *Nano Letters*, vol. 9, no. 1, pp. 383–387, Jan. 2009, ISSN: 1530-6992. DOI: 10.1021/nl803188g.

[130] D. Golberg and M. Terrones, "Heterogeneous Nanotubes: (X*CNTs, X*BNNTs)", in Wiley, Oct. 2011, pp. 323–409, ISBN: 9781119954743. DOI: 10.1002/9781119954743.ch6.

[131] P. Ayala, R. Arenal, A. Loiseau, A. Rubio, and T. Pichler, "The physical and chemical properties of heteronanotubes", *Reviews of Modern Physics*, vol. 82, no. 2, pp. 1843–1885, Jun. 2010, ISSN: 1539-0756. DOI: 10.1103/revmodphys.82.1843.

[132] F. Xu, M. Minniti, C. Giallombardo, A. Cupolillo, P. Barone, A. Oliva, and L. Papagno, "Nitrogen ion implantation in single wall carbon nanotubes", *Surface Science*, vol. 601, no. 13, pp. 2819–2822, Jul. 2007, ISSN: 0039-6028. DOI: 10.1016/j.susc.2006.12.049.

[133] W. Han, Y. Bando, K. Kurashima, and T. Sato, "Synthesis of boron nitride nanotubes from carbon nanotubes by a substitution reaction", *Applied Physics Letters*, vol. 73, no. 21, pp. 3085–3087, Nov. 1998, ISSN: 1077-3118. DOI: 10.1063/1.122680.

[134] F. Villalpando-Paez, A. Zamudio, A. Elias, H. Son, E. Barros, S. Chou, Y. Kim, H. Muramatsu, T. Hayashi, J. Kong, H. Terrones, G. Dresselhaus, M. Endo, M. Terrones, and M. Dresselhaus, "Synthesis and characterization of long strands of nitrogen-doped single-walled carbon nanotubes", *Chemical Physics Letters*, vol. 424, no. 4–6, pp. 345–352, Jun. 2006, ISSN: 0009-2614. DOI: 10.1016/j.cplett.2006.04.074.

[135] K. McGuire, N. Gothard, P. Gai, M. Dresselhaus, G. Sumanasekera, and A. Rao, "Synthesis and Raman characterization of boron-doped single-walled carbon nanotubes", *Carbon*, vol. 43, no. 2, pp. 219–227, 2005, ISSN: 0008-6223. DOI: 10.1016/j.carbon.2004.11.001.

[136] Q.-H. Yang, P.-X. Hou, M. Unno, S. Yamauchi, R. Saito, and T. Kyotani, "Dual Raman Features of Double Coaxial Carbon Nanotubes with N-Doped and B-Doped Multiwalls", *Nano Letters*, vol. 5, no. 12, pp. 2465–2469, Nov. 2005, ISSN: 1530-6992. DOI: 10.1021/nl051779j.

[137] C. Allard, L. Alvarez, J.-L. Bantignies, N. Bendiab, S. Cambré, S. Campidelli, J. A. Fagan, E. Flahaut, B. Flavel, F. Fossard, E. Gaufrès, S. Heeg, J.-S. Lauret, A. Loiseau, J.-B. Marceau, R. Martel, L. Marty, T. Pichler, C. Voisin, S. Reich, A. Setaro, L. Shi, and W. Wenseleers, "Advanced 1D heterostructures based on nanotube templates and molecules", *Chemical Society Reviews*, vol. 53, no. 16, pp. 8457–8512, 2024, ISSN: 1460-4744. DOI: 10.1039/d3cs00467h.

[138] B. W. Smith, M. Monthioux, and D. E. Luzzi, "Encapsulated C_{60} in carbon nanotubes", *Nature*, vol. 396, no. 6709, pp. 323–324, Nov. 1998, ISSN: 1476-4687. DOI: 10.1038/24521.

[139] A. Bondi, "van der Waals Volumes and Radii", *The Journal of Physical Chemistry*, vol. 68, no. 3, pp. 441–451, Mar. 1964, ISSN: 1541-5740. DOI: 10.1021/j100785a001.

[140] B. W. Smith and D. E. Luzzi, "Formation mechanism of fullerene peapods and coaxial tubes: a path to large scale synthesis", *Chemical Physics Letters*, vol. 321, no. 1–2, pp. 169–174, Apr. 2000, ISSN: 0009-2614. DOI: 10.1016/s0009-2614(00)00307-9.

[141] H. Kataura, Y. Maniwa, T. Kodama, K. Kikuchi, K. Hirahara, K. Suenaga, S. Iijima, S. Suzuki, Y. Achiba, and W. Krätschmer, "High-yield fullerene encapsulation in single-wall carbon nanotubes", *Synthetic Metals*, vol. 121, no. 1-3, pp. 1195–1196, 2001.

[142] K. Hirahara, K. Suenaga, S. Bandow, H. Kato, T. Okazaki, H. Shinohara, and S. Iijima, "One-Dimensional Metallofullerene Crystal Generated Inside Single-Walled Carbon Nanotubes", *Physical Review Letters*, vol. 85, no. 25, pp. 5384–5387, Dec. 2000, ISSN: 1079-7114. DOI: 10.1103/physrevlett.85.5384.

[143] H. Kataura, Y. Maniwa, M. Abe, A. Fujiwara, T. Kodama, K. Kikuchi, H. Imahori, Y. Misaki, S. Suzuki, and Y. Achiba, "Optical properties of fullerene and non-fullerene peapods", *Applied Physics A: Materials Science I& Processing*, vol. 74, no. 3, pp. 349–354, Mar. 2002, ISSN: 1432-0630. DOI: 10.1007/s003390201276.

[144] X. Liu, T. Pichler, M. Knupfer, M. S. Golden, J. Fink, H. Kataura, Y. Achiba, K. Hirahara, and S. Iijima, "Filling factors, structural, and electronic properties of C_{60} molecules in single-wall carbon nanotubes", *Physical Review B*, vol. 65, no. 4, p. 045 419, Jan. 2002, ISSN: 1095-3795. DOI: 10.1103/physrevb.65.045419.

[145] H. Kuzmany, R. Pfeiffer, C. Kramberger, T. Pichler, X. Liu, M. Knupfer, J. Fink, H. Kataura, Y. Achiba, B. Smith, and D. Luzzi, "Analysis of the concentration of C_{60} fullerenes in single wall carbon nanotubes", *Applied Physics A: Materials Science I& Processing*, vol. 76, no. 4, pp. 449–456, Mar. 2003, ISSN: 1432-0630. DOI: 10.1007/s00339-002-2046-8.

[146] B. W. Smith, M. Monthioux, and D. E. Luzzi, "Carbon nanotube encapsulated fullerenes: a unique class of hybrid materials", *Chemical Physics Letters*, vol. 315, no. 1–2, pp. 31–36, Dec. 1999, ISSN: 0009-2614. DOI: 10.1016/s0009-2614(99)00896-9.

[147] S. Bandow, M. Takizawa, K. Hirahara, M. Yudasaka, and S. Iijima, "Raman scattering study of double-wall carbon nanotubes derived from the chains of fullerenes in single-wall carbon nanotubes", *Chemical Physics Letters*, vol. 337, no. 1–3, pp. 48–54, Mar. 2001, ISSN: 0009-2614. DOI: 10.1016/s0009-2614(01)00192-0.

[148] Y. Sakurabayashi, "Tailoring double-wall carbon nanotubes?", in *AIP Conference Proceedings*, AIP, 2003. DOI: 10.1063/1.1628039.

[149] C. Kramberger, A. Waske, K. Biedermann, T. Pichler, T. Gemming, B. Büchner, and H. Kataura, "Tailoring carbon nanostructures via temperature and laser irradiation", *Chemical Physics Letters*, vol. 407, no. 4–6, pp. 254–259, May 2005, ISSN: 0009-2614. DOI: 10.1016/j.cplett.2005.03.089.

[150] S. Han, M. Yoon, S. Berber, N. Park, E. Osawa, J. Ihm, and D. Tománek, "Microscopic mechanism of fullerene fusion", *Physical Review B*, vol. 70, no. 11, p. 113 402, Sep. 2004, ISSN: 1550-235X. DOI: 10.1103/physrevb.70.113402.

[151] A. Stone and D. Wales, "Theoretical studies of icosahedral C_{60} and some related species", *Chemical Physics Letters*, vol. 128, no. 5–6, pp. 501–503, Aug. 1986, ISSN: 0009-2614. DOI: 10.1016/0009-2614(86)80661-3.

[152] S. Bandow, T. Hiraoka, T. Yumura, K. Hirahara, H. Shinohara, and S. Iijima, "Raman scattering study on fullerene derived intermediates formed within single-wall carbon nanotube: from peapod to double-wall carbon nanotube", *Chemical Physics Letters*, vol. 384, no. 4–6, pp. 320–325, Jan. 2004, ISSN: 0009-2614. DOI: 10.1016/j.cplett.2003.12.032.

[153] R. Pfeiffer, M. Holzweber, H. Peterlik, H. Kuzmany, Z. Liu, K. Suenaga, and H. Kataura, "Dynamics of Carbon Nanotube Growth from Fullerenes", *Nano Letters*, vol. 7, no. 8, pp. 2428–2434, Jul. 2007, ISSN: 1530-6992. DOI: 10.1021/nl071107o.

[154] F. Simon, Á. Kukovecz, C. Kramberger, R. Pfeiffer, F. Hasi, H. Kuzmany, and H. Kataura, "Diameter selective reaction processes of single-wall carbon nanotubes", *Physical Review B*, vol. 71, no. 16, p. 165 439, Apr. 2005, ISSN: 1550-235X. DOI: 10.1103/physrevb.71.165439.

[155] F. Simon and H. Kuzmany, "Growth of single wall carbon nanotubes from ^{13}C isotope labelled organic solvents inside single wall carbon nanotube hosts", *Chemical Physics Letters*, vol. 425, no. 1–3, pp. 85–88, Jul. 2006, ISSN: 0009-2614. DOI: 10.1016/j.cplett.2006.04.094.

[156] H. Shiozawa, T. Pichler, A. Grüneis, R. Pfeiffer, H. Kuzmany, Z. Liu, K. Suenaga, and H. Kataura, "A Catalytic Reaction Inside a Single-Walled Carbon Nanotube", *Advanced Materials*, vol. 20, no. 8, pp. 1443–1449, Apr. 2008, ISSN: 1521-4095. DOI: 10.1002/adma.200701466.

[157] V. Zólyomi, F. Simon, Á. Rusznyák, R. Pfeiffer, H. Peterlik, H. Kuzmany, and J. Kürti, "Inhomogeneity of C^{13} isotope distribution in isotope engineered carbon nanotubes: Experiment and theory", *Physical Review B*, vol. 75, no. 19, p. 195 419, May 2007, ISSN: 1550-235X. DOI: 10.1103/physrevb.75.195419.

[158] J. Lee, H. Kim, S.-J. Kahng, G. Kim, Y.-W. Son, J. Ihm, H. Kato, Z. W. Wang, T. Okazaki, H. Shinohara, and Y. Kuk, "Bandgap modulation of carbon nanotubes by encapsulated metallofullerenes", *Nature*, vol. 415, no. 6875, pp. 1005–1008, Feb. 2002, ISSN: 1476-4687. DOI: 10.1038/4151005a.

[159] T. Shimada, T. Okazaki, R. Taniguchi, T. Sugai, H. Shinohara, K. Suenaga, Y. Ohno, S. Mizuno, S. Kishimoto, and T. Mizutani, "Ambipolar field-effect transistor behavior of $Gd@C_{82}$ metallofullerene peapods", *Applied Physics Letters*, vol. 81, no. 21, pp. 4067–4069, Nov. 2002, ISSN: 1077-3118. DOI: 10.1063/1.1522482.

[160] Y. F. Li, T. Kaneko, and R. Hatakeyama, "Photoinduced electron transfer in C_{60} encapsulated single-walled carbon nanotube", *Applied Physics Letters*, vol. 92, no. 18, May 2008, ISSN: 1077-3118. DOI: 10.1063/1.2924300.

[161] A. Bianco, K. Kostarelos, and M. Prato, "Applications of carbon nanotubes in drug delivery", *Current Opinion in Chemical Biology*, vol. 9, no. 6, pp. 674–679, Dec. 2005, ISSN: 1367-5931. DOI: 10.1016/j.cbpa.2005.10.005.

[162] C. Tripisciano, K. Kraemer, A. Taylor, and E. Borowiak-Palen, "Single-wall carbon nanotubes based anticancer drug delivery system", *Chemical Physics Letters*, vol. 478, no. 4–6, pp. 200–205, Aug. 2009, ISSN: 0009-2614. DOI: 10.1016/j.cplett.2009.07.071.

[163] Y. Dai, C. Tang, and W. Guo, "Simulation studies of a "nanogun" based on carbon nanotubes", *Nano Research*, vol. 1, no. 2, pp. 176–183, Jul. 2008, ISSN: 1998-0000. DOI: 10.1007/s12274-008-8014-7.

[164] R. Xiang, T. Inoue, Y. Zheng, A. Kumamoto, Y. Qian, Y. Sato, M. Liu, D. Tang, D. Gokhale, J. Guo, K. Hisama, S. Yotsumoto, T. Ogamoto, H. Arai, Y. Kobayashi, H. Zhang, B. Hou, A. Anisimov, M. Maruyama, Y. Miyata, S. Okada, S. Chiashi, Y. Li, J. Kong, E. I. Kauppinen, Y. Ikuhara, K. Suenaga, and S. Maruyama, "One-dimensional van der Waals heterostructures", *Science*, vol. 367, no. 6477, pp. 537–542, Jan. 2020, ISSN: 1095-9203. DOI: 10.1126/science.aaz2570.

[165] C. Hu, V. Michaud-Rioux, W. Yao, and H. Guo, "Theoretical Design of Topological Heteronanotubes", *Nano Letters*, vol. 19, no. 6, pp. 4146–4150, May 2019, ISSN: 1530-6992. DOI: 10.1021/acs.nanolett.9b01661.

[166] R. Hoffmann, "How Chemistry and Physics Meet in the Solid State", *Angewandte Chemie International Edition in English*, vol. 26, no. 9, pp. 846–878, Sep. 1987, ISSN: 0570-0833. DOI: 10.1002/anie.198708461.

[167] S. Cahangirov, M. Topsakal, and S. Ciraci, "Long-range interactions in carbon atomic chains", *Physical Review B*, vol. 82, no. 19, p. 195 444, Nov. 2010, ISSN: 1550-235X. DOI: 10.1103/physrevb.82.195444.

[168] M. Kertesz, J. Koller, and A. Ažman, "Ab-initio Hartree–Fock crystal orbital studies. II. Energy bands of an infinite carbon chain", *The Journal of Chemical Physics*, vol. 68, no. 6, pp. 2779–2782, Mar. 1978, ISSN: 1089-7690. DOI: 10.1063/1.436070.

[169] F. Banhart, "Elemental carbon in the sp^1 hybridization", *ChemTexts*, vol. 6, no. 1, Dec. 12, 2019, ISSN: 2199-3793. DOI: 10.1007/s40828-019-0098-z.

[170] V. I. Artyukhov, M. Liu, and B. I. Yakobson, "Mechanically Induced Metal–Insulator Transition in Carbyne", *Nano Letters*, vol. 14, no. 8, pp. 4224–4229, Jul. 2014, ISSN: 1530-6992. DOI: 10.1021/nl5017317.

[171] A. La Torre, A. Botello-Mendez, W. Baaziz, J.-C. Charlier, and F. Banhart, "Strain-induced metal–semiconductor transition observed in atomic carbon chains", *Nature Communications*, vol. 6, no. 1, Mar. 2015, ISSN: 2041-1723. DOI: 10.1038/ncomms7636.

[172] A. Milani, M. Tommasini, V. Russo, A. Li Bassi, A. Lucotti, F. Cataldo, and C. S. Casari, "Raman spectroscopy as a tool to investigate the structure and electronic properties of carbon-atom wires", *Beilstein Journal of Nanotechnology*, vol. 6, pp. 480–491, Feb. 2015, ISSN: 2190-4286. DOI: 10.3762/bjnano.6.49.

[173] T. Pino, H. Ding, F. Güthe, and J. P. Maier, "Electronic spectra of the chains $HC_{2n}H$(n=8–13) in the gas phase", *The Journal of Chemical Physics*, vol. 114, no. 5, pp. 2208–2212, Feb. 2001, ISSN: 1089-7690. DOI: 10.1063/1.1338530.

[174] S. Eisler, A. D. Slepkov, E. Elliott, T. Luu, R. McDonald, F. A. Hegmann, and R. R. Tykwinski, "Polyynes as a Model for Carbyne: Synthesis, Physical Properties, and Nonlinear Optical Response", *Journal of the American Chemical Society*, vol. 127, no. 8, pp. 2666–2676, Feb. 2005, ISSN: 1520-5126. DOI: 10.1021/ja044526l.

[175] L. Shi, P. Rohringer, M. Wanko, A. Rubio, S. Waßerroth, S. Reich, S. Cambré, W. Wenseleers, P. Ayala, and T. Pichler, "Electronic band gaps of confined linear carbon chains ranging from polyyne to carbyne", *Physical Review Materials*, vol. 1, no. 7, p. 075 601, Dec. 12, 2017, ISSN: 2475-9953. DOI: 10.1103/physrevmaterials.1.075601.

[176] S. Heeg, L. Shi, L. V. Poulikakos, T. Pichler, and L. Novotny, "Carbon Nanotube Chirality Determines Properties of Encapsulated Linear Carbon Chain", *Nano Letters*, vol. 18, no. 9, pp. 5426–5431, Aug. 8, 2018, ISSN: 1530-6992. DOI: 10.1021/acs.nanolett.8b01681.

[177] M. Martinati, W. Wenseleers, L. Shi, S. M. Pratik, P. Rohringer, W. Cui, T. Pichler, V. Coropceanu, J.-L. Brédas, and S. Cambré, "Electronic structure of confined carbyne from joint wavelength-dependent resonant Raman spectroscopy and density functional theory investigations", *Carbon*, vol. 189, pp. 276–283, Apr. 2022, ISSN: 0008-6223. DOI: 10.1016/j.carbon.2021.12.059.

[178] M. Liu, V. I. Artyukhov, H. Lee, F. Xu, and B. I. Yakobson, "Carbyne from First Principles: Chain of C Atoms, a Nanorod or a Nanorope", *ACS Nano*, vol. 7, no. 11, pp. 10 075–10 082, Oct. 5, 2013, ISSN: 1936-086X. DOI: 10.1021/nn404177r.

[179] C. Lee, X. Wei, J. W. Kysar, and J. Hone, "Measurement of the Elastic Properties and Intrinsic Strength of Monolayer Graphene", *Science*, vol. 321, no. 5887, pp. 385–388, Jul. 2008, ISSN: 1095-9203. DOI: 10.1126/science.1157996.

[180] A. Timoshevskii, S. Kotrechko, and Y. Matviychuk, "Atomic structure and mechanical properties of carbyne", *Physical Review B*, vol. 91, no. 24, p. 245 434, Jun. 2015, ISSN: 1550-235X. DOI: 10.1103/physrevb.91.245434.

[181] S. Kotrechko, I. Mikhailovskij, T. Mazilova, E. Sadanov, A. Timoshevskii, N. Stetsenko, and Y. Matviychuk, "Mechanical properties of carbyne: experiment and simulations", *Nanoscale Research Letters*, vol. 10, no. 1, Jan. 2015, ISSN: 1556-276X. DOI: 10.1186/s11671-015-0761-2.

[182] C. D. Tschannen, G. Gordeev, S. Reich, L. Shi, T. Pichler, M. Frimmer, L. Novotny, and S. Heeg, "Raman Scattering Cross Section of Confined Carbyne", *Nano Letters*, vol. 20, no. 9, pp. 6750–6755, Aug. 11, 2020, ISSN: 1530-6992. DOI: 10.1021/acs.nanolett.0c02632.

[183] C. S. Casari, M. Tommasini, R. R. Tykwinski, and A. Milani, "Carbon-atom wires: 1-D systems with tunable properties", *Nanoscale*, vol. 8, no. 8, pp. 4414–4435, 2016, ISSN: 2040-3372. DOI: 10.1039/c5nr06175j.

[184] E. Parth, A. Corradini, W. Cui, D. Romanin, C. Schuster, C. Freytag, L. Shi, K. Yanagi, M. Calandra, and T. Pichler, "The resonant Raman response of confined carbyne is solely driven by anharmonic interactions", *submitted*, Oct. 2024. DOI: 10.21203/rs.3.rs-5247129/v1.

[185] K. Momma and F. Izumi, "VESTA3 for three-dimensional visualization of crystal, volumetric and morphology data", *Journal of Applied Crystallography*, vol. 44, no. 6, pp. 1272–1276, Oct. 2011, ISSN: 0021-8898. DOI: 10.1107/s0021889811038970.

[186] A. Milani, M. Tommasini, and G. Zerbi, "Carbynes phonons: A tight binding force field", *The Journal of Chemical Physics*, vol. 128, no. 6, Feb. 2008, ISSN: 1089-7690. DOI: 10.1063/1.2831507.

[187] A. Milani, M. Tommasini, M. Del Zoppo, C. Castiglioni, and G. Zerbi, "Carbon nanowires: Phonon and π-electron confinement", *Physical Review B*, vol. 74, no. 15, p. 153 418, Oct. 31, 2006, ISSN: 1550-235X. DOI: 10.1103/physrevb.74.153418.

[188] H. Tabata, M. Fujii, S. Hayashi, T. Doi, and T. Wakabayashi, "Raman and surface-enhanced Raman scattering of a series of size-separated polyynes", *Carbon*, vol. 44, no. 15, pp. 3168–3176, Dec. 2006, ISSN: 0008-6223. DOI: 10.1016/j.carbon.2006.07.004.

[189] M. Wanko, S. Cahangirov, L. Shi, P. Rohringer, Z. J. Lapin, L. Novotny, P. Ayala, T. Pichler, and A. Rubio, "Polyyne electronic and vibrational properties under environmental interactions", *Physical Review B*, vol. 94, no. 19, p. 195 422, Nov. 14, 2016, ISSN: 2469-9969. DOI: 10.1103/physrevb.94.195422.

[190] W. Cui, P. Ayala, T. Pichler, and L. Shi, "Unraveling the governing properties of confined carbyne through the interaction with its carbon nanotube host", *Carbon*, vol. 219, p. 118 784, Feb. 2024, ISSN: 0008-6223. DOI: 10.1016/j.carbon.2024.118784.

[191] A. Milani, M. Tommasini, D. Fazzi, C. Castiglioni, M. D. Zoppo, and G. Zerbi, "First-principles calculation of the Peierls distortion in an infinite linear carbon chain: the contribution of Raman spectroscopy", *Journal of Raman Spectroscopy*, vol. 39, no. 2, pp. 164–168, Dec. 2007, ISSN: 1097-4555. DOI: 10.1002/jrs.1850.

[192] R. Kuhn and K. Wallenfels, "Über Kumulene I; Synthese von Tetraphenyl-hexapentaen und Di-biphenylen-hexapentaen", *Berichte der deutschen chemischen Gesellschaft (A and B Series)*, vol. 71, no. 4, pp. 783–790, Apr. 1938, ISSN: 0365-9488. DOI: 10.1002/cber.19380710416.

[193] J. A. Januszewski and R. R. Tykwinski, "Synthesis and properties of long [n]cumulenes (n$\geq$ 5)", *Chem. Soc. Rev.*, vol. 43, no. 9, pp. 3184–3203, Mar. 27, 2014, ISSN: 1460-4744. DOI: 10.1039/c4cs00022f.

[194] P. J. Stang, "Unsaturated carbenes", *Chemical Reviews*, vol. 78, no. 4, pp. 383–405, Aug. 1978, ISSN: 1520-6890. DOI: 10.1021/cr60314a003.

[195] K. Brand and A. Busse-Sundermann, "Tetra-[2.4-xylyl]-butatrien und 1.1.4.4-Tetra-[2.4-xylyl]-butin-(2); XVI. Mitteil. über Reduktion organischer Halogenverbindungen und Verbindungen der Tetraarylbutanreihe", *Chemische Berichte*, vol. 83, no. 1, pp. 119–128, Feb. 1950, ISSN: 0009-2940. DOI: 10.1002/cber.19500830122.

[196] J. A. Januszewski, D. Wendinger, C. D. Methfessel, F. Hampel, and R. R. Tykwinski, "Synthesis and Structure of Tetraarylcumulenes: Characterization of Bond-Length Alternation versus Molecule Length", *Angewandte Chemie International Edition*, vol. 52, no. 6, pp. 1817–1821, Jan. 2013, ISSN: 1521-3773. DOI: 10.1002/anie.201208058.

[197] R. Kuhn, H. Fischer, and H. Fischer, "Über Kumulene, XVII. Darstellung von Pentatetraenen", *Chemische Berichte*, vol. 97, no. 6, pp. 1760–1766, Jun. 1964, ISSN: 0009-2940. DOI: 10.1002/cber.19640970638.

[198] G. Karich and J. C. Jochims, "Zur Darstellung und Stereochemie von Pentatetraenen", *Chemische Berichte*, vol. 110, no. 8, pp. 2680–2694, Aug. 1977, ISSN: 0009-2940. DOI: 10.1002/cber.19771100803.

[199] B. Bildstein, "Cationic and neutral cumulene sp-carbon chains with ferrocenyl termini", *Coordination Chemistry Reviews*, vol. 206–207, pp. 369–394, Sep. 2000, ISSN: 0010-8545. DOI: 10.1016/s0010-8545(00)00248-4.

[200] L. Skattebøl, "A novel route to cumulenes. The addition of dihalocarbenes to 2,5-dimethyl-2,3,4-hexatriene.", *Tetrahedron Letters*, vol. 6, no. 26, pp. 2175–2179, Jan. 1965, ISSN: 0040-4039. DOI: 10.1016/s0040-4039(00)90174-6.

[201] B. Bildstein, W. Skibar, M. Schweiger, H. Kopacka, and K. Wurst, "In situ synthesis of the first C_7 cumulene $(Fc)_2C{=}C{=}C{=}C{=}C{=}C(Fc)_2$ via deprotonation of its conjugate acid $[(Fc)_2C_7H(Fc)_2]^+$ BF_4^- (Fc=ferrocenyl)", *Journal of Organometallic Chemistry*, vol. 622, no. 1–2, pp. 135–142, Mar. 2001, ISSN: 0022-328X. DOI: 10.1016/s0022-328x(00)00882-2.

[202] P. Siemsen, R. C. Livingston, and F. Diederich, "Acetylenic Coupling: A Powerful Tool in Molecular Construction", *Angewandte Chemie International Edition*, vol. 39, no. 15, pp. 2632–2657, Aug. 2000, ISSN: 1521-3773. DOI: 10.1002/1521-3773(20000804)39:15<2632::aid-anie2632>3.0.co;2-f.

[203] C. S. Casari, "CARBON ATOMIC WIRES: FROM STARS TO NANOTECHNOLOGY", *Istituto Lombardo - Accademia di Scienze e Lettere - Rendiconti di Scienze*, Dec. 2012, ISSN: 1974-6989. DOI: 10.4081/scie.2012.130.

[204] C. Glaser, "Beiträge zur Kenntniss des Acetenylbenzols", *Berichte der deutschen chemischen Gesellschaft*, vol. 2, no. 1, pp. 422–424, Jan. 1869, ISSN: 0365-9496. DOI: 10.1002/cber.186900201183.

[205] F. Bohlmann, "Die Polyine", *Angewandte Chemie*, vol. 65, no. 15, pp. 385–389, Aug. 1953, ISSN: 1521-3757. DOI: 10.1002/ange.19530651502.

[206] W. A. Chalifoux and R. R. Tykwinski, "Synthesis of extended polyynes: Toward carbyne", *Comptes Rendus. Chimie*, vol. 12, no. 3–4, pp. 341–358, Dec. 2008, ISSN: 1878-1543. DOI: 10.1016/j.crci.2008.10.004.

[207] Q. Zheng, J. C. Bohling, T. B. Peters, A. C. Frisch, F. Hampel, and J. A. Gladysz, "A Synthetic Breakthrough into an Unanticipated Stability Regime: A Series of Isolable Complexes in which C_6, C_8, C_{10}, C_{12}, C_{16}, C_{20}, C_{24}, and C_{28} Polyynediyl Chains Span Two Platinum Atoms", *Chemistry – A European Journal*, vol. 12, no. 25, pp. 6486–6505, Aug. 2006, ISSN: 1521-3765. DOI: 10.1002/chem.200600615.

[208] C. W. Patrick, Y. Gao, P. Gupta, A. L. Thompson, A. W. Parker, and H. L. Anderson, "Masked alkynes for synthesis of threaded carbon chains", *Nature Chemistry*, vol. 16, no. 2, pp. 193–200, Nov. 2023, ISSN: 1755-4349. DOI: 10.1038/s41557-023-01374-z.

[209] E. Kano, M. Takeguchi, J.-i. Fujita, and A. Hashimoto, "Direct observation of Pt-terminating carbyne on graphene", *Carbon*, vol. 80, pp. 382–386, Dec. 2014, ISSN: 0008-6223. DOI: 10.1016/j.carbon.2014.08.077.

[210] W. Gao, W. Zheng, L. Sun, F. Kang, Z. Zhou, and W. Xu, "On-surface synthesis and characterization of polyynic carbon chains", *National Science Review*, vol. 11, no. 3, Jan. 2024, ISSN: 2053-714X. DOI: 10.1093/nsr/nwae031.

[211] M. Tsuji, S. Kuboyama, T. Matsuzaki, and T. Tsuji, "Formation of hydrogen-capped polyynes by laser ablation of C_{60} particles suspended in solution", *Carbon*, vol. 41, no. 11, pp. 2141–2148, Mar. 2003, ISSN: 0008-6223. DOI: 10.1016/s0008-6223(03)00241-0.

[212] F. Cataldo, "Synthesis of polyynes in a submerged electric arc in organic solvents", *Carbon*, vol. 42, no. 1, pp. 129–142, 2004, ISSN: 0008-6223. DOI: 10.1016/j.carbon.2003.10.016.

[213] P. Marabotti, S. Peggiani, S. Melesi, B. Rossi, A. Gessini, A. L. Bassi, V. Russo, and C. S. Casari, "Exploring the Growth Dynamics of Size-Selected Carbon Atomic Wires with In Situ UV Resonance Raman Spectroscopy", *Small*, vol. 20, no. 49, Jul. 2024, ISSN: 1613-6829. DOI: 10.1002/smll.202403054.

[214] C. Jin, H. Lan, L. Peng, K. Suenaga, and S. Iijima, "Deriving Carbon Atomic Chains from Graphene", *Physical Review Letters*, vol. 102, no. 20, p. 205 501, May 2009, ISSN: 1079-7114. DOI: 10.1103/physrevlett.102.205501.

[215] Y. Feng, W. Zhang, K. Tang, Y. Chen, J. Zhang, K. Cao, W. Cui, and L. Shi, "A robust synthesis route of confined carbyne", *Nano Research*, vol. 17, no. 7, pp. 6274–6280, Apr. 2024, ISSN: 1998-0000. DOI: 10.1007/s12274-024-6571-z.

[216] A. J. Kocsis, N. A. R. Yedama, and S. W. Cranford, "Confinement and controlling the effective compressive stiffness of carbyne", *Nanotechnology*, vol. 25, no. 33, p. 335 709, Jul. 2014, ISSN: 1361-6528. DOI: 10.1088/0957-4484/25/33/335709.

[217] Y. Zhang, J. Zhao, Y. Fang, Y. Liu, and X. Zhao, "Preparation of long linear carbon chain inside multi-walled carbon nanotubes by cooling enhanced hydrogen arc discharge method", *Nanoscale*, vol. 10, no. 37, pp. 17 824–17 833, 2018, ISSN: 2040-3372. DOI: 10.1039/c8nr05465g.

[218] W. Chang, F. Liu, Y. Liu, T. Zhu, L. Fang, Q. Li, Y. Liu, and X. Zhao, "Smallest carbon nanowires made easy: Long linear carbon chains confined inside single-walled carbon nanotubes", *Carbon*, vol. 183, pp. 571–577, Oct. 2021, ISSN: 0008-6223. DOI: 10.1016/j.carbon.2021.07.037.

[219] K. Tang, Y. Li, Y. Chen, W. Cui, Z. Lin, Y. Zhang, and L. Shi, "Encapsulation and Evolution of Polyynes Inside Single-Walled Carbon Nanotubes", *Nanomaterials*, vol. 14, no. 11, p. 966, Jun. 2024, ISSN: 2079-4991. DOI: 10.3390/nano14110966.

[220] L. Shi, R. Senga, K. Suenaga, J. Chimborazo, P. Ayala, and T. Pichler, "Photothermal synthesis of confined carbyne", *Carbon*, vol. 182, pp. 348–353, Sep. 2021, ISSN: 0008-6223. DOI: 10.1016/j.carbon.2021.05.058.

[221] W. Cui, L. Shi, K. Cao, U. Kaiser, T. Saito, P. Ayala, and T. Pichler, "Isotopic Labelling of Confined Carbyne", *Angewandte Chemie International Edition*, vol. 60, no. 18, pp. 9897–9901, Mar. 2021, ISSN: 1521-3773. DOI: 10.1002/anie.202017356.

[222] W. Cui, F. Simon, Y. Zhang, L. Shi, P. Ayala, and T. Pichler, "Ultra-Clean Isotope Engineered Double-Walled Carbon Nanotubes as Tailored Hosts to Trace the Growth of Carbyne", *Advanced Functional Materials*, vol. 32, no. 41, Aug. 2022, ISSN: 1616-3028. DOI: 10.1002/adfm.202206491.

[223] B.-W. Zhang, X.-Y. Qiu, Y. Ma, Q. Hu, A. Fitó-Parera, I. Kohata, Y. Feng, Y. Zheng, C. Zhang, Y. Matsuo, Y. Wang, S. Chiashi, K. Otsuka, R. Xiang, D. I. Levshov, S. Cambré, W. Wenseleers, S. V. Rotkin, and S. Maruyama, "Low-Temperature Synthesis of Weakly Confined Carbyne inside Single-Walled Carbon Nanotubes", 2024. DOI: 10.48550/arXiv.2411.18899.

[224] F. Wang, G. Dukovic, L. E. Brus, and T. F. Heinz, "The Optical Resonances in Carbon Nanotubes Arise from Excitons", *Science*, vol. 308, no. 5723, pp. 838–841, May 2005, ISSN: 1095-9203. DOI: 10.1126/science.1110265.

[225] J. Maultzsch, R. Pomraenke, S. Reich, E. Chang, D. Prezzi, A. Ruini, E. Molinari, M. S. Strano, C. Thomsen, and C. Lienau, "Exciton binding energies in carbon nanotubes from two-photon photoluminescence", *Physical Review B*, vol. 72, no. 24, p. 241 402, Dec. 2005, ISSN: 1550-235X. DOI: 10.1103/physrevb.72.241402.

[226] C. Voisin, S. Berger, S. Berciaud, H. Yan, J.-S. Lauret, G. Cassabois, P. Roussignol, J. Hone, and T. F. Heinz, "Excitonic signatures in the optical response of single-wall carbon nanotubes", *physica status solidi (b)*, vol. 249, no. 5, pp. 900–906, Jan. 2012, ISSN: 1521-3951. DOI: 10.1002/pssb.201100085.

[227] C. D. Spataru, S. Ismail-Beigi, L. X. Benedict, and S. G. Louie, "Excitonic Effects and Optical Spectra of Single-Walled Carbon Nanotubes", *Physical Review Letters*, vol. 92, no. 7, p. 077 402, Feb. 2004, ISSN: 1079-7114. DOI: 10.1103/physrevlett.92.077402.

[228] X. Liu, T. Pichler, M. Knupfer, M. S. Golden, J. Fink, H. Kataura, and Y. Achiba, "Detailed analysis of the mean diameter and diameter distribution of single-wall carbon nanotubes from their optical response", *Physical Review B*, vol. 66, no. 4, p. 045 411, Jul. 2002, ISSN: 1095-3795. DOI: 10.1103/physrevb.66.045411.

[229] T. Saito, S. Ohmori, B. Shukla, M. Yumura, and S. Iijima, "A Novel Method for Characterizing the Diameter of Single-Wall Carbon Nanotubes by Optical Absorption Spectra", *Applied Physics Express*, vol. 2, no. 9, p. 095 006, Sep. 2009, ISSN: 1882-0786. DOI: 10.1143/apex.2.095006.

[230] Y. Miyata, K. Yanagi, Y. Maniwa, and H. Kataura, "Optical Evaluation of the Metal-to-Semiconductor Ratio of Single-Wall Carbon Nanotubes", *The Journal of Physical Chemistry C*, vol. 112, no. 34, pp. 13 187–13 191, Aug. 2008, ISSN: 1932-7455. DOI: 10.1021/jp804006f.

[231] H. Muramatsu, T. Hayashi, Y. Kim, D. Shimamoto, Y. Kim, K. Tantrakarn, M. Endo, M. Terrones, and M. Dresselhaus, "Pore structure and oxidation stability of double-walled carbon nanotube-derived bucky paper", *Chemical Physics Letters*, vol. 414, no. 4–6,

pp. 444–448, Oct. 2005, ISSN: 0009-2614. DOI: 10.1016/j.cplett.2005.08.110.

[232] Bruker Optics GmbH & Co. KG, *VERTEX 80 FT-IR Spectrometer*, Brochure, 2021.

[233] C. Schuster, C. Freytag, W. Cui, L. Shi, E. Parth, D. Denier van der Gon, T. Saito, K. Yanagi, and T. Pichler, "Quantifying the bulk yield of carbyne confined in different carbon nanotube hosts", *Carbon*, vol. 234, p. 119 979, Mar. 2025, ISSN: 0008-6223. DOI: 10.1016/j.carbon.2024.119979.

[234] S. D. M. Brown, A. Jorio, P. Corio, M. S. Dresselhaus, G. Dresselhaus, R. Saito, and K. Kneipp, "Origin of the Breit-Wigner-Fano lineshape of the tangentialG-band feature of metallic carbon nanotubes", *Physical Review B*, vol. 63, no. 15, p. 155 414, Mar. 2001, ISSN: 1095-3795. DOI: 10.1103/physrevb.63.155414.

[235] K. T. Nguyen, A. Gaur, and M. Shim, "Fano Lineshape and Phonon Softening in Single Isolated Metallic Carbon Nanotubes", *Physical Review Letters*, vol. 98, no. 14, p. 145 504, Apr. 2007, ISSN: 1079-7114. DOI: 10.1103/physrevlett.98.145504.

[236] M. Abe, H. Kataura, H. Kira, T. Kodama, S. Suzuki, Y. Achiba, K.-i. Kato, M. Takata, A. Fujiwara, K. Matsuda, and Y. Maniwa, "Structural transformation from single-wall to double-wall carbon nanotube bundles", *Physical Review B*, vol. 68, no. 4, p. 041 405, Jul. 2003, ISSN: 1095-3795. DOI: 10.1103/physrevb.68.041405.

[237] O. Jost, A. A. Gorbunov, W. Pompe, T. Pichler, R. Friedlein, M. Knupfer, M. Reibold, H.-D. Bauer, L. Dunsch, M. S. Golden, and J. Fink, "Diameter grouping in bulk samples of single-walled carbon nanotubes from optical absorption spectroscopy", *Applied Physics Letters*, vol. 75, no. 15, pp. 2217–2219, Oct. 1999, ISSN: 1077-3118. DOI: 10.1063/1.124969.

[238] C. Freytag, C. Schuster, E. Parth, D. Denier van der Gon, T. Saito, K. Yanagi, P. Ayala, and T. Pichler, "Systematic Optimization of the Synthesis of Confined Carbyne", *Small Methods*, Apr. 2025, ISSN: 2366-9608. DOI: 10.1002/smtd.202500075.

[239] L. Shi, P. Rohringer, P. Ayala, T. Saito, and T. Pichler, "Carbon nanotubes from enhanced direct injection pyrolytic synthesis as templates for long linear carbon chain formation: CNTs from eDIPS for LLCC formation", *physica status solidi (b)*, vol. 250, no. 12, pp. 2611–2615, Nov. 2013, ISSN: 0370-1972. DOI: 10.1002/pssb.201300148.

[240] W. Cui, T. Saito, P. Ayala, T. Pichler, and L. Shi, "Oxidation stability of confined linear carbon chains, carbon nanotubes, and graphene nanoribbons as 1D nanocarbons", *Nanoscale*, vol. 11, no. 32, pp. 15 253–15 258, 2019, ISSN: 2040-3372. DOI: 10.1039/c9nr04924j.

[241] S. Yu, W. Zheng, Q. Wen, and Q. Jiang, "First principle calculations of the electronic properties of nitrogen-doped carbon nanoribbons with zigzag edges", *Carbon*, vol. 46, no. 3, pp. 537–543, Mar. 2008, ISSN: 0008-6223. DOI: 10.1016/j.carbon.2008.01.006.

[242] P. Wang, Y. Zheng, T. Inoue, R. Xiang, A. Shawky, M. Watanabe, A. Anisimov, E. I. Kauppinen, S. Chiashi, and S. Maruyama, "Enhanced In-Plane Thermal Conductance of Thin Films Composed of Coaxially Combined Single-Walled Carbon Nanotubes and Boron Nitride Nanotubes", *ACS Nano*, vol. 14, no. 4, pp. 4298–4305, Apr. 2020, ISSN: 1936-086X. DOI: 10.1021/acsnano.9b09754.

[243] Y. Wang and G. H. Robinson, "Unique homonuclear multiple bonding in main group compounds", *Chemical Communications*, no. 35, p. 5201, 2009, ISSN: 1364-548X. DOI: 10.1039/b908048a.

[244] H. Braunschweig, R. D. Dewhurst, K. Hammond, J. Mies, K. Radacki, and A. Vargas, "Ambient-Temperature Isolation of a Compound with a Boron-Boron Triple Bond", *Science*, vol. 336, no. 6087, pp. 1420–1422, Jun. 2012, ISSN: 1095-9203. DOI: 10.1126/science.1221138.

[245] M. Zhou, N. Tsumori, Z. Li, K. Fan, L. Andrews, and Q. Xu, "OCBBCO: A Neutral Molecule with Some Boron-Boron Triple Bond Character", *Journal of the American Chemical Society*, vol. 124, no. 44, pp. 12 936–12 937, Oct. 2002, ISSN: 1520-5126. DOI: 10.1021/ja026257+.

[246] V. V. Nascimento, W. Q. Neves, R. S. Alencar, G. Li, C. Fu, R. C. Haddon, E. Bekyarova, J. Guo, S. S. Alexandre, R. W. Nunes, A. G. Souza Filho, and C. Fantini, "Origin of the Giant Enhanced Raman Scattering by Sulfur Chains Encapsulated inside Single-Wall Carbon Nanotubes", *ACS Nano*, vol. 15, no. 5, pp. 8574–8582, Apr. 2021, ISSN: 1936-086X. DOI: 10.1021/acsnano.1c00390.

[247] M. Hart, J. Chen, A. Michaelides, A. Sella, M. S. P. Shaffer, and C. G. Salzmann, "One-Dimensional Arsenic Allotropes: Polymerization of Yellow Arsenic Inside Single-Wall Carbon Nanotubes", *Angewandte Chemie International Edition*, vol. 57, no. 36, pp. 11 649–11 653, Aug. 2018, ISSN: 1521-3773. DOI: 10.1002/anie.201805856.

[248] M. Hart, E. R. White, J. Chen, C. M. McGilvery, C. J. Pickard, A. Michaelides, A. Sella, M. S. P. Shaffer, and C. G. Salzmann, "Encapsulation and Polymerization of White Phosphorus Inside Single-Wall Carbon Nanotubes", *Angewandte Chemie International Edition*, vol. 56, no. 28, pp. 8144–8148, Jun. 2017, ISSN: 1521-3773. DOI: 10.1002/anie.201703585.

[249] F. Hu, C. Zeng, R. Long, Y. Miao, L. Wei, Q. Xu, and W. Min, "Supermultiplexed optical imaging and barcoding with engineered polyynes", *Nature Methods*, vol. 15, no. 3, pp. 194–200, Jan. 2018, ISSN: 1548-7105. DOI: 10.1038/nmeth.4578.

[250] C. D. Tschannen, M. Frimmer, G. Gordeev, T. L. Vasconcelos, L. Shi, T. Pichler, S. Reich, S. Heeg, and L. Novotny, *Raman Sideband Thermometry of Single Carbyne Chains*, 2021. DOI: 10.48550/ARXIV.2104.02347.